UNIVERSITY OF CALIFORNIA

Santa Barbara

Factors affecting the streamflow and in-stream nitrate concentration in semi-arid areas: sub-surface flow-generation, vertical distribution of soil nitrate and drainage properties, and the connectivity of impervious areas.

A dissertation submitted in partial satisfaction of the

requirements for the degree

Doctor of Philosophy

in Environmental Science & Management

by

Xiaoli Chen

Committee in charge:

Professor Christina Tague, Co-Chair

Professor Arturo Keller, Co-Chair

Professor John Melack

Professor Jeff Doizer

March 2017

The dissertation of Xiaoli Chen is approved.

_____
John Melack

_____
Jeff Doizer

_____
Arturo Keller, Committee Co-Chair

_____
Christina Tague, Committee Co-Chair

March 2017

Factors affecting the streamflow and in-stream nitrate concentration in semi-arid areas: sub-surface flow-generation, vertical distribution of soil nitrate and drainage properties, and the connectivity of impervious areas.

by

Xiaoli Chen

I dedicate this thesis to my grandmother. It is her unconditional love that motivates me to set higher targets.

Acknowledgements

The completion of the dissertation will not be possible without the guidance and patience from my four committee members: Professor Arturo Keller, Professor Christina Tague, Professor John Melack and Professor Jeff Dozier.

I would like to express my thanks to my lab manager Janet Choate who guided me through modeling using RHESSys.

I also want to thank my lab mates from Keller's lab and Tague's lab. I learned a lot from discussing with all of you.

I would like to extend my thanks to Bren Assistant: Kristine Faloon and Casey Hankey for their help on my PhD journey in Bren.

Curriculum Vitæ

Xiaoli Chen

Education

2017	Ph.D. in Environmental Science & Management (Expected), University of California, Santa Barbara.
2009	B.S. in Mechanical Engineer, Peking University.

Publications

Arturo A. Keller, Xiaoli Chen, Jessica Fox, Matt Fulda, Rebecca Dorsey, Briana Seapy, Julia Glenday, and Erin Bray. 2014. Attenuation Coefficients for Water Quality Trading. *Environmental Science & Technology* 2014 48 (12), 6788-6794. DOI: 10.1021/es500202x

Xiaoli Chen, Nathan Emery, Elizabeth S Garcia, Erin J Hanan, Heather E Hodges, Tyronne Martin, Matthew A Meyers, Lindsey E Peavey, Hui Peng, Jaime Sainz Santamaria, Kellie A Uyeda, Sarah E Anderson, Christina Tague. 2013. Perspectives on disconnects between scientific information and management decisions on post-fire recovery in Western US. *Environ Manage*. 2013 Dec; 52(6):1415-26. DOI: 10.1007/s00267-013-0165-y.

Xiaoli Chen, Naomi Tague, John Melack, Janet Choate, Jeff Dozier, Arturo Keller. 2016. Comparisons of the Fill & Spill Model and the Continuous Model for Hydrologic Modeling of Subsurface Flow in Semi-Arid Areas. *Hydrological Processes*. In revision.

Abstract

Factors affecting the streamflow and in-stream nitrate concentration in semi-arid areas: sub-surface flow-generation, vertical distribution of soil nitrate and drainage properties, and the connectivity of impervious areas.

by

Xiaoli Chen

The Southern California coastal region is one of the five areas in the world with Mediterranean climate. The long dry summer and cool wet winter not only attract a large population, but also create a unique hydrologic signature with strong temporal and spatial heterogeneity in soil moisture, streamflow and vegetation water use.. The sandy soil, fractured and uplifting bedrocks in undeveloped areas result in flashy and non-linear hydrologic responses to storms. Urbanization in this area further alters the hydrograph by changing the land cover and drainage patterns . These changes alter both water and nitrate fluxes, which may have substantial impacts on the downstream and coastal ecosystems, such as Great Kelp forest in the Santa Barbara channel. To understand and ultimately manage of water resources in this region must take these multiple factors climate, soil and urbanization into account. Study and modeling of flow generation and nitrate transport mechanisms in the undeveloped area, and disturbance of nitrate cycling and nitrate export in the urban areas in this region may reveal new insight and improve the understanding of hydrologic processes, and provide sustainable watershed management strategies.

Southern California coastal mountain watersheds are characterized by a Mediterranean climate, sandy soil, shallow rock, flashy hydrologic responses and drought tolerant vegetation such as oak and chaparral [51, 93]. The geological condition in this area may fit

the requirement condition of 'Fill & Spill' hypothesis of subsurface flow generation mechanism. We adapted 'Fill & Spill' submodel in an eco-hydrologic model, Regional Hydro-Ecologic Simulation system (RHESSys) [23], implemented it in the semi-arid area, and compare its model performance with the traditional 'Continuous Transmissivity' model which assume the soil hydraulic conductivity follows a continuous exponential function [3]. Our results show that in the recession period, the modeled discharge from 'Fill & Spill' model dropped much faster than the one from 'Continuous Transmissivity' model, and fit the observed discharge data better. 'Fill & Spill' model is also less sensitive to small precipitation events, and tends to increased estimates of peak flow. Assessment of whether peak flow responses by the 'Fill & Spill' model are a better representation of observed dynamics is challenging given that peak flow observed data is prone to uncertainties from different sources such as heterogeneity in precipitation distribution and errors in stream gauge stations, and may not reflect the true hydrologic response of watershed behavior. In summary, model assessments show that the 'Fill & Spill' model results in substantially different recession behavior and that, for the study watershed, the 'Fill & Spill' model may be a better predictor of the watershed hydrologic responses to precipitation events better than 'Continuous Transmissivity' model.

The long dry summer and cool wet winter of semi-arid climate in the undeveloped watersheds results in uneven vertical distribution of nitrate, with most of the nitrate concentrated at surface layer and limited in the deep soil [53]. In our conceptual model, we showed that the vertical distribution of nitrate and its interaction with soil hydraulic conductivity controls the nitrate concentration-discharge patterns in the downstream. The uneven distribution of nitrate tends to produce an enrichment pattern, and the more evenly distributed nitrate will lead to a stable or weak dilution. In the eco-hydrologic model, we tested a combination of different hydraulic conductivity and vertical distribution of soil nitrate. Results show that at both patch and watershed scales, nitrate

concentration-discharge patterns are sensitive to the hydraulic conductivity and vertical distribution of soil nitrate. In patch scale, modeling results match with the conceptual model. In watershed scale, because of the lateral replenishment of nitrate, concentration-discharge patterns are more complex and showing a 2-stage pattern with a transition point where patterns shift from enrichment to dilution. The hydraulic conductivity controls the transition point, and the interactions between conductivity and vertical nitrate distribution still affects the concentration-discharge pattern. This result is different from previous researches, which attributes the enrichment and dilution in the nitrate concentration-discharge relationship as the consequences of lateral expansion and contraction of saturated area [60, 59]. Our results indicate that, besides the analysis from horizontal hydrologic connectivity, the distribution of nitrate in the vertical direction and its interaction with the hydraulic conductivity also contributes to the nitrate concentration-discharge pattern.

The urbanization and expansion of impervious areas have great impact on the downstream nitrate concentration. Previous studies focus on the impact of impervious surface on collecting nitrate and other pollutant [94, 96]. How the water availability in vegetated area affecting the nitrate concentration in urban area is less well known and may be particularly important in semi-arid regions. Our results show that the total impervious area (TIA), effective impervious area (EIA), and vegetation types all have impacts on the downstream nitrate concentration. The TIA and EIA control the water availability in the vegetated land. The reduced TIA and EIA will increase the water availability in vegetated land and decrease the stream flow. As growth of vegetation and microbial activity in semi-arid areas is water limited, increased water availability can lead to more nitrate uptake by plant, but may also lead to increased nitrate released through soil decomposition processes. Results show that, the impact of the enhanced vegetation uptake is the dominant factor and consequently reducing TIA and EIA generally tends to

reduce downstream nitrate flux and concentration. In some cases, however, the impact of a reducing EIA on reducing the stream discharge may offset the influence from the enhanced plant nitrate uptake and increase the nitrate concentration. These results suggest that improve water quality in urbanizing regions, a low EIA will generally but not always reduce nitrate concentration and the magnitude of this effect varies strongly with TIA and vegetation type. Thus the design of effective strategies may be improved by model-based assessments that account for interactions among EIA, TIA, and vegetation types. These findings are specific to semi-arid regions where additional water availability has great impacts. In humid environment where the biochemical activities are generally not water limited, some of the interactions in this study may not occur.

Contents

List of Figures

Tables

Chapter 1

Comparisons of Fill & Spill Model and Continuous Transmissivity Mechanisms for Hydrologic Modeling of Subsurface Flow in a Mountainous Semi-Arid Areas

1.1 Introduction

Subsurface flow is an important component of watershed responses to storm events in areas with conductive soils. Controlled by the hydrological connectivity on hillslopes, subsurface flow redistributes soil moisture and nutrients in watersheds [1]. Various factorssuch as antecedent soil moisture, the permeability of underlying bedrock, soil depth, existence of macropores and local slopeaffect subsurface flow. Ecological processes also influence subsurface flow by controlling antecedent soil moisture through evapotranspi-

ration, and creating preferential flow paths via root channels [2].

In hydrological models, 'Continuous Exponential Transmissivity' model [3] for subsurface flow is widely used, where the subsurface transmissivity decays exponentially with soil saturation deficit:

$$K(sat_{df}) = Ksat_0 \times e^{-\frac{sat_{df}}{m}} \tag{1.1}$$

$$T(sat_{df}) = \int_{max\_sat_{df}}^{sat_{df}} K(sat_{df}) \tag{1.2}$$

$K(sat_{df})$ is described as the hydraulic conductivity when soil saturation deficit equals sat_{df}, which is calculated as the difference between the soil porosity per unit area and the water storage per unit area. max_sat_{df} is the maximum of saturation deficit, $Ksat_0$ is the saturated hydraulic conductivity at soil surface, $T(sat_{df})$ is the transmissivity when soil saturation deficit equals sat_{df}, and m is the coefficient controlling the decreasing rate of transmissivity against soil saturation deficit.

Tromp-van Meerveld and McDonnell [4] proposed the Fill & Spill hypothesis as an alternative model to explain hillslope threshold-based hydrological responses. Observations following rainfall show that responses of the subsurface flow are not significant until a threshold of cumulative precipitation is reached [5, 4, 6, 7]. The Fill & Spill model explains the threshold behavior as follows: the infiltrated water first fills bedrock depressions, and then follows the preferential flow along the bedrock-soil interface. The Fill & Spill hypothesis differs from the traditional Continuous Exponential subsurface model by emphasizing a threshold soil water level above which there is an abrupt change in transmissivity in contrast to assuming that subsurface transmissivity decays continuously and exponentially with soil saturation deficit [3].

While Continuous Transmissivity approach is still widely used in hydrological models,

some models have implemented the Fill & Spill alternative to understand the subsurface connectivity [8, 9, 10, 11, 12, 13, 14], especially in environments with bedrock near the surface and with seasonal variability in precipitation that causes water tables to rise and fall. For example, Weiler & McDonnell (2007) used the modified Hill-vi model, which includes a pipe network to model preferential flows, to highlight the importance of the inclusion of the bedrock leakage for long-term subsurface flow responses. Hopp & McDonnell (2009) conducted a series of virtual experiments using a 3-D physics-based model and identified the interactions between slope angles, soil depth and the storm size as the hillslope controls on connectivities. Janzen & McDonnell (2015) incorporated stochastic percolation theory into the virtual experiments and successfully reproduced the threshold of 55mm cumulative precipitation for nonlinear hydrological responses. They also explored effects of different factors on subsurface connectivity and suggested the need to account for the detailed pattern of the delivery of rainwater to the soil-bedrock interface. Most of these studies were conducted in small hillslope ($0.1 < \text{km}^2$), partly because the high computational complexity of 3-D models that prohibits their use at the watershed scale.

None of the studies above have implemented or tested the Fill & Spill hypothesis in semi-arid watersheds. Compared with humid or arid areas, the succession of dry/wet periods and wetting up transitions in semi-arid areas can lead to high spatial heterogeneity in soil moisture, increasing the complexity of hydrological responses that depends on catchment wetness [15]. The interactions of processes at different spatial or temporal scales often result in non-linear dynamics and poses additional difficulties for hydrological modeling in semi-arid areas [16]. As studies have argued that the threshold based response and lateral preferential flow seem to be a common property of the hillslope drainage [17], the Fill & Spill hypothesis may still be valid for semi-arid areas, especially for mountainous area with steep slopes and bedrock near the surface such as southern

California coastal mountain area [18]. The existence of macropores and interactions between preferential flow, soil matrix and bedrock irregularities were found in a study of semi-arid catchments in Spain [19] and observations indicate similar conditions to those described in the Fill & Spill conceptual model [4]. The Fill & Spill hypothesis may explain the non-linear responses to storm events and capture the non-linear dynamics of catchment connectivity in semi-arid watersheds.

Appropriate temporal resolution is another important factor for numerical modeling in semi-arid areas. Precipitation characteristics such as the storm duration/intensity, and temporal variability often controls the catchment runoff in semi-arid areas [20, 21]. Modeling the hydrologic consequences of short-duration storms together with the flashy hydrological characteristics in semi-arid areas may depend on model time step and require hourly or sub-hourly time step [22].

In this study, we implement the Fill & Spill mechanism in the Regional Hydro-Ecologic Simulation system (RHESSys) [23] in a semi-arid undeveloped watershed in southern California and examine the impact on estimates of watershed connectivity. We address the following questions:

1. Do the Fill and Spill and Continuous Transmissivity models lead to different estimates of streamflow responses to precipitation inputs in semi-arid regions?

2. Which model more accurately represents the observed flow data during the storm events? And during the recession periods?

3. Will a more frequent timestep in model simulations improve the predictions compared to the observed flow data?

Two modifications to RHESSys are made: adaptation from the daily time step to an hourly time step, and integration of a threshold-based Fill & Spill mechanism into the

subsurface flow sub-model, replacing the Continuous Transmissivity mechanism. Four model scenarios were compared: Continuous Transmissivity and Fill & Spill, each with daily and hourly time steps.

We use these scenarios to compare model behavior between daily and hourly time steps and between the two different conceptual models of subsurface flows. The comparisons consider model performance when evaluated against the stream discharge, and model estimates of hydrograph characteristics and spatial patterns of soil moisture under different wetness conditions.

1.2 Methodology

1.2.1 Model Description

The physical process-based, distributed hydrological model, RHESSys [23], has been widely implemented and evaluated in different climate zones [24, 25, 26], including in semi-arid regions [27, 28, 29].

RHESSys explicitly models hydrologic connectivity and lateral hydrological fluxes. The soil profile is represented in two layers: an unsaturated layer and a saturated zone. The root zone is within the unsaturated layer. Infiltration is modeled as a 1-D vertical process using a modified version of the Green and Ampt [30] approximations. Lateral flow from upland areas can be diverted to more than one receiving patch in the downslope based on the topography. Precipitations in excess of interception and connected upslope areas can generate surface flow when soil is saturated or when infiltration capacity is exceeded. RHESSys also models the macropore preferential flow in two ways: (1) the use of an effective hydraulic conductivity in the shallow subsurface flow model, which is typically higher than measured soil hydraulic conductivity values, and (2) by diverting

part of surface detention water directly to a deeper groundwater storage, which drains directly to the stream.

RHESSys uses the Penman Monteith approach [31] to calculate both the evaporation and the transpiration, including evaporation of the rain intercepted by each canopy layer, sublimation of intercepted snow, and transpiration of vascular layers. Soil evaporation is estimated by incorporating energy and atmospheric drivers as well as a maximum exfiltration rate, as determined by soil properties and the soil moisture. The potential capillary rise is limited by the water table and soil properties. To account for the subdaily plant responses, half of the potential capillary rise is allocated to the unsaturated zone at the start of the day, and the other half left to meet the plant transpiration needs.

Although RHESSys includes biogeochemical cycling and vegetation growth sub-models to account for the carbon/nutrient cycling, in this paper, we will only focus on hydrologic implications.

1.2.2 Adapting from daily to hourly time step

RHESSys daily time step runs most processes and sub-models at the end of each day. To model the effect of temporal variation on runoff during the storm events, we have adapted hydrological routing code in RHESSys to an hourly time step that including processes: plant interceptions and throughfall, soil infiltration and lateral flows, drainages to deep groundwater and discharge of groundwater to streams.

During storms, the impact of hourly evapotranspiration (ET) and phenological processes on water availability is small compared with other hydrological processes like drainage and interception; therefore, for computationally efficiency we continue to model ET and plant phenological processes at a daily time step. Modeling ET at an hourly time step would require adding substantial complexity to the plant model to account for

the transport time between roots and leaves.

After these adaptations, RHESSys runs in a hybrid time step that depends on the time step of the input data. When hourly climate data are available, RHESSys runs the hydrological processes with the hourly time step for days with hourly data. This adaptation improves computationally efficiency by allowing the user to switch between 'daily' and 'hourly' within a given simulation and use the 'hourly' model only when processes are likely to be sensitive to the time step (e.g., runoff during storms).

1.2.3 Adapting from Continuous Transmissivity to Fill & Spill implementation

Unlike the Continuous Transmissivity model, where the hydraulic conductivity decreases exponentially and continuously with the soil saturation deficit level (equation 1.1 1.2), the Fill & Spill model uses a discontinuous relationship. A threshold '*saturation deficit threshold*' is explicitly set (Figure 1). For the Fill & Spill concept, when the saturation deficit falls below this threshold, the soil water is trapped by bedrock depressions, and there is a little leakage from the depressions. When saturation deficit exceeds the threshold, the infiltrated water has already filled the bedrock depressions and begins to spill over along macropores at the interface of the soil and the bedrock as lateral preferential flows. Due to the preferential flow, the soil hydraulic conductivity has an abrupt increase at the saturation deficit threshold and exceeds the value in the Continuous Transmissivity model. Some leakage does occur through bedrock fractures and accounting for this is necessary for modeling subsurface flow responses to multiple storms [12].

When implemented in RHESSys, three new parameters were used for the Fill & Spill model. First, the '*Saturation Deficit Threshold*' is defined as the soil saturation deficit

needed to fill the bedrock depression. This is the threshold beyond which preferential flow will emerge and dominate the subsurface flow in a patch, shown as the dashed line in Figure 1.2. Second, the '*leakage*' is defined as the multiplier to the original hydraulic conductivity K that is applied when the saturation deficit falls below the threshold (bedrock leakage). We assume the leakage coefficient is less than 1. Third, the '*spillover*' is defined as the multiplier to original hydraulic conductivity k when the saturation deficit is above the '*Saturation Deficit Threshold*', representing the abrupt increase in soil hydraulic conductivities due to the emergence of the preferential flow. The spillover coefficient is always larger than 1.(Figure 1.2)

$$K(sat_{df}) = \begin{cases} Ksat_0 \times e^{-\frac{sat_{df}}{m}} \times Leakage, & \text{if } sat_{df} > Saturation\_Deficit\_Threshold\ . \\ Ksat_0 \times e^{-\frac{sat_{df}}{m}} \times Spillover, & \text{if } sat_{df} \leq Saturation\_Deficit\_Threshold\ . \end{cases} \tag{1.3}$$

$$T(sat_{df} = \int_{max\_sat_{df}}^{sat_{df}} K(sat_{df}) \tag{1.4}$$

1.3 Study Area and Data

1.3.1 Study Area

Rattlesnake Creek catchment is a headwater catchment located on the southern facing slopes of the coastal Santa Ynez Mountains. Three dominated shrub speciesIt covers the 5.8 km^2 area: *Ceanothus megacarpus* (big pod ceanothus), *Adenostoma fasciculatum* (chamise) and *Arctostaphylos spp.* (Manzanita) [32]. Slope steeper than $> 20°$ and sandy loams characterize the watershed, which eventually flows into the Santa Barbara Channel. Investigation shows that the headwater is covered by shallow highly fractured

bedrock [18, 33]. Catchment elevation ranges from 270 to 1262 m (Figure 1.3).

The climate is semi-arid Mediterranean with warm summers and cool winters. The year-round average temperature is 18 °C, with an average maximum of 23 °C and an average minimum of 13 °C. Most of the precipitation events are in the winter, and the long dry summer has very little precipitation. The annual precipitation averages around 470 mm/year [28]. The intensity of storms is mild, ranging from 10 mm/day to 100 mm/day. During storm events, the orographic lift has substantial effects on the distribution of precipitations. The gauge at the ridgeline with 1000 m elevation shows 210% higher precipitation than the one at 30 m elevation [34].

1.3.2 Data

The observed climate and discharge data come from the Santa Barbara Channel Long Term Ecological Research (SBC LTER) website `http://sbc.lternet.edu/`. The discharge records come from the streamflow gauge station 'RS02' (Lon: -119.6922, Lat: 34.4576) at the outlet of watershed. Both water pressure and water temperature were collected and reported hourly with some missing data in 2007. Stage height was calculated from water pressure and atmospheric pressure, then was converted to discharges using a rating curve developed with stream channel cross-sections, roughness estimates using the HEC-RAS model [35]. The observed climate and stream discharge data [36, 37] from 2004-10-01 to 2005-10-05 are used for the model calibration, and the observed climate and stream discharge data from 2001-09-01 to 2008-09-01 are used for the model evaluation. For precipitations, the ridgeline gauge 'El Deseo' (Longitude: -119.6958, Latitude: 34.4917) is used because it is the closest precipitation gauge station to the study area. The precipitation was collected with a tipping bucket gauge and the data are reported in 5 minute intervals. In the model, precipitation inputs were interpolated from

a single rain gauge based on elevation and a precipitation scaling factor. The precipitation for a given elevation (P_E) was interpolated as:

$$P_E = P_{base} \times [s \times (E - E_{base}) + 1] \tag{1.5}$$

E is the elevation of given point, E_{base} is the elevation of the main precipitation gauge, and the P_{base} is the precipitation at the main gauge [28]. The precipitation scaling factor s is 0.0015 m^{-1}.

1.4 Model Calibration and Evaluation

We compared the performance of the four different model implementations: (1) Continuous Transmissivity model with daily time step (daily continuous); (2) Fill & Spill with daily time step (daily Fill & Spill); (3) continuous model with hourly time step (hourly continuous); (4) Fill & Spill with hourly time step (hourly Fill & Spill).

1.4.1 Model Calibration (Monte Carlo Simulation S1)

3600 Monte Carlo simulations (described below) were implemented for each of the four models, using the observed climate and discharge rate records from 2004-10-01 to 2005-10-07. Hourly simulation outputs were aggregated to a daily time step so that the output of the four model implementations could be compared. The Nash-Sutcliffe Efficiency [38] was used to evaluate the model performance against the observed stream discharge.

$$NSE = 1 - \frac{\sum (\hat{Q}_i - Q_i)^2}{\sum (Q_i - \bar{Q})^2} \tag{1.6}$$

Q_i is the observed stream discharge at time i, $\bar{Q}_i$ is the mean observed stream discharge and $\hat{Q}_i$ is the simulated stream discharge. NSE ranges from -∞ to 1. An NSE

value equals to 1 indicates the best model performance. When NSE is negative, it indicates that the model performance is no better than choosing the average value. The NSE value is sensitive to high discharges, and it is less sensitive to performance in low flow or recession periods.

In the Rattlesnake Creek watershed, the modeled peak flow is likely to show substantial errors because of the uncertainty in the precipitation input data and in particular in the estimation of the spatial distribution in the precipitation data during storms. In mountain areas, the strong orographic effect can result in high uncertainties while interpolating the precipitation over the whole watershed from a single meteorological station for a particular event [39]. The uncertainty in interpolated precipitation propagates into errors in the estimation of the peak flow. Hydrograph recession characteristics and low flow estimates are less sensitive to these errors in storm precipitations [28]. To avoid over fitting the uncertainty-prone peak flow, the multi-objective calibration that accounts for the performance of different components of the hydrograph was used to evaluate the model performance. The multi-objective function is:

$$Obj_{NSE_{all}} = \frac{1}{3} \times NSE + \frac{1}{3} NSE_{recession1} + \frac{1}{3} NSE_{recession2} \tag{1.7}$$

NSE is the Nash-Sutcliffe Efficiency as defined in equation 1.6. $NSE_{recession1}$ is the Nash-Sutcliffe Efficiency for the recession period from Jan 13, 2005 to Feb 5, 2005. $NSE_{recession2}$ is the Nash-Sutcliffe Efficiency for the second major recession period from 2005-02-23 to 2005-03-10. The recession period is defined as the period from 4 days after the streamflow peak to 4 days before the next peak. These two recession periods are chosen because they are the longest in the observed data. While using the average of these three NSE values as the objective function, the model's performance weigh more on the recession flow.

The parameter sets for the Monte Carlo calibration were generated by randomly varying the value of the five drainage-rate-control parameters. The five parameters are: (1). m, the coefficient controlling the decreasing rate of the transmissivity against the soil saturation deficit as in Equation 1.1. (2). $Ksat_0$, the saturated hydraulic conductivity at soil surface. (3). sd, soil depth. (4). $gw1$, the percentage of water in detention store drained to the groundwater directly; this parameter controls the macro-pore flow in the soil. (5). $gw2$, the percentage of groundwater storage drained to stream. For the Fill & Spill model, three more parameters were evaluated: *leakage* is the leakage multiplier; *spillover* is the spillover multiplier; *Saturation Deficit Threshold*, the threshold for Fill & Spill and defined as the portion of max saturation deficit. The range of drainage-rates-control parameters is based on Shields & Tague (2012).

1.4.2 Model Sensitivities to the Spatial Heterogeneity in Saturation Deficit Threshold (Monte Carlo Simulation S2)

Previous studies indicate that in the Fill & Spill model, spatial heterogeneities in the threshold-related soil properties can help explain the non-linear behavior of stream discharge [40, 6]. To test the impact of spatial heterogeneities of soil drainage properties on stream discharge, during the calibration period, another 3600 simulations are implemented in hourly Fill & Spill scenarios with a set of threshold-related values for the Fill & Spill parameter *Saturation Deficit Threshold*, based on four soil types in the watershed that in turn are selected as quantiles in the remotely sensed normalized difference vegetation index (NDVI).

Soil Types and Ranges of the *Saturation Deficit Threshold*

According to the Fill & Spill conceptual model (equation 1.3, patches with a smaller *Saturation Deficit Threshold* may drain in high volumes only when the saturation deficit

(sat_{df}) is small (high water table), and result in more soil moisture. Patches with a higher *Saturation Deficit Threshold* may drain in high volumes even when the saturation deficit (sat_{df}) is high (low water table), and result in less soil moisture. As a result, soil moisture can be used to at least partly infer the *Saturation Deficit Threshold*. However, neither the value of *Saturation Deficit Threshold* nor direct measurements of the soil moisture are available. NDVI can be used as an indicator for soil moisture [41, 42], and we first use NDVI to classify the soil into 4 types and then infer the *Saturation Deficit Threshold* range according to the soil types. The 25%, 50%, and 75% quantile from NDVI histogram (0.69, 0.77, 0.82) is used as threshold to separate the 4 soil types (Figure 1.4). Soil type 1 covers most of upslope dry areas and is given the highest value of *Saturation Deficit Threshold*. Soil type 4 is usually the one in the riparian zone and given the lowest value of *Saturation Deficit Threshold*. In these scenarios, all 3600 parameter sets share the same set of soil drainage parameter, chosen from the initial calibration as the baseline parameter set, except for the spatial-based *Saturation Deficit Threshold*, which is randomly selected from the range of value according to its soil type (Table 1.2). The performance evaluation metrics are the same as it is in the calibration period.

1.4.3 Model Validation (Simulation S3)

The period from 2001-12-06 to 2008-09-12 is used for model validation. All daily and hourly stream discharge records are used in the validation. The top 900 parameter sets with the highest $Obj_{NSE_{all}}$ values were used to validate the model performance. Part of the observed data are missing from Oct 2007 to Nov 2008. As a result, this period was excluded for the model validation. The period of time for calibration is also excluded for model validation. The performance metrics used for the validation are similar to that for calibration, with the weighted average of NSE and the NSE for recession period, as

described above.

1.4.4 Uncertainty Estimation

Uncertainty bounds around stream discharge estimates are computed using the Generalized Likelihood Uncertainty Estimation method (GLUE) [43]. The 97.5% and 2.5% uncertainty bounds and the maximum likelihood predictions of model's output are identified by this process.

1.5 Results

1.5.1 Calibration Results Based on NSE Value

The NSE values of the four models are summarized in Table 1.3. Generally, model performance with an hourly time step is slightly better than with the daily time step. This improvement exists with both the Fill & Spill and Continuous Transmissivity implementations. The performance during recession periods is substantially improved from the Continuous Transmissivity to the Fill & Spill implementation,

1.5.2 Model Behavior Comparison

To better illustrate the differences between the four model implementations, results from 2005-01-06 to 2005-03-16 are plotted in Figure 1.5. The top 150 parameter sets with the $Obj_{NSE_{all}}$ greater than 0.5 are used for to determine GLUE uncertainty bounds. Figure 5 shows three interesting patterns. First, the Fill & Spill models matched the observed discharge better than the Continuous Transmissivity models by producing a lower discharge, during the first recession period. The predicted discharge from the Continuous Transmissivity models begins to deviate from the observed values on 2005-

01-13 for recession Period 1 and on 2005-02-24 for recession Period 2. In comparison, the Fill & Spill implementations had satisfactory fitness to the observed data over the recession period. Second, Fill & Spill models predicts higher peak discharges than the one from Continuous Transmissivity models. The difference between the two rates is significant ($p < 0.01$) based on a t-test for the multi-day mean peak-flow discharge for the top 150 parameters. Third, the difference between the hourly model and daily model in peak flow is very small. The differences in mean peak flow between the hourly and daily model are less than 5% of the mean peak flow for the top 150 parameters. Also, there is no evidence that the difference grows as mean peak flow increases.

1.5.3 Uncertainty

The range of the uncertainty for the Fill & Spill models is larger than the Continuous Transmissivity models (Figure 1.6), especially for the two small precipitation events around 2004-02-11 and 2005-02-04. Although the uncertainty bandwidth tends to be wider for storm events than low flow conditions, the relation between the width of uncertainty and discharge is not simply linear. The observed discharge shows that the largest uncertainty width is for storm on 2005-02-20, which is the second largest storm. For the storm on 2005-01-10, which is the largest storm in this year, the uncertainty width grows to a peak during the recession period, not during the peak flow. The cumulative width of the uncertainty also shows that the steepest slope is around the median level discharge rather than the highest discharge (Figure 1.7).

1.5.4 Parameter Distribution

The top 150 parameter sets with $Obj_{NSE_{all}}$ larger than 0.5 from performance ranking were selected out of 3600 parameter sets as the 'good parameter sets' from Monte

Carlo Simulation S1. To examine how performance responds to individual parameters we plot the cumulative frequency of 'good' parameter values (Figure 1.8). The original sampling distribution of parameters will plot as a one-to-one line on this figure. Departures from this line in distributions of 'good parameter sets' reflect parameter values that are selected through calibration. A steep upward curve indicates the clustering of 'good parameters'. We show results only for parameters where 'good parameter' distributions showed substantial differences across model implementations.

All models favor m with a value less than 0.5 (Figure 1.8). However, models with an hourly time step generally prefer smaller m values than the models with daily time step. The Fill & Spill models prefer smaller m values than Continuous Transmissivity models. As m is the denominator in a negative exponential expression referenced in Equation (1), the larger m values means the hydraulic conductivity decreases more slowly against the soil saturation deficit. The smaller m values mean the soil hydraulic conductivity sharply decreases from surface soil to deep soil. The accumulative frequency plot of m indicates that the models with daily time step prefer hydraulic conductivity more gently decreasing across the soil profile than the hourly time step models, while models with Fill & Spill setting prefer hydraulic conductivity more sharply decreasing across the soil profile than the Continuous Transmissivity ones.

The $gw2$ parameter is the parameter that defines the percentage of groundwater draining from the deeper groundwater storage to the downstream. The cumulative frequencies plot of parameter $gw2$ for 'daily Fill & Spill' model leans to the right of the one for 'hourly Fill & Spill' model (Figure 1.8); this indicates that the 'daily Fill & Spill' model needs more rapid drainage from groundwater stores than the 'hourly Fill & Spill' model. The distribution plot of the 'daily Continuous' model lies on the left of the one of the 'daily Fill & Spill' model, indicating that in a daily time step, the Continuous Transmissivity model favors slower groundwater drainage than the Fill & Spill model.

Both frequency plots are close to 1 once the spillover multiplier reaches 80, indicating that both 'daily' and 'hourly' models prefer spillover multipliers less than 80 (Figure 1.8). The cumulative frequency of 'hourly Fill & Spill' model follows a more linear relationship when the spillover multiplier is less than 80, indicating that the model does not have a particular preference for the value of this parameter. However, the cumulative frequency plot for 'daily' model skews to the left and reaches 0.9 when the spillover multiplier is around 40. This means that the 'daily Fill & Spill' model favors the spillover multiplier with a value less than 40.

The cumulative frequency distributions of parameters like the soil depth and gw1, which determines the amount of bypass flow to deep groundwater stores, show only small differences between different models. It indicates that these parameters are not as sensitive to model selections as the three parameters mentioned above.

1.5.5 Spatial heterogeneity of *Saturation Deficit Threshold* and Its Impact on Model Performance

When assessing the impact of the spatial heterogeneity of *Saturation Deficit Threshold* on stream discharge, the top 150 parameter sets with $Obj_{NSE_{all}}$ larger than 0.4 from performance ranking were selected out of 3600 parameter sets as the good parameter sets in Monte Carlo Simulation 2. Figure 1.9 is the cumulative frequency plots of these parameters. SDT1 through SDT4 represent the *Saturation Deficit Threshold* of soil type 1, 2, 3, 4, which are generated (Section 4.2) by random selecting from the range of value corresponding to the soil type in Table 1.2. Figure 1.9 shows that the cumulative frequency curves of the 4 parameters are straight line and nearly identical, indicating that the spatial heterogeneity in *Saturation Deficit Threshold* may not results in substantial impact on the stream discharge.

1.5.6 Model Validation

The performances in the validation period (Simulation S3) (Table 1.4) are similar to the ones in calibration period (Simulation S1) (Table 1.3). The 'hourly' models did not differ substantially from the 'daily' models. The Fill & Spill models improve the performance for the recession flow, but not for the peak flow. When considering the weighted averaged $Obj_{NSE_{all}}$, the Fill & Spill models have a little wider range of $Obj_{NSE_{all}}$ than the Continuous Transmissivity models.

1.5.7 The Spatial Moisture Distribution

One set of parameters with good performance ($Obj_{NSE_{all}} > 0.6$) for each of the four models was selected as an example to illustrate the spatial moisture distribution during low flows, recessions and storm events. Table 1.5 summarizes the percentage of saturated area for the four different model settings.

Figure 1.10 shows the spatial distribution of soil moisture during a low flow period, with little difference between the four models. None of the patches are saturated during the low flow condition (Table 1.5). All plots show that the soil is drier in the upland and wetter in the riparian zone. The south-faced slopes are drier than the north-faced slopess. This pattern is typical of semi-arid Northern Hemisphere region since south facing slopes receive more solar radiation and have higher ET leading to lower soil moisture values during period between storms.

During recession periods, the differences in soil moisture patterns between models are more apparent 1.11. Fill & Spill models (Figure 1.11 B and D) tend to have greater area in relatively dry soils than the Continuous Transmissivity models (Figure 1.11 A and C). Around 0.3% of the total area in 'daily/hourly Fill & Spill' is fully saturated, while over 6% of the total area in 'daily/hourly Continuous' is fully saturated (Table 1.5). All

of these model results show that the south facing slopes are drier than the north facing slopes. The differences between daily time-step models and hourly time-step models are small.

During storms, the differences of heterogeneity in soil moisture distribution between models are less obvious (Figure 1.12). The Fill & Spill models (Figure 1.12 B and D) display a little more heterogeneities in the soil moisture than the Continuous Transmissivity models (Figure 1.12 A and C) during storms. Uphill regions have more rapid drainages in the Fill & Spill models, which results in a drier (lighter color) areas in the uphill regions in Figure 1.12 B/D than Figure 1.12 A/C. Table 1.5 also shows that during the storm, Fill & Spill models have less saturated area. However, while the whole watershed has been wet up during the storm events, the difference in soil moisture distribution is small comparing with the ones in the recession period.

1.6 Discussion

1.6.1 Evaluation Metrics

NSE values for the Fill & Spill implementation are substantially lower than those for the Continuous model (Table 1.3). We note that in mountainous semi-arid system, the NSE is not always a good indicator of model performances. Modeling of peak flow is prone to significant uncertainties in semi-arid coastal mountain areas because of uncertainty in the interpolation of point rainfall measurements over the watershed during storm, when the strong orographic effects non-linearly enhance the heterogeneity in the spatial distribution of precipitation, often leading to a poor representation of the spatial pattern [39, 28]. The uncertainties in observed precipitations make it difficult for a hydrology model to match the observed peak flow especially when there is only one pre-

cipitation station in the watershed. As a result, this difference in NSE value may not be a good indicator for overall performances. In this sense, the $NSE_{recession1}$, $NSE_{recession2}$ and weighted average objective function $Obj_{NSE_{all}}$ are the better metrics than the NSE in performance evaluations. Based on these metrics, models with Fill & Spill implementations have similar overall performance to the Continuous Transmissivity models but achieve better performances in recession periods, when compared with Continuous Transmissivity models.

1.6.2 Model Responses in Peak Flow and Recession/Low Flow Period

Peak Flow

As the soil moisture increases, adjacent patches become hydrological connected when soil saturation deficit level is above the Fill & Spill *Saturation Deficit Threshold*. With this approach, subsurface preferential flow will dominate subsurface flow because the hydraulic conductivity is much higher than the Continuous Transmissivity models. As a result, Fill & Spill models have higher runoff rates during peak flows, as reflected by model estimates for storms in 2005-01-09 and 2005-02-20. This result is consistent with previous modeling work on preferential flows [14].

Recession Flow

Once the water table falls during recession/low flow periods, the soil saturation deficit falls below the Fill & Spill threshold *Saturation Deficit Threshold* and the subsurface hydrological connectivity is lost. In that case, Fill & Spill models have lower soil conductivity than the Continuous Transmissivity models, and thus generate less subsurface flow and slower recessions. As a result, Fill & Spill models' results match observed runoff rates better during recession periods than the Continuous Transmissivity models (Figure

1.5).

However, runoff rates from Continuous Transmissivity models respond more sensitively to any additional small precipitation events during the recession period than runoff rates from Fill & Spill models. For example, around 2005-01-29 and 2005-03-05, Continuous Transmissivity models reproduce the small responses to precipitation events, while Fill & Spill models do not (Figure 1.5). Because of the threshold mechanism in Fill & Spill models, the small precipitation fails to meet the threshold and trigger the runoff generating mechanism. In contrast, a study in a humid system using Fill & Spill found that responses to small events were over-predicted [12], These results suggest that there are threshold runoff production conditions that are missed by the current implementation of the Fill & Spill approach.

1.6.3 Parameter Distributions

The patterns revealed by cumulative frequency curves (Figure 1.8) reflect the differences in subsurface flow generating mechanisms. The cumulative frequency curve for parameter m shows that 'hourly' models and Fill & Spill models prefer the hydraulic conductivity to be decreasing more sharply with an increasing saturation deficit. The hourly time steps and 'Fill and Spill' models tend to generate more flow following precipitation events than the 'daily' or Continuous Transmissivity models. Hourly models may infiltrate more water into the soil during larger storms and consequently generate more subsurface flow following storms rather than overland flow during the storm. The 'Fill and Spill' model maintain greater flow immediately following a storm while the *Saturation Deficit Threshold* is not reached. The 'daily' and Continuous Transmissivity models may require a lower m (slower decay of hydraulic conductivity with depth) to maintain a similar volume of subsurface flows following a storm event, as the satura-

tion deficit begins to decrease. In other words, the lower values of m selected for in the 'daily' or Continuous Transmissivity models be compensating for the more non-linear episodic/threshold behavior that can be captured by 'hourly' or Fill & Spill models respectively. Substantial differences in behavioral parameter selection between models in general suggest that calibrated parameter values may be compensating for limitations in process representations [44]. The inclusion of additional information (hourly precipitations) in the 'hourly' model suggests that it is the more realistic representation. For the Fill & Spill versus Continuous Transmissivity the choice is less clear but the improved recession flows as discussed above may suggest that Fill & Spill is more realistic and that the differences in behavior parameters for the Continuous Transmissivity approach are partially a compensation for a poorer conceptual model.

While the cumulative frequency curves for $gw1$, (not shown) which determines the amount of bypass flow to deep groundwater stores, shows no obvious differences in sensitivity between the four models, the cumulative frequency curves for parameter $gw2$ shows that 'daily' models require a faster drainage rate of the deeper groundwater stores (Figure 1.8). As described above, this may reflect difference in process representations between the models. If the 'hourly' model produces greater infiltration during storm events and consequently greater post-storm subsurface flows than the 'daily' model, the calibrated $gw2$ parameter in the 'daily' models may be larger to compensate and produce more flow during this post-storm period. Models with Fill & Spill implementation favor faster groundwater drainage relative to the Continuous Transmissivity approach. In the Fill & Spill model, deep groundwater drainages will generally contributes to greater proportion of streamflow in the low flow period because subsurface flow is very small once the saturation deficit falls below *Saturation Deficit Threshold*. To match with the observed discharge rate, models with Fill & Spill implementations will select relatively higher groundwater drainage rates $gw2$ compared with the Continuous Transmissivity

model. As noted above, these parameter selection differences point to the importance of differences in process representations that are partially masked by parameter calibration.

While other studies indicate that the spatial heterogeneities of threshold-related soil parameters may have some influences in explaining the performance of Fill & Spill model [40, 6], our results indicate that the hydrological performance is not substantially sensitive to the spatial heterogeneities in our model. This finding may result from the lack of a correct spatial distribution of soil properties; deducing the parameters range of the saturation deficit threshold from NDVI is not sufficiently accurate. The range of value assigned to different soil types determined by the NDVI quantile may not effectively represent real spatial characteristics of the soil.

1.6.4 Spatial moisture distribution

The spatial difference in soil moisture distribution across the implementations vary for different meteorological and antecedent moisture conditions (Figures 1.10, 1.11, 1.12). The most substantial difference in spatial moisture distribution occurs during the recession period (Figure 1.11). During the transition periods between wetting up and drying down (recession period), spatial soil moisture redistribution depends mainly on non-local factors such as upslope contributing areas and hillslope hydrological connectivity [45, 15]. In models, these factors are reflected by soil parameters and model structures. In order to generate the observed hydrograph, calibrated parameters in the Fill & Spill models tends to lead to higher drainage at the beginning of the recession and during the peak period, resulting in more rapid drainage and lower water tables in the uphill areas than Continuous Transmissivity models and greater recharge of riparian areas. As the system continues to dry, spatial patterns of soil moisture for Fill & Spill and Continuous Transmissivity model converge (Figure 1.10).

During the storm event, the difference in spatial moisture distribution is less substantial than the recession period. During storm events soil moisture redistribution depends more on the lateral water movement that is controlled by subsurface flow generating mechanism rather than local factors (such as ET). During wet periods, more patches are hydrologically connected in both Fill & Spill and Continuous Transmissivity approaches. Following initial period of wet up, the soil in many patches is closer to saturation and show less spatial variance regardless of which method is used for lateral routing. As a result, the differences between the two models on soil moisture during storms is sensitive to the storm intensity.

The low flow period has the least differences in spatial moisture distribution between the four model implementations. During the low flow period, most patches in the watersheds are dry and hydrologically disconnected. The soil moisture distribution depends mainly on local factors such as ET [45] rather than the lateral water movements. While Fill & Spill and Continuous Transmissivity models are directly controlling the lateral flow but not ET, they may not directly bring substantial changes to the distribution of soil moisture during the low flow period.

Although soil moisture patterns generated two approaches are similar during the wettest and driest periods, spatial differences in soil moisture during the recession period may have important implications for ecological processes. In semi-arid area, soil moisture is often the controlling factor for ecological structures and patterns. Because the Fill & Spill models maintain greater differences in soil moisture distributions between upland and riparian areas during recession periods, it may have long-term implications for vegetation patterns in these water-limited environments. Previous studies have pointed out that the riparian zone in semi-arid areas has more biodiversity than upland and the water availability during growing season is the major factor controlling the ecological patterns in semi-arid area [46, 47]. However, this long-term effect on ecosystem and its feedbacks

to hydrological processes is beyond the scope of this paper.

Ideally, observed spatial soil moisture data should be collected, converted to numbers using metrics comparable for model outputs, and the model performance evaluated to validate the soil spatial moisture distribution. However, there is no soil spatial moisture data with appropriate resolution in the study area and the comparisons are only aimed to illustrate the differences resulting from model implementations. Incorporating remote sensing products of spatially variable soil moisture into the model evaluation in much larger watershed may be a logical next step.

1.7 Summary and Conclusion

Subsurface flow has been recognized as the dominant hydrological path as well as an important control for the hydrological connectivity of hillslope in steep terrains. In this paper, the Fill & Spill hypothesis for the subsurface flow was implemented in an eco-hydrological model RHESSys and implications explored in a mountains semi-arid watershed. Unlike other studies that incorporate percolation theory and explicitly create a stochastic pipeline network for subsurface preferential flow [10, 11], we integrated the preferential flow by adjusting the soil conductivity profile with an abrupt increase at the threshold of soil saturation deficit level.

Results show that when the streamflow has been aggregated to daily timesteps, the simulated streamflow and spatial soil moisture patterns have small difference between 'hourly' models and 'daily' models. Different sub-model representations of the subsurface flow show substantial differences in calibrated parameters and in estimated hydrographs. In general, Fill & Spill seems to better capture the streamflow recession characteristics of the study watershed. It is both the semi-arid climate and the geology condition that leads to this recession characteristics. The heterogeneity, fractured and uplifted bedrock likely

leads to a discontinuous set of depressions and small aquifers that are only connected to the stream under in frequent events. The Fill & Spill models also produce higher peak flows, but the high sensitivity of peak flows in semi-arid regions to errors in input precipitation data precludes determining which approach is more realistic. The threshold behavior of the Fill & Spill approaches leads to greater spatial soil moisture differences between upland and riparian zones during recession periods relative to the Continuous Transmissivity models. Difference in soil moisture patterns during this dry period may have important implications for ecological processes such as vegetation growth and the soil biogeochemical cycling.

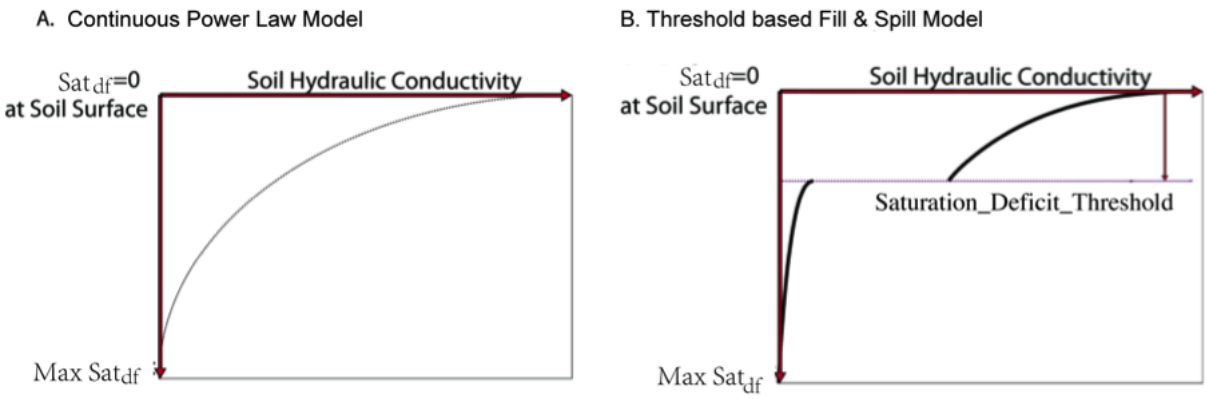

Figure 1.1: Hydraulic conductivity against soil sat deficit for the Continuous Transmissivity model (left) and Fill & Spill model (right). The y-axis is downward in both plots. Sat_{df} is the saturation deficit. Max_Sat_{df} is the maximum saturation deficit. *Saturation Deficit Threshold* is the threshold above which preferential flow will emerge.

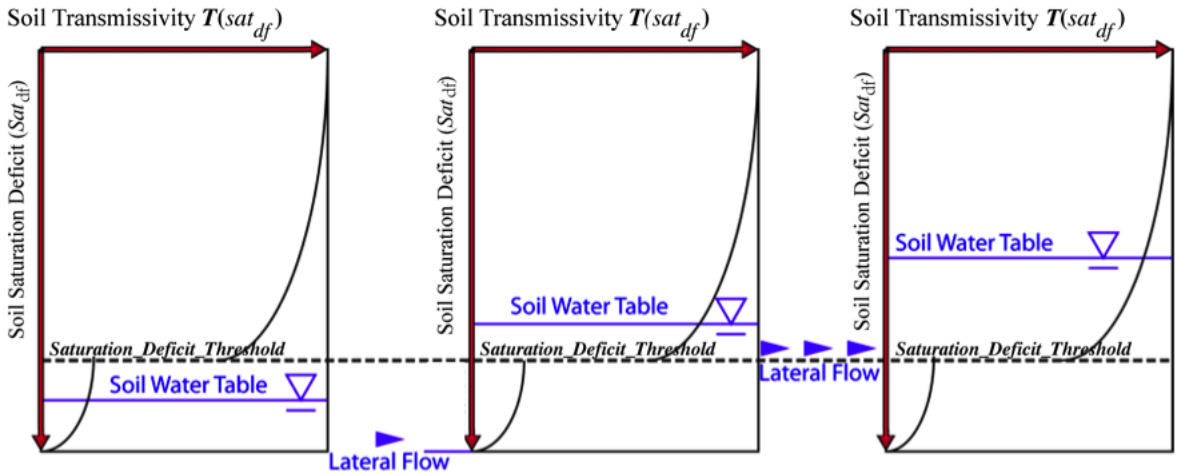

Figure 1.2: The implementation of Fill & Spill model in patch level. When saturation deficit (Sat_{df}) fall below the threshold (*Saturation Deficit Threshold*), a limited amount of subsurface flow will be generated (original K times *Leakage*). Once saturation deficit (Sat_df) rises above the threshold (*Saturation Deficit Threshold*), a significant amount of subsurface flow will be generated (original K times *Spillover*) representing the abrupt increase in soil hydraulic conductivity due to the emergence of the preferential flow. The y-axis is downward plotted.

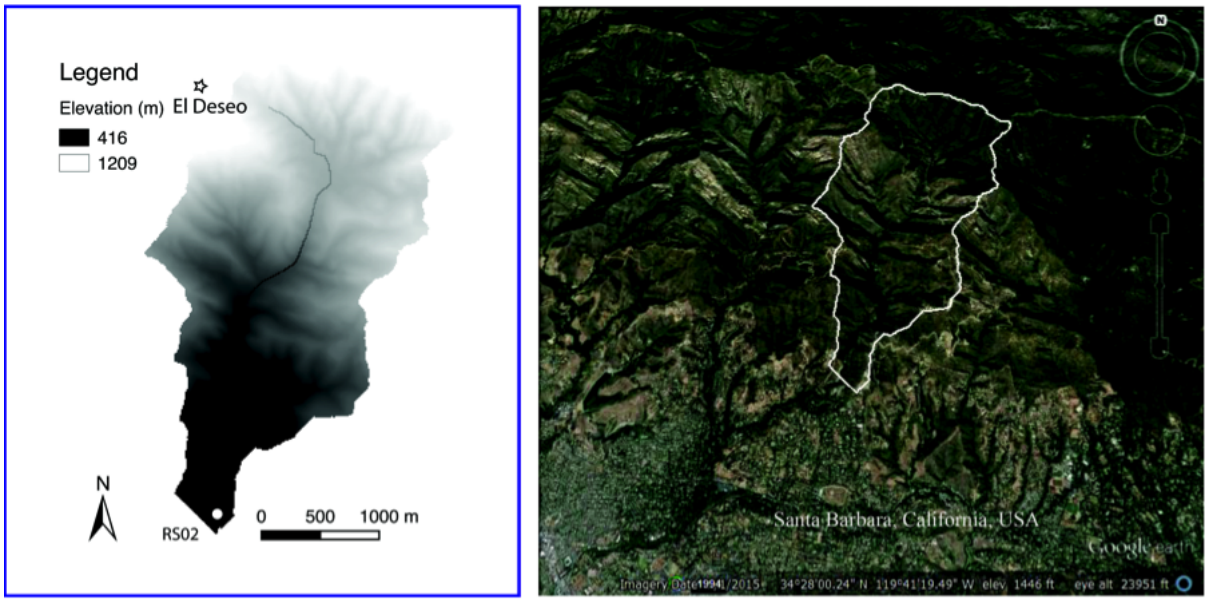

Figure 1.3: Map for Rattlesnake Creek Watershed. 'El Deseo' is the meterologic station used for climate input and 'RS02' provides streamflow data. (Image Source: 'Rattlesnake.' Google Earth. 34°28′24″N and 119°41′19.49″W. May 1, 2015. Nov 20, 2015.)

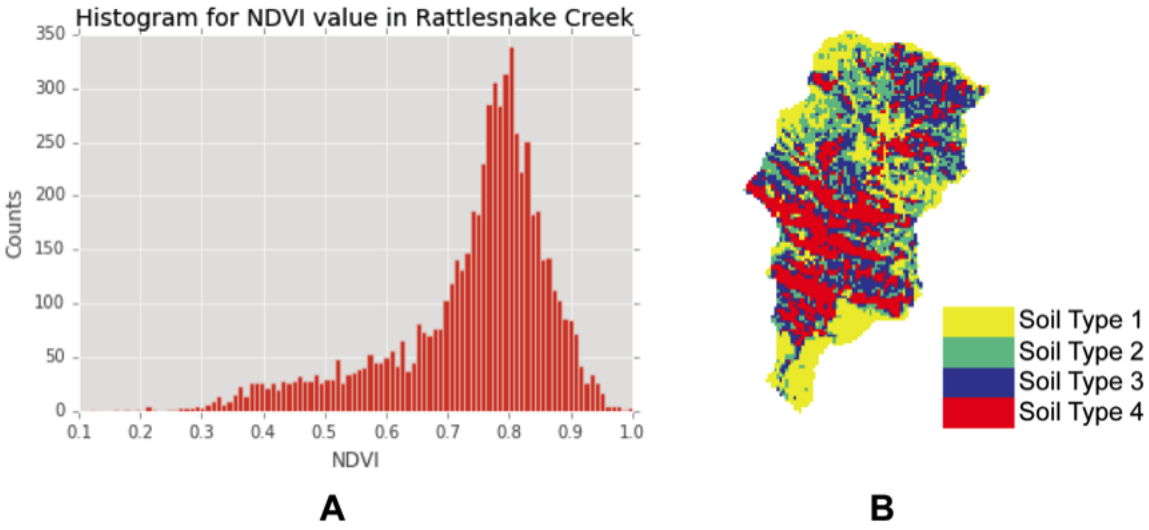

Figure 1.4: Soil types in Rattlesnake watershed are classified into four types according to the NDVI image. A: the histogram for the NDVI image. The 25%, 50%, 75% quantile of NDVI (0.69, 0.77, 0.82) are used to classify the four soil types. Soil type 1 has lowest *Saturation Deficit Threshold* value range. Soil type 4 has the highest *Saturation Deficit Threshold* value range.

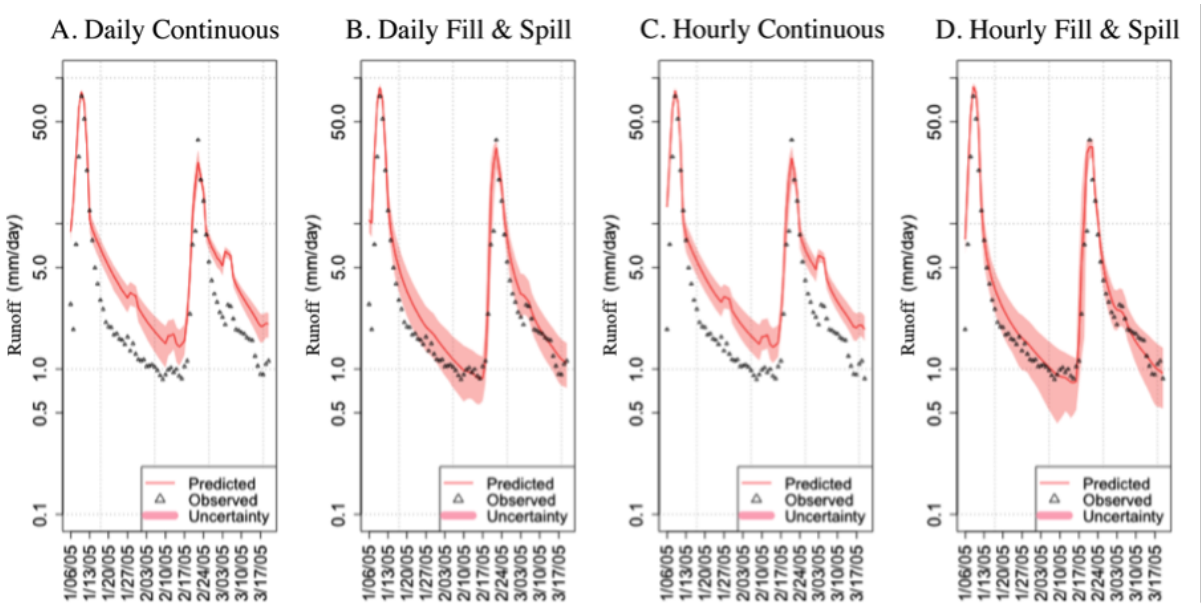

Figure 1.5: Comparisons of model performance during storm and recession periods. Triangles represent observed runoff rates while the solid red line and red shadow represent the weight average runoff rate and the uncertainty bounds, respectively, as calculated by the GLUE method.

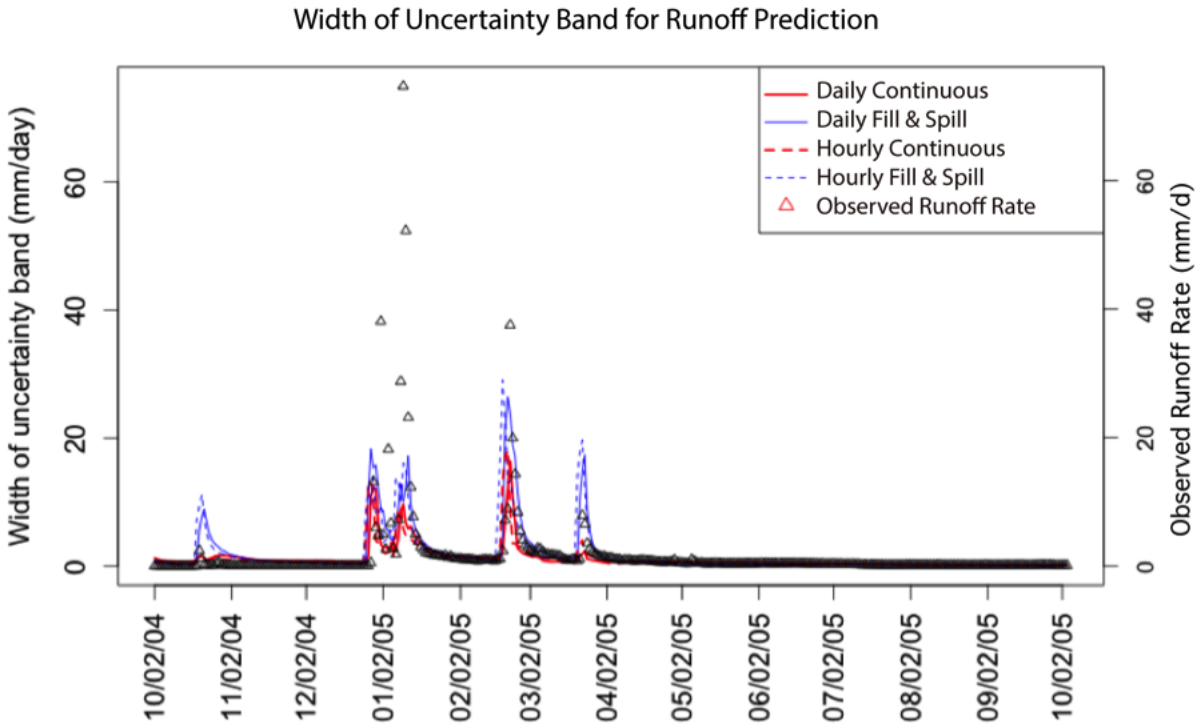

Figure 1.6: Width of the uncertainty bands during the calibration period.

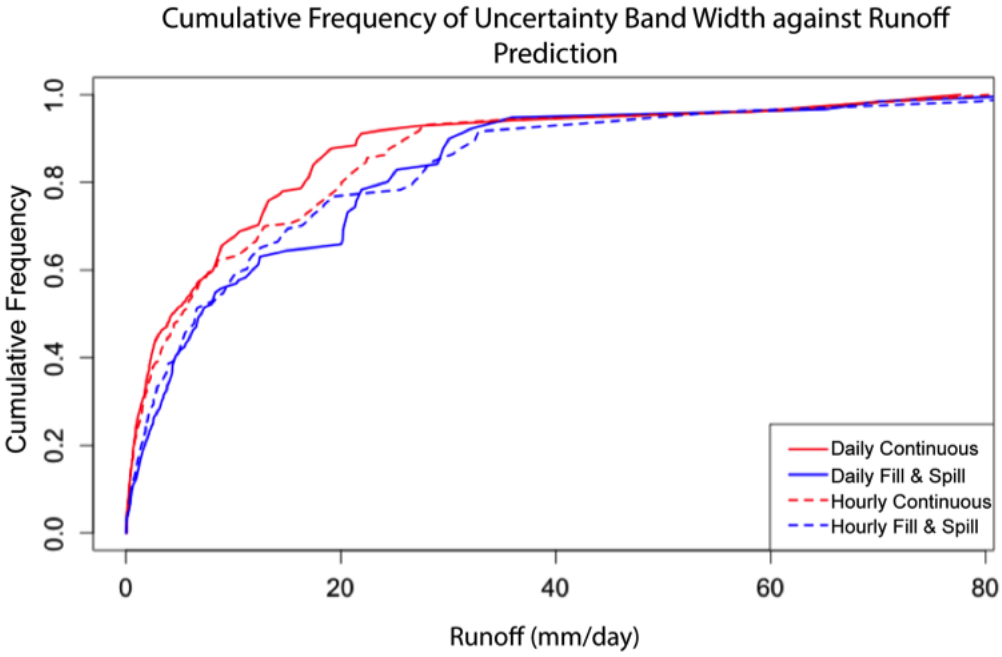

Figure 1.7: Cumulative frequency of uncertainty bandwidth against runoff.

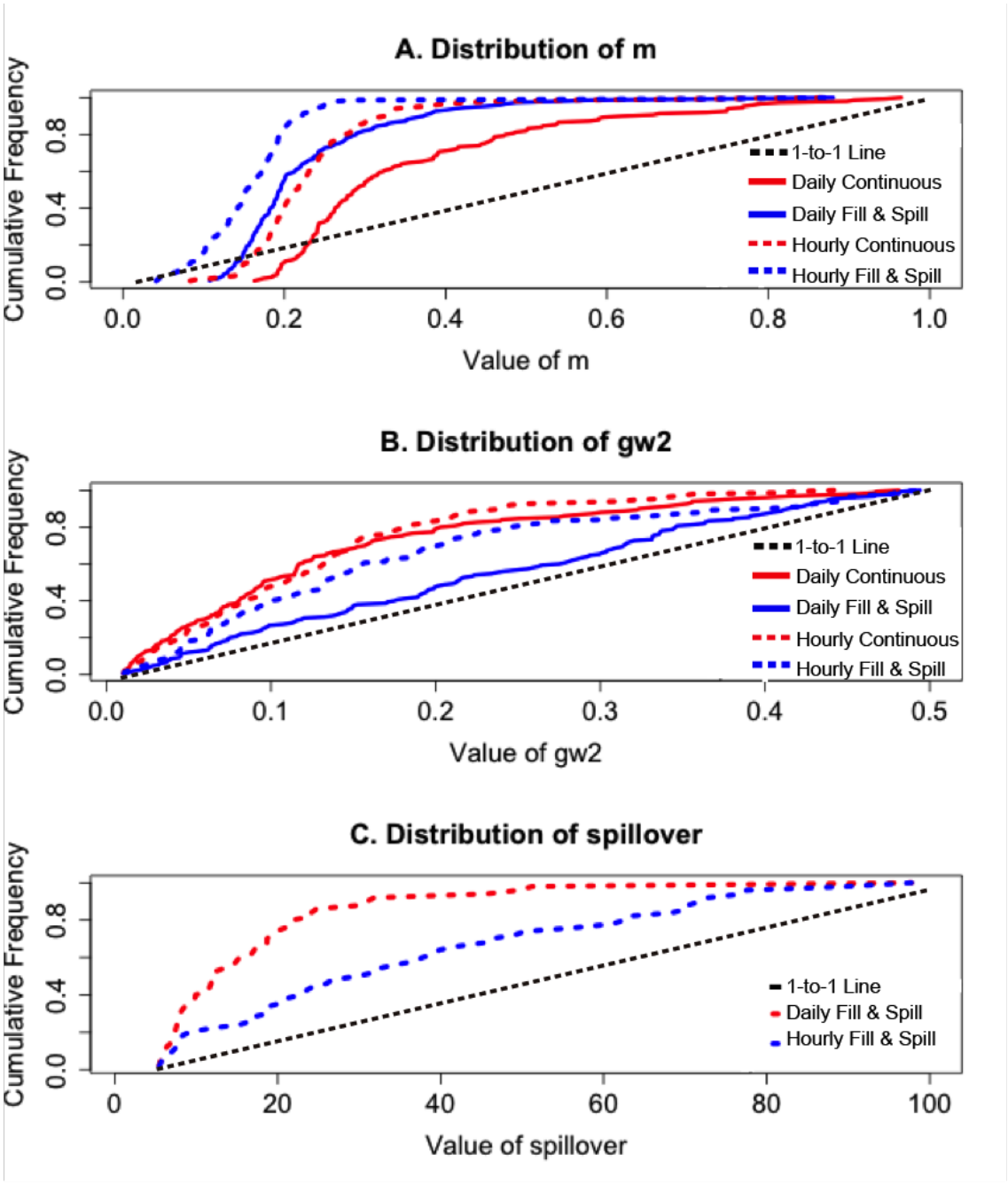

Figure 1.8: Cumulative frequency distribution for model parameters.

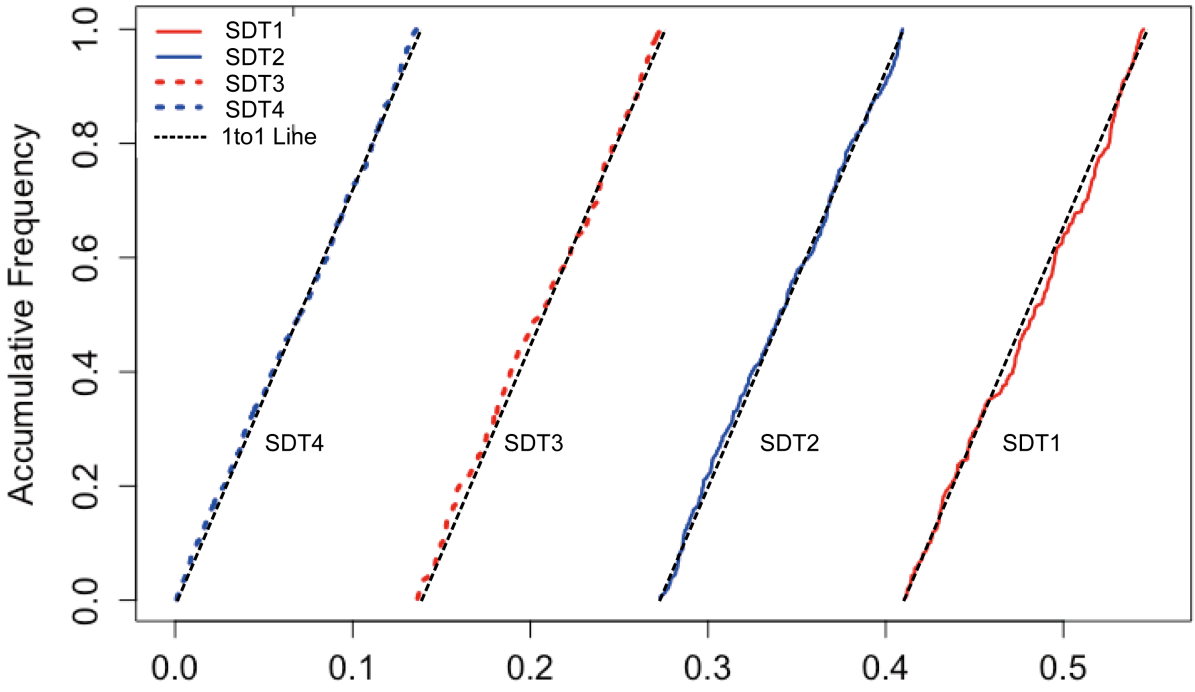

Figure 1.9: Cumulative frequency distribution for *Saturation Deficit Threshold* with spatial heterogeneity. The solid red curve, the soil blue curve are the cumulative frequency plot for *Saturation Deficit Threshold* of soil type 1 and soil type 2 (SDT1, SDT2). The dash red curve and the dash blue one are cumulative frequency plots for *Saturation Deficit Threshold* of soil type 3, 4 (SDT3, SDT4)..

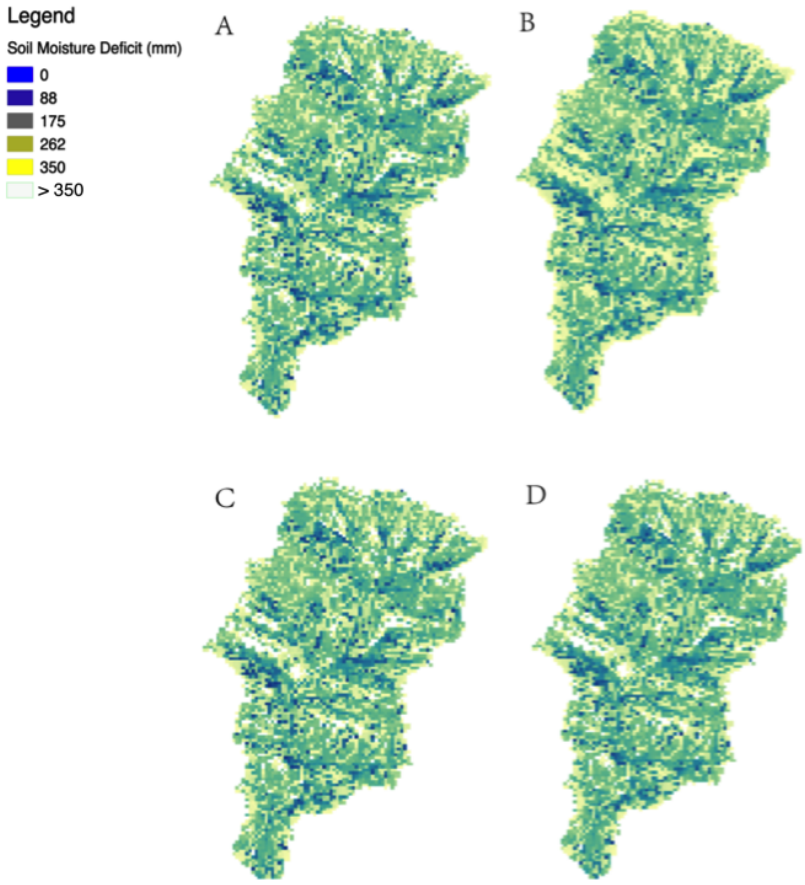

Figure 1.10: Spatial distribution of soil moisture before significant precipitation (precipitation > 5mm/day) at 12:00 am, Dec 2, 2004. 'daily Continuous Model' (A), 'daily Fill & Spill Model' (B), 'hourly Continuous Model' (C) and 'hourly Fill & Spill Model' (D)

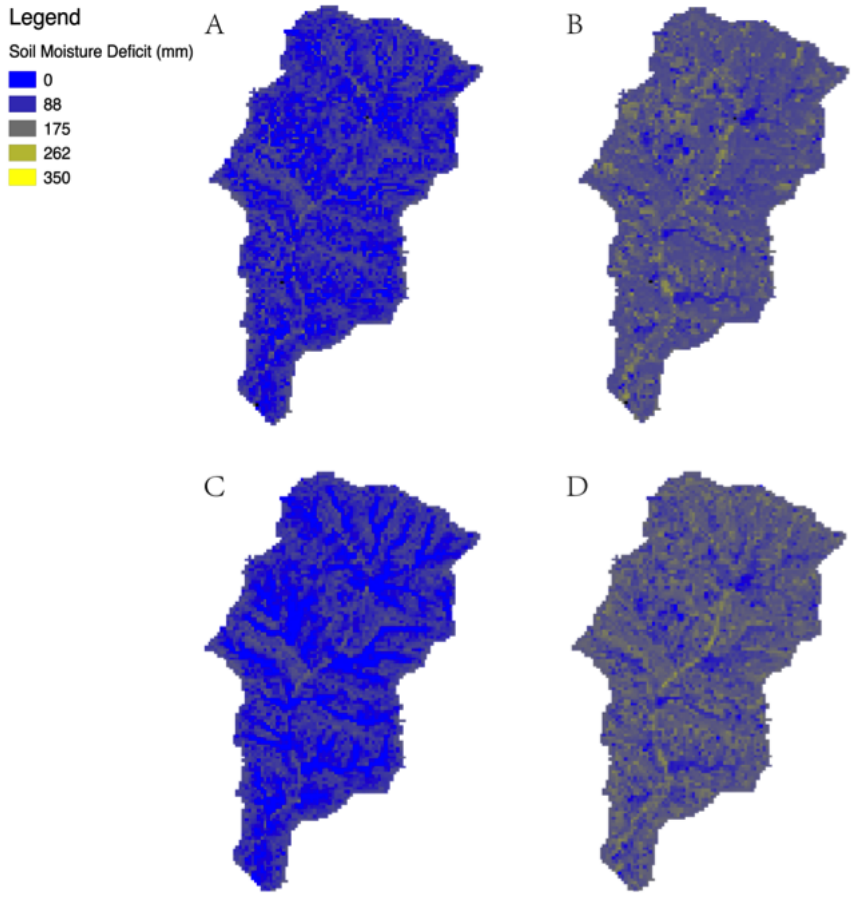

Figure 1.11: Spatial distribution of soil moisture during the recession at 12:00 am, Jan 27, 2005. 'daily Continuous Model' (A), 'daily Fill & Spill Model' (B), 'hourly Continuous Model' (C) and 'hourly Fill & Spill Model' (D)

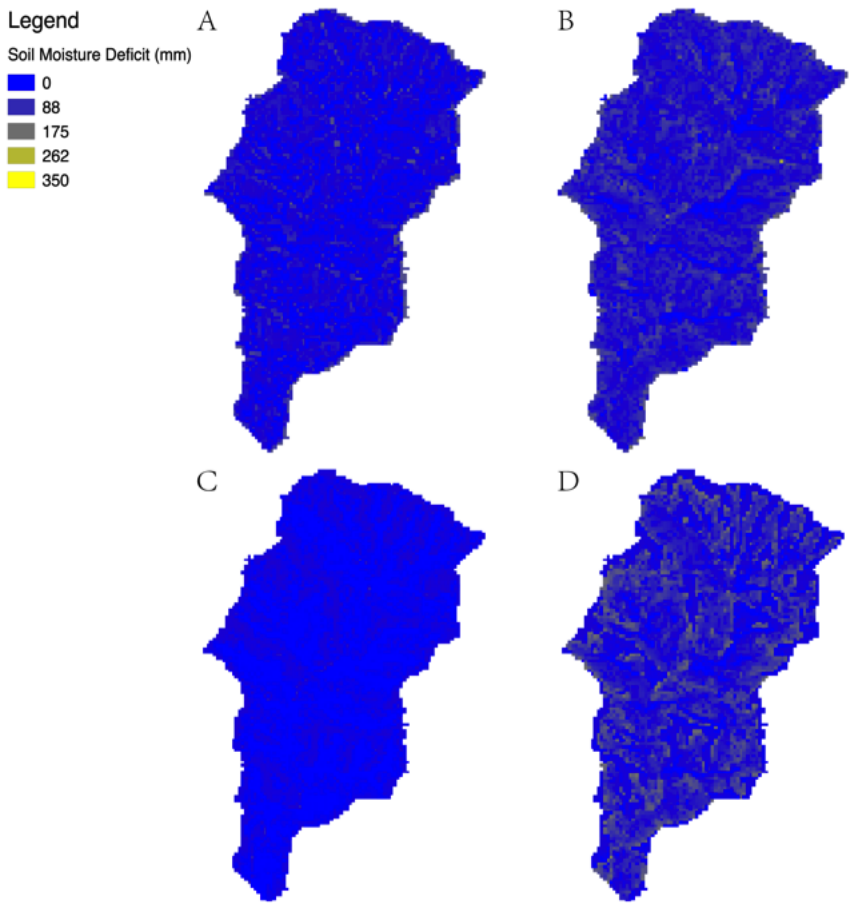

Figure 1.12: Spatial distribution of soil moisture during the storm period at 12:00 am, Jan 28, 2008. 'daily Continuous Model' (A), 'daily Fill & Spill Model' (B), 'hourly Continuous Model' (C) and 'hourly Fill & Spill Model' (D)

Table 1.1: Range of Parameters for Model Calibration

	M	$Ksat_0$ (mm/day)	sd(m)	$Gw1$	$Gw2$	$Spillove$	$Leakage$	Saturation Deficit Threshold
Min	0.01	40	0.1	0.01	0.01	5	0.1	0.1
Max	1	5000	3	0.5	0.5	100	0.4	0.4

Table 1.2: Range of value for *Saturation Deficit Threshold* (SDT) for different soil types. SDT1 to SDT4 represent the *Saturation Deficit Threshold* (SDT) of soil type 1 to 4, respectively. Soil type 1 represents soil in the upland, and soil type 4 represents soil in the riparian area.

	Soil Type 1	Soil Type 2	Soil Type 3	Soil Type 4
Range of $Saturation\_Deficit\_Threhold$ (SDT)	[0.41, 0.54]	[0.27, 0.41]	[0.14, 0.27]	[0, 0.14]

Table 1.3: Model performance during calibration period. The 'F&S' means Fill & Spill model. 'Continuous' is the continuous transmissivity model.

Timestep	Daily		Hourly	
Model Implementation	Continuous	$F\&S$	Continuous	$F\&S$
Highest NSE	0.8	0.64	0.81	0.67
Highest $NSE_{recession1}$	0.81	0.99	0.86	0.99
Highest $NSE_{recession2}$	0.95	0.99	0.92	0.99
Top 150 $Obj_{NSE_{all}}$	0.6 3$\sim$ 0.79	0.55 $\sim$ 0.84	0.54 $\sim$ 0.82	0.55 $\sim$ 0.82

Table 1.4: Model performance during validation period. 'Continuous' is the continuous transmissivity model. 'F & S' is the Fill & Spill model.

		Daily		Hourly	
Model Implementations		Continuous	F&S	Continuous	F&S
Highest NSE		0.63	0.51	0.74	0.62
2003/3/18 - 2003/3/28	Highest NSE	0.92	0.99	0.82	0.98
	80% quantile	-1.8	-7.3	-1.5	-3.7
2005/1/13 - 2005/2/5	Highest NSE	0.89	0.99	0.86	0.99
	80% quantile	0.83	0.94	0.80	0.92
2005/2/23 - 2005/3/10	Highest NSE	0.94	0.93	0.92	0.99
	80% quantile	0.72	0.62	0.90	0.96
2006/4/6 - 2006/4/20	Highest NSE	0.64	0.96	0.71	0.96
	80% quantile	-0.72	0.11	0.63	0.78
2008/1/6 - 2008/1/17	Highest NSE	0.28	0.95	0.59	0.95
	80% quantile	0.36	-0.27	-2.0	-0.66
2008/2/1 - 2008/2/12	Highest NSE	0.99	0.99	0.95	0.99
	80% quantile	0.65	0.94	0.89	0.95
Top 150 $Obj_{NSE_{all}}$		$0.48 \sim 0.63$	$0.24 \sim 0.51$	$0.60 \sim 0.74$	$0.38 \sim 0.62$

Table 1.5: Percentage of saturated area during sample events for different model settings. 'Continuous' is the continuous transmissivity model. 'F & S' is the Fill & Spill model.

Saturated Area(%)	Daily		Hourly	
	Continuous	$F\&S$	Continuous	$F\&S$
Low Flow (2004/12/02)	0.0	0.0	0.0	0.0
Recession (2005/1/27)	$6.7 \sim 8$	$0.02 \sim 0.1$	$6.6 \sim 8.2$	$0.02 \sim 0.1$
Storm (2008/1/28)	$5.5 \sim 20.5$	$0.1 \sim 12$	$6.2 \sim 18$	$0.1 \sim 3.2$

Chapter 2

Sensitivity of Nitrate Concentration-Discharge Patterns to Soil Nitrate Distribution and Drainage Properties in the Vertical Dimension

2.1 Introduction

Nitrate loss from subsurface soil to streams is an important nitrate-exporting path and has several impacts on the terrestrial and coastal ecosystems, such as reducing nitrate availability for terrestrial plants, increasing nutrient downstream fluxes and possibly triggering eutrophication [48, 49, 50]. Due to drought in summer and episodic rainfall in winter and early spring, most nitrate is exported during wet seasons in semi-arid regions, such as southern California [51, 52, 53]. In order to estimate the subsurface

nitrate losses from land to streams, it is important to understand the dominant controls on nitrate-export and how they vary with climate, land cover/land use and disturbance [51, 54].

Previous studies have developed several hypotheses that link nitrate-export to the interaction between flow paths and nitrate sources. 'Concentration-Discharge' relationships are often studied as clues to understand these controlling factors [55, 56]. The 'Nitrate Flushing' hypothesis has been proposed to explain nitrate concentration peaks during storm events [57, 58]. When soil saturation deficit (i.e., the difference between soil porosity and soil water storage) is high, this hypothesis assumes nitrates accumulate in the upper layer of the soil. As soil saturation deficit decreases, nitrates in saturated subsurface layers will be washed way from upper layers soil to streams [59]. Further development of the 'Flushing Hypothesis' shows how topographic properties and their influences on variable source area would regulate the 'Nitrate Flushing' mechanism and concentration-discharge relationship [60, 61, 62]. Creed & Band (1998a) emphasize that the rate of expansion of the variable source area, not the total variable source area, regulates the export of nitrates. Other processes or factors including macropore flow [63], shallow groundwater linkage [64], hillslope hydrologic connectivity [65] and antecedent soil moisture conditions [66] also contribute to the regulation of nitrate export.

Most of these studies have focused on hydrologic linkages in the horizontal direction. Only a few studies look into the vertical dimension and these studies indicate that soil vertical stratigraphy regulates hydrologic flow paths and water quality dynamics in semi-arid soil [67]. However, due to substantial uncertainties and lack of details for the semi-arid soils, the implications of the vertical nitrate distribution and drainage profiles on nitrate transport have not been extensively examined.

When interpreting enrichment or dilution patterns in the 'Concentration-Discharge' relationship, most studies indicate that it is the connection with additional nitrate source,

after a sufficiently long period of disconnection, that brings high nitrate concentration flow downstream [68, 51]. However, nitrate concentration is the combined result of nitrate-outflux and water-outflow from a given location, and a more complete explanation may require simultaneously considering both characteristics that determine nitrate-outflux and water-outflow at different levels of local saturation deficit. In this paper, we consider how discharge and nitrate-export interact over a vertical profile and how that interaction may be influenced by the vertical distribution of nitrate and hydraulic conductivity.

In semi-arid regions, nitrate mass distribution and hydraulic conductivity decrease with increasing soil depth. During the periods between rainfall events, that are likely to flush nitrate, nitrate accumulates in the upper layer because organic material inputs and decomposition rates are higher in near surface layers [51, 32, 53]. Soil saturated-hydraulic-conductivity typically decays with depth due to soil structural characteristics such as pore-size distribution and is commonly represented with an exponential declining function [69, 3, 70]. As a result, the distributions of both soil nitrate and soil hydraulic conductivity are biased towards the upper soil layer. When the water table increases, it reaches the upper soil layer with more nitrate and higher hydraulic conductivity, which means it can release more nitrate and produce higher volumes of water. During this process, the change of nitrate concentrations in released water with declining saturation deficit (or high water tables) is determined by the change in soil nitrate flux and the change in water flux as the water table rises. This scenario offers a new conceptual model that posits how the vertical distribution of nitrate in soil interacts with the vertical distribution of hydraulic-conductivity, to influence the pattern of concentration-runoff relationships. In this paper, we will explore this conceptual model and how different configurations of soil hydraulic-conductivity and soil vertical nitrate distribution determine concentration-discharge relationships. We will answer the following questions:

1. How do different configurations of the proposed model (e.g different combinations of vertical nitrate distribution and hydraulic conductivity distribution) lead to different Concentration-Discharge patterns at a patch scale in a semi-arid climate? The patch scale represents an average condition where there is no lateral replenishment of water and nitrate flux from upslope areas.

2. Will the different configurations of the proposed model change the Concentration-Discharge relationship at the watershed scale, where the lateral replenishment between the upland and the downstream patches can also influence nitrate-export?

2.2 Study Sites and Data

2.2.1 Study Sites

The undeveloped headwater catchment, Rattlesnake Creek, is the study area for this paper. Rattlesnake Creek watershed is located on the southern facing slopes of the coastal Santa Ynez Mountains. It covers 5.8 km^2 area, with three dominated shrub species: *Ceanothus megacarpus* (big pod ceanothus), *Adenostoma fasciculatum* (chamise) and *Arctostaphylos spp.* (Manzanita) [32]. Steep slopes (slopes $> 20°$) and sandy soil (sandy loams) are the characteristics of the Rattlesnake Creek watershed. In this semi-arid Mediterranean climate, the rainy season lasts from October to April. Large storm events, which last for only a few days, contribute to a substantial portion of the annual precipitation (30%∼60%) [36]. From 2000 to 2009, the mean annual precipitation is 645 mm/year, with remarkable inter annual variance (>360 mm/year). The year-round average temperature is 18 $°C$, with a maximum of 23 $°C$ and a minimum of 13 $°C$. Shrubs re-sprout and herbaceous species establish after rain, greening up the watershed from winter to late spring. The biomass of vegetation reaches its peak in June [32].

Shrubs re-sprout and herbaceous species establish after rain, greening up the watershed from winter to late spring. The mean biomass of vegetation reaches its peak in June [71].

2.2.2 Data

The observed climate and discharge data come from the Santa Barbara Channel Long Term Ecological Research (SBC LTER). Both the stream discharge data and the stream chemistry data are from the gauge station 'RS02' (Longitude: -119.6922, Latitude: 34.4576), which is located at the outlet of Rattlesnake watershed. The stream hydrologic record was collected as hourly stage values, then converted to discharge using a rating curve with stream channel cross-sections and roughness estimated by the HEC-RAS model [37]. The stream chemistry records are collected weekly during non-storm flows in winter, and bi-weekly during summer. During the winter storms, stream chemistry samples are collected hourly on rising limbs and at 2-4 hour intervals on falling limbs. The stream nitrate is measured as 'nitrite + nitrate' in micro-moles per liter [72], then converted to micro-gram per liter in this paper. The precipitation was collected in the gauge 'El Deseo' (Longitude: -119.6958, Lattitude: 34.4917) with a tipping bucket gauge and reported in 5 minutes' interval [36] (Figure 2.1). The observed data from 2004-10-01 to 2005-10-07 is used for this study.

In an analysis of these nitrate measurements, Goodridge and Melack (2012) found that the Concentration-Discharge relationship in Rattlesnake watershed shows an enrichment pattern for storm events. In their paper, Goodridge and Melack (2012) provide an explanation based on catchment connectivity and suggest that during storm events, more nitrate sources in upland may be connected and more nitrates are flushed to downstream, resulting in the enrichment pattern [51]. We will provide a model-based analysis that examines how vertical properties described by our conceptual model contribute to

this explanation of the observed concentration-discharge pattern. We configure an eco-hydrologic model, RHESSys (Regional hydro-ecosystem simulation system), to reproduce the enrichment pattern, and discuss the general implications of the soil vertical nitrate distribution and the hydraulic conductivity distribution on the Concentration-Discharge relationship.

2.3 Methods

2.3.1 Concepts Review

Saturated Hydraulic Conductivity

Soil hydraulic conductivity describes the rate with which water can move through soil and deeper saprolite layers. Hydraulic conductivity depends on factors like the soil properties and the degree of saturation. Saturated hydraulic conductivity is the hydraulic conductivity when soil layer is saturated. Note that in this paper we focus on hydrologic soil that may include both organic and mineral soil layers as well as underlying saprolite and fractured bedrock. We use the term 'soil' since most of the activity occurs in upper layers that are traditional defined as soil but our conceptual framework does not preclude the flux of water or nitrate through deeper layers. We do not define an explicit soil depth, but rather relay on the exponential decay of saturated conductivity with depth to define an 'effective' soil depth at which low hydraulic conductivity values result in negligible lateral flux. In order to model lateral flux we divide the soil into discrete 1000 layers/meter) and the total lateral flux is the summation of lateral flux for each layer.

Soil Water Outflow Rate

Soil water outflow rate is calculated as the integration of hydraulic conductivity over soil layers below the current water table. A rising water table will lead to an increase of

soil water outflow rate and an increase of runoff.

Soil Nitrate Distribution in Vertical Dimension

In semi-arid area, nitrates accumulate on surface during the dry summer and initial wet up process due to the nitrification and the establishments of micro scale water linkage between microbial sites and substrates needed for nitrification [51, 32, 53]. As a result, we assume more nitrates in the upper soil layers. Moreover, we assume this nitrate mass distribution is static over time. That is, although the total mass of nitrate in soil column will change, the nitrate mass distribution in vertical dimension will not change.

Total Soil Nitrate Flux in Vertical Dimension

Nitrate is weakly retained by soil matrix. In our conceptual model, nitrate within the water table can be transported by saturated subsurface flow; we assume no patch-scale lateral transport of nitrate through flux in unsaturated soil. Nitrate outflux from a patch is proportional to the soil nitrate mass within the soil layer where saturated later flux occurs. The total soil nitrate flux is calculated as the integration of the nitrate-outflux for each soil layer below the soil water table.

Nitrate Concentration in Soil Releasing Water

Nitrate concentration is calculated as

$$Concentration = \frac{\text{Total Nitrate Outflux}}{\text{Soil Water Outflow}} \tag{2.1}$$

Nitrate concentration is dynamic in model simulations and is determined by both *Total Nitrate Outflux* and *Soil Water Outflow*. Since the vertical distribution of nitrate mass and hydraulic conductivity control *Total Nitrate Flux* and *Soil Water Outflow*, these two parameters also influence the nitrate concentration in the releasing water.

2.3.2 Vertical Profile Controls on the Concentration-Discharge Relationship at the Patch Scale: A Simple Demonstration

In Figure 2.2 we present a hypothetical illustration of a case where soil nitrate distribution increases faster than the hydraulic conductivity distribution as the water table rises (or saturation deficit decreases). These soil nitrate and soil hydrological parameter setting results in an enrichment pattern in the Concentration-Discharge relationship (subplot 2.2 F).

Following this same approach, in Figure 2.3, we create a scenario to explain a dilution pattern. The key difference between Figure 2.2 and Figure 2.3 is the nitrate mass distribution in subplot 2.2 A and 2.3 A. In Figure 2.3, although the nitrate mass still increases in upper soil layers, it is more evenly distributed (Figure 2.3 A). Water flux, controlled by the distribution of hydraulic conductivity with depth, is the same as in Figure 2.2. The difference in vertical nitrate distribution between subplot 2.2 C and subplot 2.3 C is relatively small. However, with a rising water table or increasing discharge/runoff, the nitrate concentration in this scenario shows a dilution pattern (as opposed to an enrichment pattern that occurred with a slightly more uneven vertical distribution of nitrate) (Figure 2.3 F vs Figure 2.2 F).

The uneven nitrate distribution in Figure 2.2 can be transformed into the more even distribution in Figure 2.3 under certain conditions. For example, after long drought, nitrate will accumulate on top layer, resulting in a more uneven N distribution more like Figure 2.2. After sequences of strong precipitations, the nitrate from top layer will infiltrate into deeper soil layers, resulting in a nitrate distribution more like Figure 2.3. However, in this study, we focus on longer-term-controls on vertical nitrogen distribution related to soil structure that do not change with time.

2.3.3 Vertical Profile Controls on the Concentration-Discharge Relationship at the Watershed Scale

At the watershed scale, sources of nitrate include lateral inputs from upslope patches with replenishment of soil nitrate in receiving patches during the storm events.

Figure 2.4 shows an example of consequence of the lateral nitrate replenishment: at the watershed scale, lateral flow combines with vertical nitrate distribution and hydraulic conductivity to regulate the Concentration-Discharge relationship. Without the lateral nitrate replenishment, the Concentration-Discharges relationship would show a dilution pattern. However, with additional nitrate replenishment from upslope area, the Concentration-Discharge relationship would be shifted from dilution to enrichment. If this patch is a riparian patch, then the resulting nitrate export will influence the Concentration-Discharge relationship of the stream.

2.3.4 Assumptions of the Conceptual Model

In the conceptual model, we emphasize the importance of soil vertical nitrate distribution and its interactions with lateral subsurface flow, based on three assumptions:

1. Lateral nitrate export exists only in the saturated layer.
2. Soil vertical nitrate mass distribution is proportional to the lateral nitrate out flux distribution at each soil layer.
3. Although the total nitrate mass in soil column may change, the soil vertical nitrate mass distribution is static.

The first and second assumptions can be written as:

$$NO3_{flux}(d) = \frac{\partial NO3(d)}{\partial t} = Sat\_d \times NO3(d) \tag{2.2}$$

Where $NO3\_flux(d)$ is the lateral nitrate out flux from soil layer at depth d, $NO3(d)$ is the nitrate mass from soil layer at the depth d, Sat_d is a dummy variable representing whether this layer is saturated or not. If soil layer at depth d is not saturated, then Sat_d is 0. Otherwise, it is a none-zero constant. Using this assumption, the distribution of nitrate flux at each soil layer is deduced from the distribution of nitrate mass, and the total nitrate flux is calculated by the summation of nitrate flux from each soil layer under current water table.

These assumptions are the simplified settings comparing with the definition of nitrate flux in existing transportation models, such as SOIL & WATER ASSESSMENT TOOL (SWAT) [73] and Integrated Nitrogen in Catchments model (INCA) [74], where the lateral nitrate exports in unsaturated layer are calculated and Sat_d is a continuous function of both water content and soil porosity. However, in our conceptual model, lateral nitrate export in saturated layer alone is enough to demonstrate the conceptual model. Future studies can explore the results of considering lateral nitrate exports in both saturated and unsaturated layers.

The third assumption assumes that the shape of nitrate mass distribution with depth does not vary with time. In other words, even though the total nitrate mass in soil column changes, how it is distributed with depth does not change. This assumption follows the nitrate-flushing hypothesis [59, 23]. Field investigation also suggests that the infiltrating water may moves through unsaturated layer via macropore, without significant contact with soil matrix [75, 76]. As a result, this simplification may be reasonable.

2.3.5 RHESSys Model Description

In our conceptual model, illustrated by the example above, we suggest that nitrate concentration pattern is sensitive to the soil vertical distribution of nitrate and

soil drainage properties. To assess how these controls influence nitrate Concentration-Discharge relationships for a more realistic situation where water and nitrate evolve dynamically, we configure vertical nitrate distribution and hydraulic conductivity in the Regional Hydro-Ecologic Simulation system (RHESSys) and test the sensitivity of the concentration-discharge relationship to these different configurations. RHESSys is a physical process-based, distributed hydrological model, which has been widely implemented in a variety of bioclimatic regions, including in semi-arid regions [27, 28, 29]. RHESSys explicitly models the catchment connectivity by calculating the volume of water exported from upland to downstream via lateral movement through adjacent patches [23]. The soil profile is represented in three layers: a root zone, an unsaturated layer, and a saturated zone. The modified version of Green and Amt approximation is used to calculate the 1-D vertical infiltration process. The water held in saturated and unsaturated layer will be updated following the infiltration process. The traditional 'Continuous Exponential' transmissivity model [3] for subsurface flow sub-model is used to calculate the subsurface lateral flow, where both the subsurface conductivity and transmissivity decays exponentially with the soil saturation deficit:

$$K(sat_{df}) = Ksat_0 \times e^{(-sat_{df} \times K_{decay})} \tag{2.3}$$

$$T(sat_{df}) = \int_{max\_satdf}^{sat_{df}} K(sat_{df}) \tag{2.4}$$

$K(sat_{df})$ is the hydraulic conductivity when the soil saturation deficit equals to sat_{df}, max_sat_{df} is the maximum of saturation deficit, $Ksat_0$ is the saturated hydraulic conductivity at surface soil, $T(sat_{df})$ is the transmissivity when the soil saturation deficit equals to sat_{df}, and K_{decay} is the coefficient controlling the decreasing rate of transmissivity

against the soil saturation deficit. For the lateral flow, more than one receiving patches in the downslope get the lateral flow from the upland area.

Evaporation and transpiration including evaporation of rain intercepted by each canopy layer, and transpiration of vascular layers, are calculated using Penman Monteith approach [31] in a daily timestep. Soil evaporation is calculated based on energy and atmospheric drivers as well as a maximum exfiltration rate. The maximum exfiltration rate is determined by soil parameters and soil moisture. Potential capillary rise is constrained by soil parameters and the water table. For each day, half of the potential capillary rise is allocated to the unsaturated zone at the start of the day to account for the subdaily plant responses, left the other half at the end of the day to meet the plant transpiration needs.

RHESSys calculates biogeochemical cycling similar to those in BIOME-BGC [77]. Photosynthesis and respiration process are included in the carbon and nitrogen cycling in a daily timestep [23]. In RHESSys, carbon and nitrogen stores are partitioned into leaves, roots, stems, and coarse roots. Both live and dead wood components in stem and coarse-root stores are considered to account for the differences in respiration and C:N ratios. Vegetation nitrogen stores and carbon stores are linked following the stoichiometric relationships. N-cycling processes such as nitrification and denitrification are modeled following the $CENTURY_{NGAS}$ approach [78]. Decomposition is based on litter and soil pools, which are determined by organic material and microbial biomass. Potential nitrification rates are calculated following the approach by Parton et al.(1996), and the actual nitrification rate is determined by soil moisture, carbon substrate availability, soil temperature and soil ammonia. Only mineralized soil nitrogen is used for nitrification. Denitrification is determined by maximum denitrification rate, soil moisture and soil respiration. In the soil column, the vertical distribution of nitrate is assumed to follow an

exponential distribution.

$$N(depth) = Coeff_1 \times N_{all} \times e^{(-N\_decay \times depth)} \times N\_decay \tag{2.5}$$

$$\int_{Max_d}^{depth} N(depth) = Coeff_1 \times N_{all} \times (e^{-N\_decay \times depth} - e^{-N\_decay \times Max_d}) \tag{2.6}$$

Where, $depth$ is the soil depth, Max_d is the max soil depth, $N(depth)$ is the nitrate mass of the patch in the soil layer at depth = $depth$. $Coeff_1$=$\frac{1}{1-e^{(-N\_decay \times Max_d)}}$ is the coefficients for $N(depth)$ calculation. N_{all} is the total amount of nitrate in that patch, and N_decay controls the vertical decay rate of the nitrate distribution. A high N_decay corresponds to more unevenly distributed nitrate in soil, with most of the nitrate gathering in top layers, and a lower N_decay corresponds to a less unevenly distributed situation. The integration of $N(depth)$ from Max_d to $depth$, which can be interpreted as the total nitrate flux below soil depth = $depth$, also follows the exponential distribution.

2.3.6 Simulations and Analysis

RHESSys model was used to show the sensitivity of the Concentration-Discharge patterns to the vertical distribution of nitrate and soil drainage parameter. A constant decay rate for soil hydraulic conductivity (K_decay) was used from preliminary streamflow calibration. By varying the vertical soil nitrate distribution parameter N_decay, we assess the impact of nitrate vertical distribution on nitrate Concentration-Discharge pattern in stream. A range of saturated soil hydraulic conductivity ($Ksat$) was implemented to vary the relationship between water flux and nitrate flux and evaluate the effects on nitrate concentration. All of the simulations were run on both the patch scale and watershed scale.

1. Simulations for different pairs of N_decay and $Ksat$ on single patch scale. RHESSys model was implemented using Rattlesnake watershed as a case study. Simulations were based on observed meteorological data from 2004-10-01 to 2005-10-07. For the patch scale simulations, the whole watershed is treated as a single patch, and assigned a set of spatially averaged soil & vegetation parameters. In this lumped case there is no lateral subsurface flow within the watershed. 336 different pairs of N_decay and $Ksat$ are tested, with 21 values between [2, 6] for N_decay and 16 values between [1, 1200] (m/day) for $Ksat$ (2.1). The lowest value of N_decay corresponds to the more even nitrate distribution in the vertical dimension. The highest value of N_decay refers to the vertical nitrate distribution where nitrate is most preferentially distributed near to the surface.

2. Simulations with RHESSys model at the watershed scale. RHESSys model were set up with approximately 2,000 patches using DEM map with 30-meter resolution from SBC LTER database [36]. Lateral subsurface replenishment is included in this scenario. Based on preliminary simulation results, the parameter sensitivity of N_decay on stream nitrate concentration varies under different spatial scale. As a result, a wider range of N_decay than that from the patch scale simulations is used in the watershed scale simulation. Together with the hydraulic conductivity, 336 parameter sets are tested (2.1), with observed input data from 2004-10-01 to 2005-10-07. Parameters were assumed to be homogeneous throughout the watershed.

2.4 Results

2.4.1 RHESSys Modeling on Single Patch Scale

By varying N_decay and $Ksat$, 336 scenarios were simulated using RHESSys model. Figure 2.5 compares the results for several examples with $Ksat$=4, 30, 190, 1200 m/day and $N\_decay = 2$ (evenly distributed) and 6 (concentrated near surface layers).

When $N\_decay = 2$ (blue circles, relatively evenly distributed nitrate), the nitrate concentration-discharge patterns show a flat or a weak dilution pattern across a wide range of $Ksat$ values. In contrast, when nitrate is preferentially located near to the surface ($N\_decay = 6$ red circle), the nitrate concentration tends to show enrichment patterns. This is consistent with our simple illustrative model where more evenly distributed soil nitrate tends to produce a dilution pattern (Figure 2.2) and scenarios where nitrate is concentrated nearer to the surface produces an enrichment pattern. The higher N_decay (red circle) scenario leading to enrichment is more sensitive to changing $Ksat$ than the dilution pattern associated with a lower N_decay (blue circle). When N_decay is high, for lower values of $Ksat$, enrichment tends to plateau at higher runoff levels. For higher $Ksat$ values, however, we continue to see enrichment even for very high runoff levels. When N_decay is high, concentrations tend to be lower for lower $Ksat$'s across most runoff values.

To show how 'Concentration-Discharge' patterns vary across a wider range of N_decay and $Ksat$ values, we calculated the regression slope in the 'Concentration-Discharge' plots for storm flow to show the overall trend of the concentration patterns. We define the storm flow as any runoff larger than 97.5% of the runoff of water year 2005 (1.3 mm/hour). Then, we computed the regression slope as the average rate of change in Concentration-Discharge between 97.5th percentile and 100th percentile runoff and then plotted this average slope of Concentration-Discharge plots for N_decay and $Ksat$ from

the 336 simulations (Figure 2.6).

Both N_decay and hydraulic conductivity $Ksat$ control average slopes of the concentration discharge relationship during storm flow (Figure 2.6). Similar to results from the simple illustrative example in Figure 2.2, higher N_decay scenarios (yellow & red) generally result in a steeper slope, corresponding to a stronger enrichment pattern. Lower N_decay cases (blue & black) result in a flat or negative slope, representing a stable or weak dilution pattern. Hydraulic conductivity $Ksat$ also affects the average slope. With the increase of hydraulic conductivity, the average slope of enrichment curve in high N_decay cases (red) increases, and the average slope in low N_decay cases (blue & black) is low. However, there is a threshold conductivity value (500 m/d) at which the slope of enrichment curve of high N_decay case (red) reaches its maximum and then declines. This is because soil with higher hydraulic conductivity drains water faster than soil with lower hydraulic conductivity. With higher soil hydraulic conductivity, it is more difficult for subsurface flow to reach top layer, export the nitrate from the surface soil layer, and harder to produce the stronger enrichment pattern. As a result, while exceeding the conductivity threshold, the slope of enrichment curve will decline.

2.4.2 Simulations with RHESSys Model in Watershed Scale

We will first examine results for several illustrative scenarios at the watershed scale (Figure 2.7 a, 2.7 b, 2.7 c), and then show summary metrics for simulations across all values of N_decay and $Ksat$ (Figure 2.8 a & 2.8 b). Since these are at the watershed scale, subsurface lateral flow need to move from upland to riparian zone through series of adjacent patches, resulting in a different pattern and magnitude of responses to precipitation than that in patch scale (Figure 2.5). To better show the patterns of Concentration-Discharge relationships, we plot the x-axis in log-plot and use the regres-

sion line to represent the general trend of Concentration-Discharge relationship. We also include Concentration-Discharge relationships derived from observed measurements for comparison.

Figure 2.7 a is the result from $N\_decay = 0.1$ and $Ksat = 8$ m/day. The modeled Concentration-Discharge plot (black circles) show a 2-stage pattern: an enrichment for runoff < 0.07 mm/hour, then a dilution for runoff > 0.07 mm/hour, with the 'transition point' at peak concentration with Runoff $= 0.07$ mm/hour. The observed Concentration-Discharge also shows a 2-stage patterns, however, its transition period comes at runoff $= 0.2$ mm/hour, which is greater than the simulated transition runoff value. In order to evaluate the impact of parameters on the Concentration-Discharge relationship, two regression lines are plotted to represent the average slope for the enrichment stage and dilution stage. The sensitivity of these slopes to parameter values are presented in figures 8a and 8b and discussed in more detail below. To help explain modeled watershed scale patterns, we use 'Percent Saturated Area' (green dots), which defines the percent of the watershed where the water table is at the surface. Percent Saturated Area shows a 3-stage pattern with transitions when runoff reaches 0.005 mm/hour and again at 0.07 mm/hour. During the 'dry period'- between runoff from 0.0001 mm/hour to 0.005 mm/hour - the water table is below the surface for the entire watershed (0% saturated area). Then, during the initial wetting up following precipitation, patches near stream become saturated and the saturated area expands with more precipitation. As runoff increases from 0.005 mm/hour to 0.07 mm/hour, the percent saturated area increases from 0 to 41% (transition period). After the transition period, it goes into the 'plateau' stage. At this stage, the percent saturated area stays at 41% but the runoff increases from 0.07 mm/hour to over 7 mm/hour, indicating that fast flowpath such as macropore flow or overland flow are contributing to the increase in runoff. In Figure 2.7 a, at the x-axis (runoff), this 'plateau' stage also corresponds to a 'transition point' where the

Concentration-Discharge shifts from enrichment to dilution (black circles).

Figure 2.7 b shows the saturated area and Concentration-Discharge relationship for N_decay =0.1 and $Ksat$ = 1200 m/day. While the overall pattern is similar to that for N_decay =0.1 and $Ksat$ = 8 m/day (Figure 2.7 a), the transition point, between enrichment and dilution, occurs at higher runoff values, from 0.07 mm/hour to 0.2 mm/hour. The lowest nitrate concentration also increases from 0.04 mg/l to 0.1 mg/l. As a result, the slope of regression line of the 'enrichment stage' is flatter in Figure 2.7 b than in Figure 2.7 a. Increases in saturated area occur at higher runoff values, such that initiation of the 'rising' stage in 'Percent Saturated Area' shifts from 0.005 mm/hour to 0.01 mm/hour. The starting runoff value for the 'plateau' stage shifts from 0.07 mm/hour to 0.2 mm/hour. However, the transition period of 'Percent saturated Area' still overlap with the transition period of Concentration-Discharge relationship.

The overlap of the transition periods in Figure 2.7 a & 2.7 b indicates that there may be a shared reason for the transition to the 'plateau' in 'Percentage Saturated Area' plot and to the 'dilution' in the Concentration-Discharge plot. As mentioned above, the 'plateau' stage for 'Percent saturated Area' reflects an increase in the importance of fast flow paths such as macropore flow or overland flow that result in an increase in runoff without an expansion in saturated area. In RHESSys, overland flow on saturated surfaces and flow through macropores, which drain water from ponding surface to groundwater and to streams, are the two fast flow paths. These fast flow paths may also contribute to dilution since water traveling through these pathways is unlikely to access additional nitrate once initial wash-off of surface nitrate from the deposition has been depleted earlier in the storm. As a result, although the fast flow paths can drain a substantial amount of water into streams, the lateral nitrate replenishment is limited. Thus as contributions from these flow paths increase, nitrate concentrations decrease.

Figure 2.7 c is the result with N_decay = 10 and $Ksat$ = 1200 m/day. The increase

of *N_decay* from 0.1 to 10 contributes to several differences between Figure 2.7 b and Figure 2.7 c: the most substantial change is that the lowest nitrate concentration is lower for the 'enrichment' stage (left of the transition point) in Figure 2.7 c. With higher *N_decay*, when the water table is low and lateral drainage only exports the nitrate from deeper soil, nitrate export is much less than that in low *N_decay* scenario (Figure 2.7 a). However, Figure 2.7 c is more close to the Concentration-Discharge pattern from the observed data than the other two scenarios.

To reveal the patterns in the Concentration-Discharge relationship in 'enrichment' and 'dilution' stages, regression lines are constructed and the slope of regression lines are calculated to compare the sensitivity of Concentration-Discharge relationship to the vertical soil nitrate distribution and soil drainage parameters.

Figure 2.8a summarizes the slopes of regression lines for 'Concentration-Discharge' relations in the enrichment stage. Red and yellow represents higher *N_decay* with more nitrates in upper soil layer, and blue & black represents lower *N_decay*, with soil nitrate more evenly distributed in the vertical dimension. Figure 8a indicates that higher *N_decay* will lead to steeper slope of the regression line, representing stronger enrichment. This is similar to results from our conceptual and numerical models for the patch scale.

Figure 2.8 b summarizes the slope of regression lines for 'Concentration-Discharge' relations during dilution stage. Although the slopes of unevenly distributed scenarios are higher (less negative) than that of evenly distributed scenarios, the difference is small (0.1) compared with the differences associated nitrate distribution in the enrichment stage in Figure 8a (0.8). The lower sensitivity to vertical nitrate distribution in the dilution stage occurs because once the dilution state has been reached, most of the nitrate has been exported (during the 'enrichment' stage) from the nitrate reservoir. Low total nitrate means that the soil nitrate distribution has a smaller impact on nitrate export.

Nevertheless, the slope is steeper and the variance of slope across N-decay gets widened with higher hydraulic conductivity, showing that under higher hydraulic conductivity, the more evenly distributed nitrate cases will result in the stronger dilution relationship. Higher hydraulic conductivity and more evenly distributed nitrate will exhaust the soil nitrate reservoir faster than cases with lower hydraulic conductivity and less evenly distributed nitrate. If soil nitrate is more evenly distributed, more nitrate is allocated to middle or lower soil layers than the less evenly distributed cases, and more nitrate in the lower layers will be exported to downstream with a rising water table. When water table reaches the top layer and creates saturated area in near-stream riparian zone ('dilution' stage in Figure 2.8 b), fewer nitrates will be left and the nitrate concentration will be lower in the more evenly distributed nitrate cases, resulting a stronger dilution relationship.

2.5 Discussion

This study focuses on the implications of the interactions between the soil nitrate and hydraulic properties on vertical distribution in both patch and watershed scale. Given the assumptions that both soil nitrate and hydraulic conductivity are higher on surface soil and lower in deeper soil, even a small difference in the rate of change in vertical soil nitrate distribution would result in substantially different concentration-discharge patterns. At the watershed scale, the subsurface lateral nitrate replenishment from upslope would be another factor that changes the concentration-discharge pattern.

2.5.1 Important Features of This Study

This paper extends previous analysis of nitrate concentration pattern [60, 61], by showing how interactions between the vertical distribution of soil nitrate and hydraulic

properties can give rise to both enrichment and dilution patterns.

Previous hypotheses or conceptual models (such as 'nitrate flushing' hypotheses) usually explain the enrichment pattern through the establishment of greater horizontal hydrologic connection with more nitrate sources, as water table rises and the spatial extent of saturated area increases [59, 60, 61]. Our analysis provides an explanation for nitrate concentration patterns focused on the vertical dimension, specifically the impact of soil nitrate vertical distribution on the nitrate concentration-discharge relationship. Nitrate flushing emphasizes that the saturated area contributes not only to the increase of water flow, but also to the chemical flux where the chemicals have accumulated near or at the surface [61]. Creed & Band (1998a) state that it is the rate of expansion of the variable source area, not the total variable source area, that regulates the export of NO3 [60]. Our findings are consistent with this nitrate flushing hypothesis but also indicate that the relative rate of change in soil nitrate distribution in the vertical dimension, together with the rate of change in how soil releases water across its vertical profile, controls the pattern in the nitrate concentration-discharge relationship.

By providing quantitative analysis of the sensitivity of the Concentration-Discharge relationship to parameters that control nitrate and water flux rates in the vertical dimension, we show that even a small change in the vertical soil nitrate distribution will result in substantial transition in patterns of the Concentration-Discharge relationship. For the semi-arid undeveloped watershed, with the nitrate concentrated at surface, the Concentration-Discharge relationship may show an enrichment pattern. However, in the humid area or irrigated cropland, soil nitrate may accumulate at deeper soil (>1.3 m) [79, 80], the enrichment pattern may be replaced by a dilution pattern.

2.5.2 Discussions on RHESSys Model Implementations

In the RHESSys model, an exponential function is used to represent the nitrate distribution. In semi-arid areas, nitrate accumulates on surface because of the nitrate dry deposition and suitable environments for microbial activity of mineralization and nitrification [51, 53]. An exponential distribution is likely to reflect the nitrate distribution in our semi-arid watershed. Other distributions including non-monotonic increasing/decreasing functions may also occur and could be considered in future research.

In Figure 2.7 a and 2.8 b, the 'dilution' stage in the watershed scale simulation results requires a fast increase in the volume of overland flow and insufficient lateral nitrate replenishment on surface. In semiarid area like Rattlesnake Creek watershed, the limitation on nitrate supply fits the requirement as the nitrate dry deposition is quite low (2 kg/ha/year) [71] and there is no substantial sediment flow during water year 2004-2005. However, this requirement may not be satisfied in some other situations. If with sufficient surface nitrate replenishment or nitrate supply provided by sediment flow, the 'dilution' stage on the right side of the transition period may change to an enrichment stage. For example, for area with high nitrate deposition or area after fire, there will be much more N available on the surface [81]. In that case, the 'dilution' stage in Figure 2.7 a, 2.7 b, 2.7 c may not exist.

2.6 Conclusion

In this study, we proposed a conceptual model, which uses vertical soil nitrate distribution and its interaction with soil hydraulic conductivity to quantitatively explain the nitrate concentration-discharge relationship in a semi-arid watershed. We showed that in Eco-Hydrologic model RHESSys, the resulting concentration-discharge relationship from model output is sensitive to the parameter governing soil vertical nitrate distribution

and soil hydraulic conductivity, in both patch scale and watershed scale. In patch scale, the uneven distribution of nitrate in vertical direction with majority portion of nitrate on surface soil tends to result in an enrichment pattern in the nitrate concentration-discharge relationship. The evenly distributed nitrate will produce a stable or a weak dilution pattern. In watershed scale, because of the lateral replenishment, the nitrate concentration-discharge relationship shows a 2-stage pattern (first enrichment, and then dilution) and a transition point. The hydraulic conductivity and soil vertical nitrate distribution controls the degree of enrichment or dilution on both stages, and the location of the transition point. It is the first study to explain the concentration-discharge relationship from the vertical dimension with quantitative analysis and emphasis on the importance of change in vertical distribution of soil nitrate and hydraulic properties. Future studies can explore the scenarios that vary the assumptions in the conceptual model, such as introducing heterogeneity in soil depth and varying the vertical nitrate distribution with infiltration water, or assess the impact of vegetation uptake and microbial activity on the nitrate concentration-discharge relationship in short term vs. long term.

Table 2.1: Parameter value range for model simulations in single patch scale and watershed scale

	N_decay rate for patch scale (unitless)	*N_decay* rate for watershed scale	`Hydro_Conductivity`
Min	2 (more evenly distributed)	0.1 (more evenly distributed)	1
Max	6 (more in upper layer)	10 (more in upper layer)	1,200

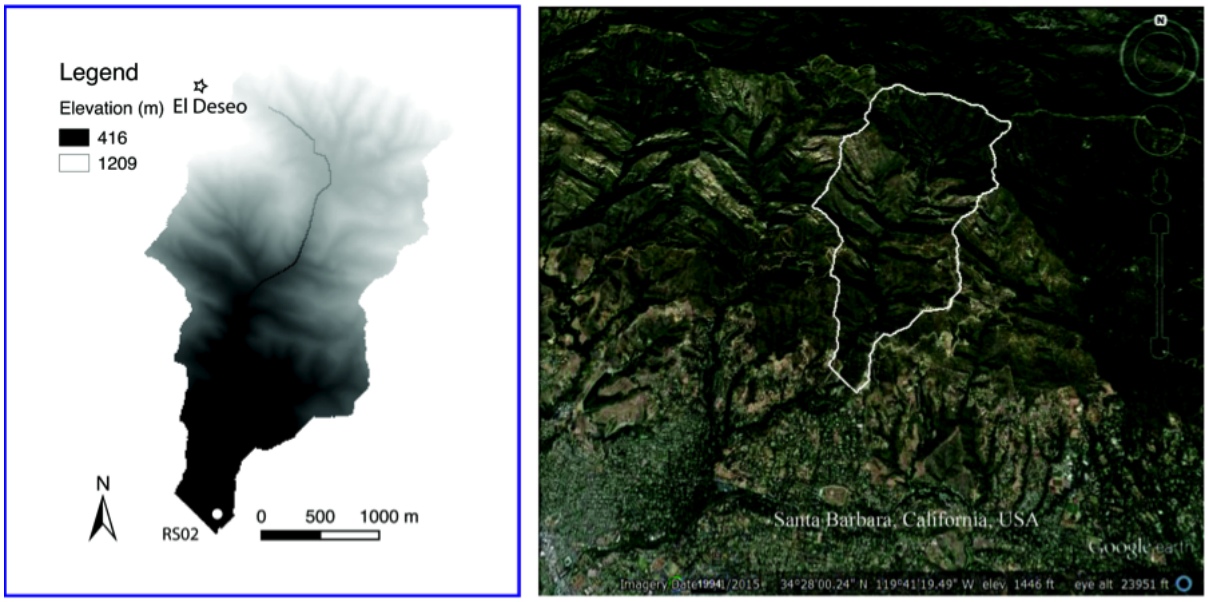

Figure 2.1: Map for Rattlesnake Creek. 'El Deseo' is the meteorological station used for climate input and 'RS02' provides streamflow data. ((Image Source: 'Rattlesnake.' Google Earth. 34°28′24″N and 119°41′19.49″W. May 1, 2015. Nov 20, 2015.)

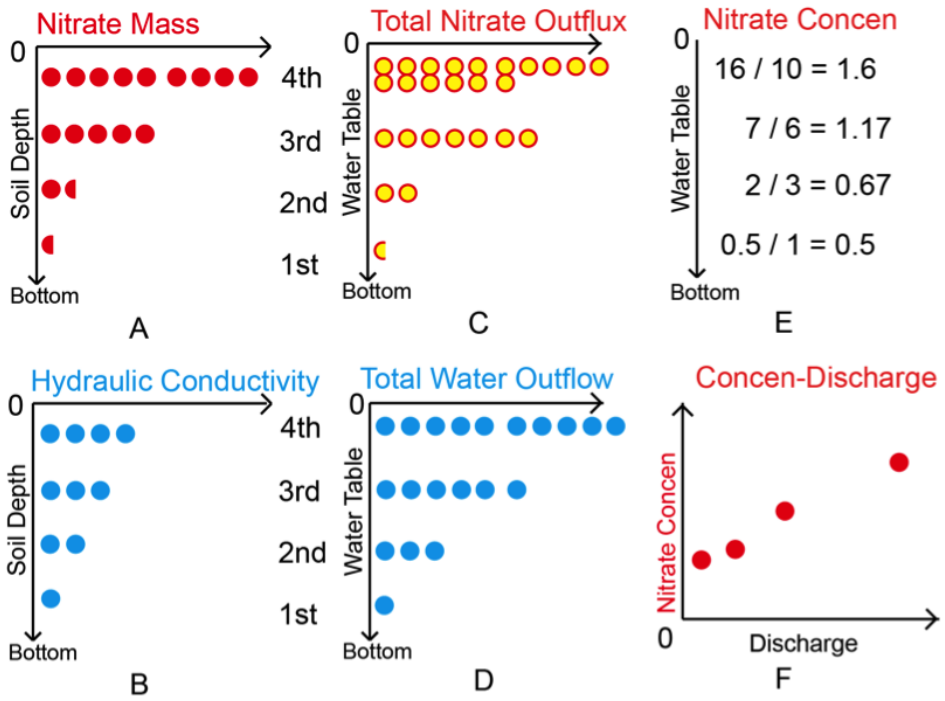

Figure 2.2: Consider a case where soil nitrate is distributed unevenly with soil depth (A), while hydraulic conductivity is less unevenly distributed (B). This scenarios results in an enrichment Concentration-Discharge pattern (F) as the water table rises from the 1st to 4th soil layer (nearer to the surface). Circles in subplot A, B, C, D, F represent: one unit of nitrate (A), one unit of hydraulic conductivity (B), one unit of total nitrate outflux (C), one unit of water outflow (D) and one unit of concentration (F). Subplots C and D are derived from subplots A and B by integrating water and nitrate flux from the corresponding soil layers. For example, the total nitrate outflux when water table reaches the 3rd soil level is the summations of nitrate fluxes for lower three layers, proportional to the nitrate mass distribution in these three layers, which is $0.5 + 1.5 + 5 = 7$. Following the same method, the total nitrate out flux when water table reaches the surface is: $0.5 + 1.5 + 5 + 9 = 16$ unit flux. The total water outflow when water table reaches the 3rd level is: $1 + 2 + 3 = 6$ unit water flow. When the water table reaches the surface, water flux is: $1 + 2 + 3 + 4 = 10$ unit water flow. Subplot E shows how the nitrate concentration at each water table level computed using the total nitrate outflux divided by total water outflow (Equation 2.1).

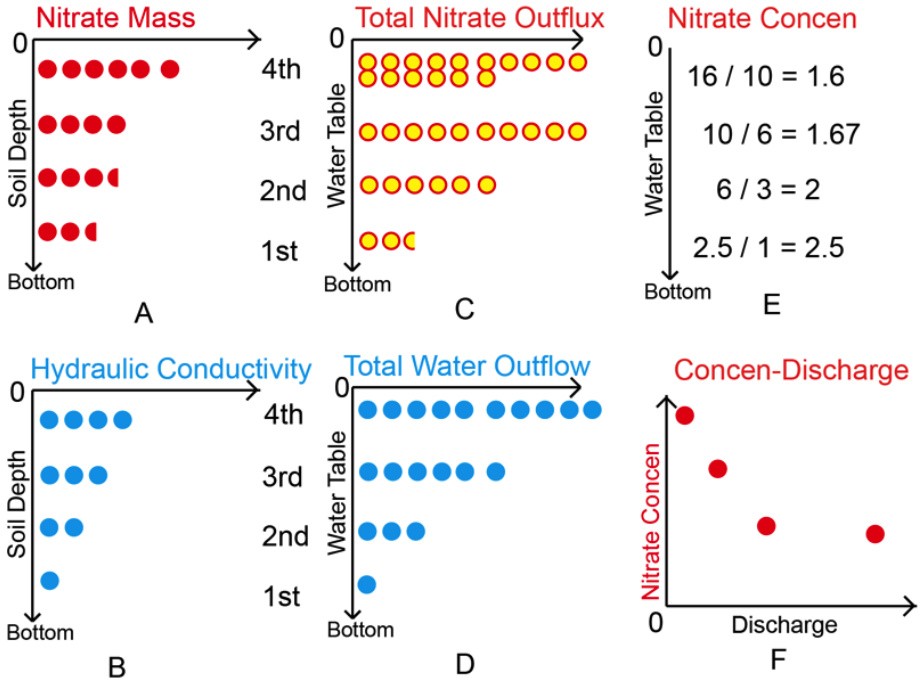

Figure 2.3: A scenario where nitrate is less unevenly distributed compared with Figure 2.2, resulting a dilution pattern. Circles in subplot A, B, C, D, F represent: one unit of nitrate (A), one unit of hydraulic conductivity (B), one unit of nitrate flux (C), one unit of water out flow (D) and one unit of concentration (F). Subplots C and D are derived from A and B by integrating water and nitrate flux from the corresponding soil layers. For example, total nitrate outflux when water table reaches top layer in subplot C is calculated as: $16 = 2.5 + 3.5 + 4 + 6$, the integration of all layers from subplot A. The water out flux when water table reaches top layer in subplot D is: $10 = 1 + 2 + 3 + 4$ unit water flow. Subplot E shows the nitrate concentration at each water table level computed using the total nitrate outflux divided by total water outflow

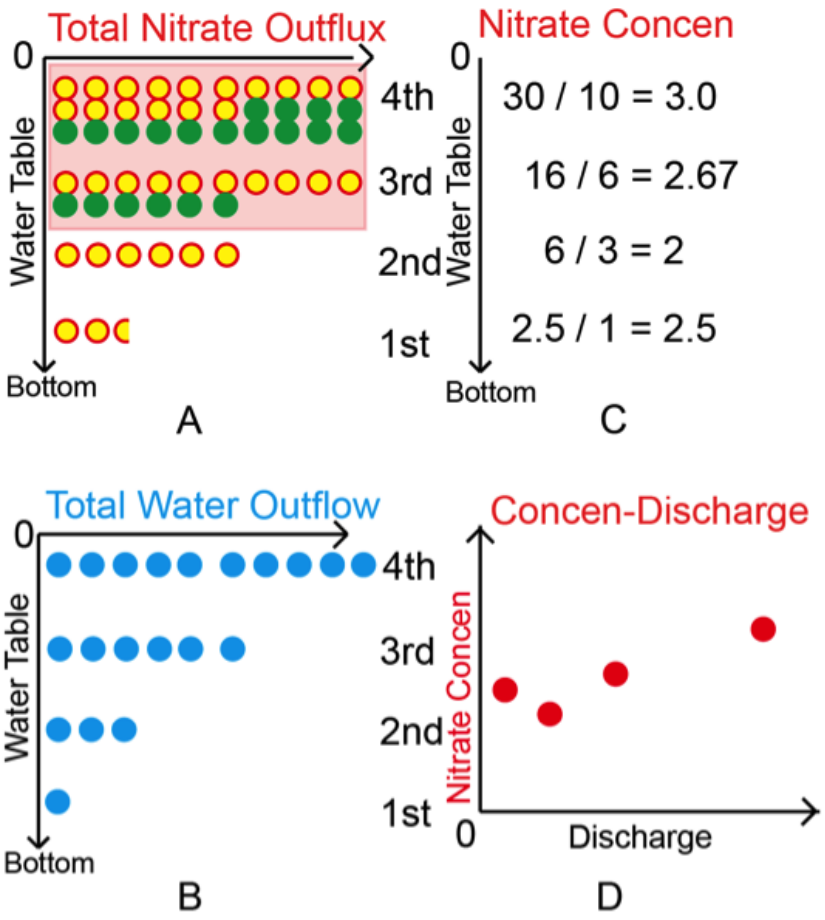

Figure 2.4: In watershed scale, the lateral nitrate replenishment will change the concentration-discharge relationship from dilution in Figure 2.3F to enrichment in Figure 2.4 D. The green points are results of lateral nitrate replenishments from upland. All the other labels follow the same definition as Figure 2.2 and Figure 2.3. Without the lateral nitrate replenishment, the nitrate outflux is the same as that in Figure 2.3 and the Concentration-Discharges relationship would show a dilution pattern. However, assuming that when the water table rises to the third level, lateral water movements brings nitrate replenishments from upland to this patch, increase the total nitrate outflux and changes the nitrate concentration. The resulting nitrate concentration with the rising water table is now: 2.5, 2, 2.67 and 3.0 units, and is thus an enrichment rather than dilution pattern in Figure 2.3 E and 2.3 F.

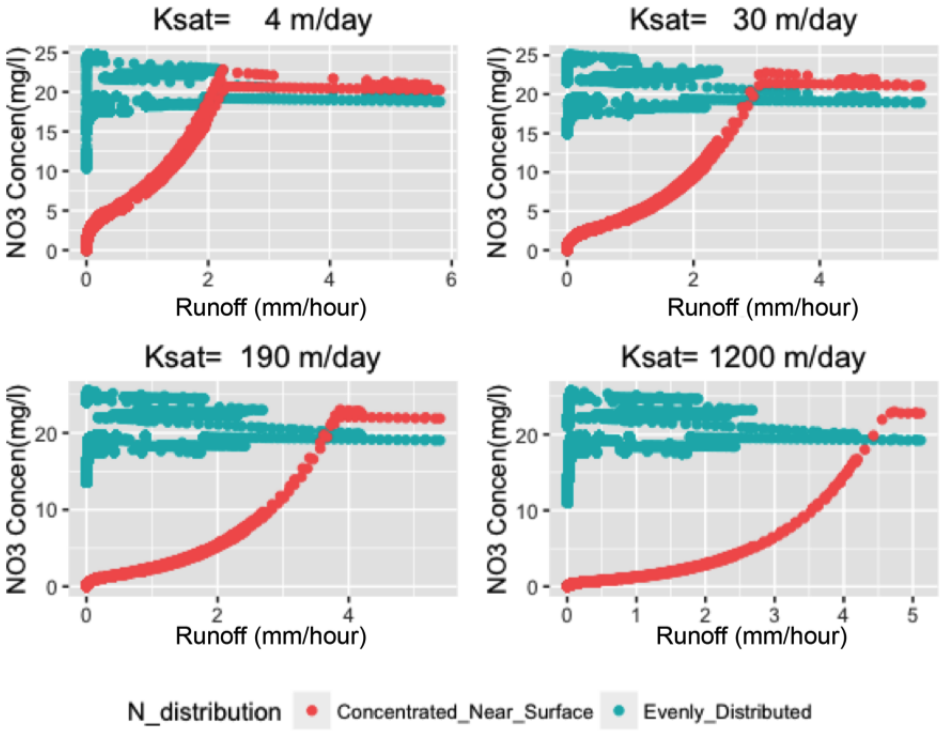

Figure 2.5: The 'Concentration-Discharge' plot for a single patch for increasing values $Ksat$ and two contrasting vertical distributions of nitrate. The red circles show results when nitrate distribution is concentrated hear to the surface (N_decay=6). The blue circles are the nitrate concentration plots for distribution where nitrate is more evenly distributed (N_decay=2).

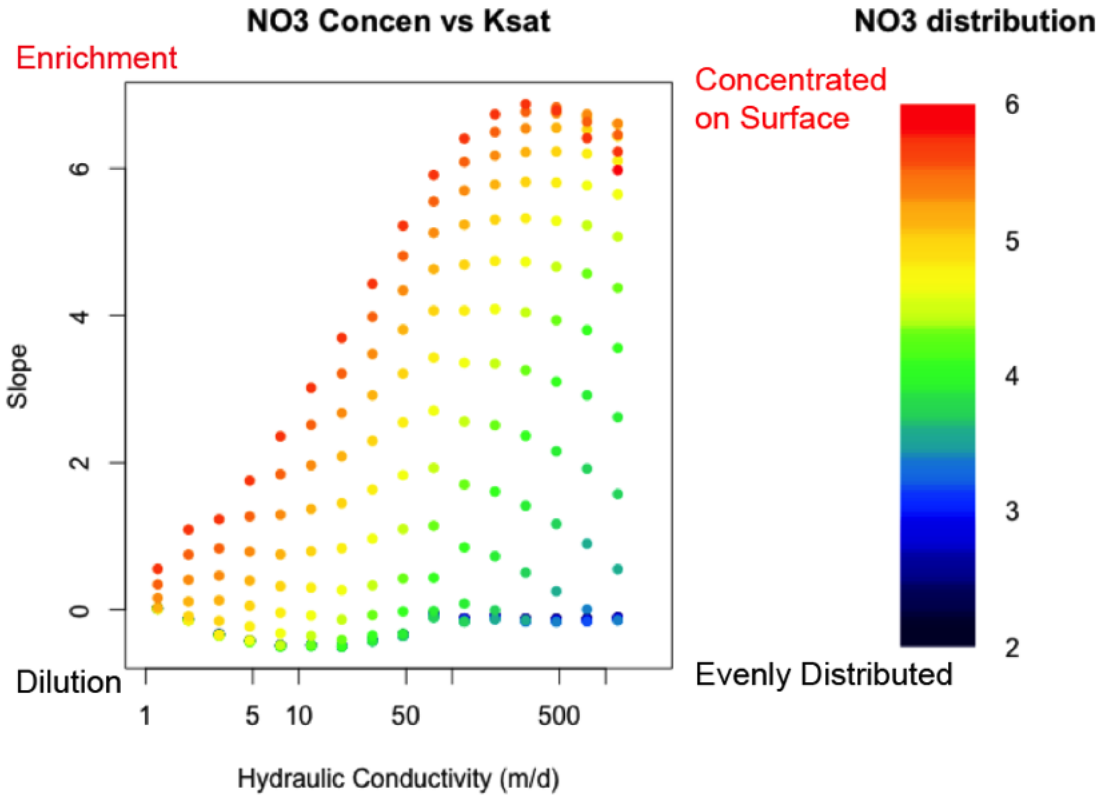

Figure 2.6: Average slope for nitrate concentration plots for storm runoff in the 336 simulations. Each point represents the average slope of the Concentration-Discharge relationship. Red points represent scenarios with a more uneven distribution of nitrate (e.g nitrate more concentrated at the surface). Black or blue represents more evenly distributed scenarios. The x-axis is the hydraulic conductivity. Y-axis is the average slope. A greater positive average slope corresponds to a stronger enrichment pattern, while a more negative average slope corresponds to a stronger dilution pattern.

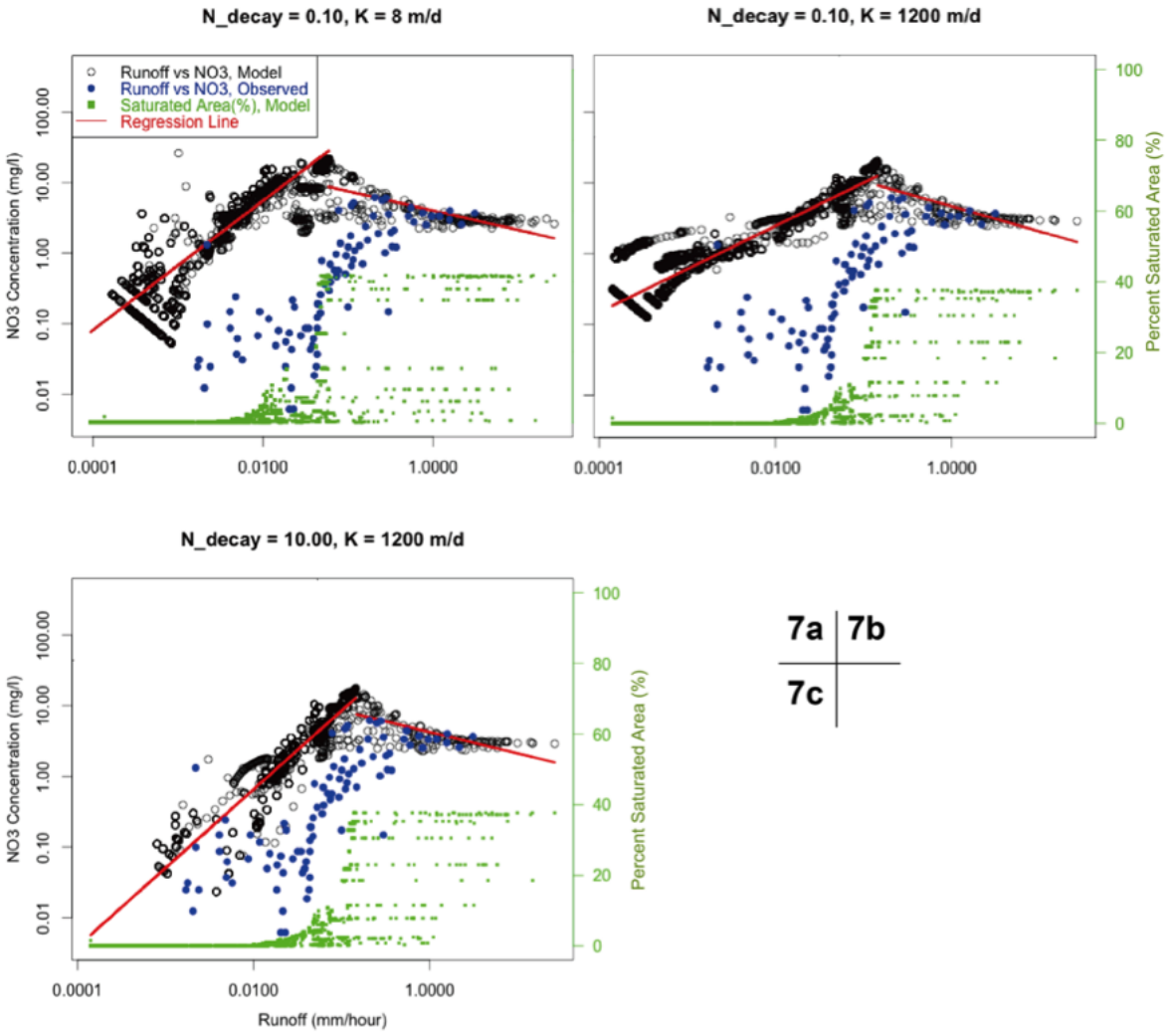

Figure 2.7: Concentration v.s Discharge a) $N\_decay = 0.1$, `Hydro_Conductivity` ($Ksat$) = 8 (m/day). b) $N\_decay = 0.1$, `Hydro_Conductivity` ($Ksat$) = 1200 (m/day). c) $N\_decay = 10$, `Hydro_Conductivity` ($Ksat$) = 1200 m/day. Blue points are the observed Concentration-Discharge points, black circles are the Concentration-Discharge results from model, the green dots are the percent saturated area from model, and the red line is the regression line for the modeled Concentration-Discharge relationship.

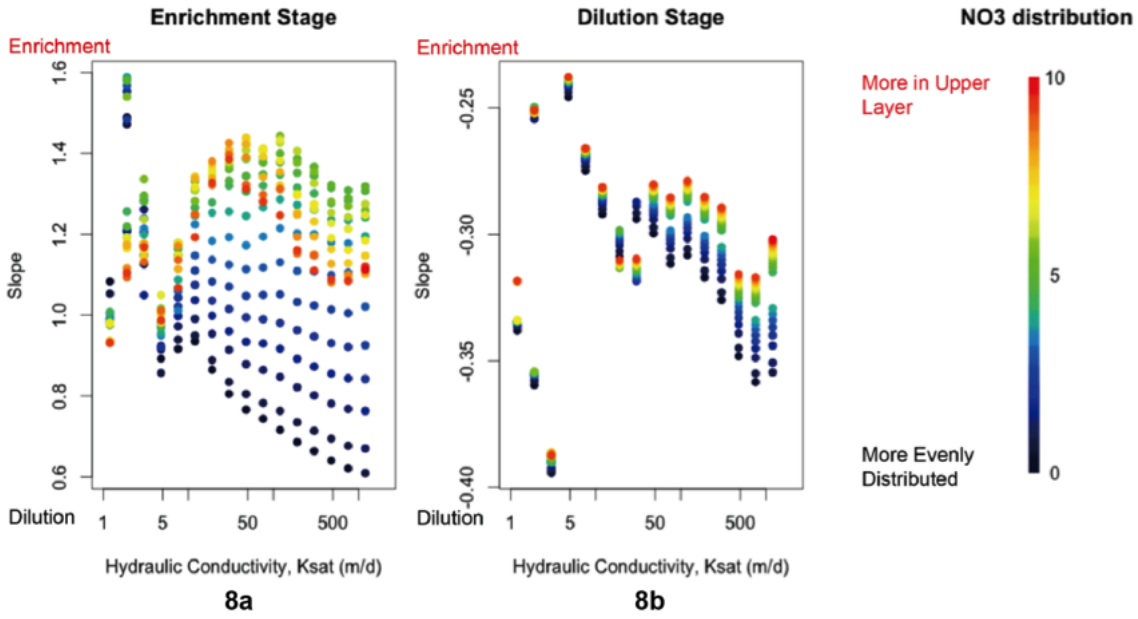

Figure 2.8: Slope of regression lines for 'Runoff-Concentration' plot during the 'Enrichment' stage (a) and the 'Dilution' stage (b). X-axis is the hydraulic conductivity, and y-axis is the slope of the regression line. Red and yellow points represent scenarios with higher N_decay. Blue and black points represent scenarios with lower N_decay.

Chapter 3

The Effect of Total Impervious Surface, Impervious Surface Connectivity and Vegetation Types on Nitrate Concentration in Urban Hillslope

3.1 Introduction

In 2014, more than 54% of the world's population lives in urban area. This number is projected to reach 66% in 2050 [82]. The fast growing impervious urban surface has dramatically changed the urban hydrology [83, 84]. While rapidly exporting runoff via the storm drainage, urban impervious surface area reduces infiltration and evapotranspiration, resulting in the increased frequency and volume of storm flow, decrease of the base flow, and ecological impact [85, 86, 87, 88]. However, if the impervious area

is disconnected from downstream receiving stream, water from these hydrologic disconnected impervious areas (HDIA) are diverted to nearby vegetated areas. In contrast, if impervious areas are directly connected with the downstream receiving water body, retention time will be reducd and result in more rapid drainage than that from hydrologic disconnected impervious areas. These connected impervious areas are called 'Effective Impervious Areas (EIA)' [**?**].

Previous studies have suggested that it is the effective impervious area (EIA), instead of the total impervious area (TIA), that drives the changes in the urban hydrology [89, 90, 88]. In semi-arid areas where the ecosystems are generally water-limited, the decline of water and carbon fluxes from an increase of TIA may be partially or completely offset by an increase of transpiration and NPP in the remaining vegetated area supported by additional water from disconnected impervious areas [93].

In addition to the hydrologic impact of impervious surfaces on flow regimes, urbanization and growing impervious surface area have a substantial influence on urban stream water quality. Pollutants collected on impervious surfaces will be carried by urban storm water runoff, leading to degradation of water quality in receiving urban streams [94, 95, 96, 97, 98]. As one of the important nutrients and major factor for eutrophication in the downstream, an increasing nitrate concentration is the major concern for urban watershed [**?**, **?**]. However, how the connectivity of urban impervious surface affects nitrate concentration by controlling the water availability in the remaining vegetated area is less well studied.

Conceptually in semi-arid areas, the decrease of EIA affects the influence of TIA on downstream nitrate concentration primarily through increasing water retained in and transported through the remaining vegetated areas. An increase of retained water provides additional water availability for plant growth and stimulates nitrate uptaking by plants, as well as providing more moisture for the litter decomposition. The enhanced

infiltration associated with additional water inputs may also result in increased nitrate transport from soil. However this effect may be offset by, an increase in transpiration by the vegetation [93] and plants with adequate water supply may uptake more nitrate than the plants under drought stress [99].

How additional inputs of water and nitrogen from surrounding impervious surfaces influences the function of vegetation patches and ultimately nitrogen export is likely to vary both with climate, particularly the timing and magnitude of water inputs and vegetation characteristics. For example, different plants have distinctive needs for water and nitrate, which will determine how they make use of additional water and nutrient inputs. In semi-arid areas, grass usually has less evapotranspiration than oaks or chaparral [93], resulting in higher discharge. Conversely, grass forms less litter and uptakes less nitrate than oak or chaparral.

The multiple factors and interactions and feedbacks between factors that determine the responses of vegetated patches to both TIA and EIA make assessing water quality impacts challenging. We use computer models to synthesize these interacting effects and compare the impacts of different EIA and plants scenarios on nitrate cycling and identify dominant factors that alter the influence of TIA on nitrate concentration.

We will answer the following three questions:

1. How will impervious surface connectivity affect the mean stream flow rate in three vegetation scenarios?

2. What is the impact of impervious surface connectivity on mean stream nitrate flux in three vegetation scenarios?

3. Which one of the scenarios has the lowest mean nitrate concentration and what are the implications for watershed management?

We focus on how the downstream water quality is affected by the connectivity of impervious surface and nitrogen and water inputs from these surfaces and do not consider potential for additional nitrate sources such as lawn fertilizer and the leaking sewer pipes within vegetated patches to influence nitrogen cycling.

3.2 Method

3.2.1 Study Area

The study area is in the northeastern Santa Barbara city within the Mission Creek catchment. Land cover within the catchment includes both vegetated areas and impervious surfaces. The local climate Mediterranean type with a long dry summer and a cool wet winter, which is right for the drought tolerant plant such as chaparral and oak. The majority of the precipitation falls in winter and early spring. The mean annual precipitation from 2005 to 2014 was 427 mm, with a standard deviation of 249 mm [100]. During the rainy season, the predominant southwest winds and south orientation of the watersheds result in substantial orographic rainfall enhancement [34]. The mean annual precipitation at 1000 m elevation can be 210% greater than that at the elevation of 31 m [51]. Mission Creek catchment is an urban/suburban mixed catchment. The headwater is characterized with undeveloped chaparral land and steep slope (slope $> 20°$), but the downstream is developed area with relatively gentle slope (slope $< 6°$). In the developed area, an average of 21% surface is covered by impervious area and the most developed area has the highest percentage coverage (81%) of impervious surface [93]. In this study, a single hillslope (#259) is extracted to represent the moderately urbanized hillslope, with an area of 0.56 km^2 and an average slope of 8° (Figure 3.1). This hillslope has an average elevation of 200 m, with 39% of the area covered by impervious surface, including

road, roof area, and parking area [93].

3.2.2 Data

To develop model scenarios, nine years of hourly precipitation data was obtained from Santa Barbara County Flood Control District at Botanic Garden with elevation of 243 m (Lon/Lat: -119.70694, 34.45388) [100], adjusted with orographic effects following method described in previous study [28]. Daily temperature data is from the National Climate Data Center monitoring station (HCND:USC00047902) near the outlet of Mission Creek catchment. Msonthly irrigation is estimated and interpolated following data from Shields and Tague [28] (Figure 3.2). The total impervious area (TIA) and effective impervious area (EIA) were held constant over the 9 years.

3.2.3 RHESSys Model

RHESSys is a physical process-based, distributed hydrological model. It has been widely implemented in a variety of bioclimatic regions, including in semi-arid regions like Mission Creek Catchment [27, 28, 29]. RHESSys explicitly models the catchment connectivity by calculating the volume of water drained to downstream from upland via lateral movement through adjacent patches [23]. Two layers are modeled in soil profile: an unsaturated layer, and a saturated zone. RHESSys calculate the 1-D vertical infiltration process by the modified version of Green and Amt approximation, where the time to ponding is constrained by porosity, initial soil moisture content and infiltration intensity. Following the infiltration process, the water held in saturated and unsaturated layer will be updated. RHESSys uses the traditional Continuous Transmissivity model [3] to calculate the subsurface lateral flow for subsurface flow sub-model, where both the subsurface conductivity and transmissivity decays exponentially with the soil saturation

deficit.

The Penman Monteith approach [31] is implemented at a daily timestep to estimate the canopy evaporation and transpiration. Soil evaporation is estimated based on energy, atmospheric factors and the maximum exfiltration rate. The maximum exfiltration rate is determined based on soil properties and the soil moisture. Potential capillary rise is controlled by soil properties and the water table. Only half of the potential capillary rise is left to meet the plant transpiration needs at the end of day, with the rest of potential capillary rise allocated to the unsaturated zone at the start of the day to account for the subdaily plant responses.

Biogeochemical cycling and vegetation growth are modeled in RHESSys sub-models to account for the carbon and nutrient cycling [23] at a daily timestep. Photosynthesis is modeled following the Farquhar model, where the net assimilation rate per unit LAI is constrained by nitrogen availability, electron transport and stomatal conductance [101]. Total maintenance respiration integrates respiration of leaves, roots and stems, following the model developed by Ryan (1991).

Carbon and nitrogen stores are partitioned into leaves, stems, coarse roots and fine roots. Vegetation nitrogen stores and carbon stores are linked through the stoichiometric relationships. Soil nitrification and denitrification are modeled following the $CENTURY_{NGAS}$ approach [78]. Decomposition is calculated based on litter and soil pools of different C:N ratios to account for labile, slow and recalcitrant pools. Potential nitrification rates are computed following the method by Parton et al. (1996). The actual nitrification rate is calculated based on the soil moisture, carbon substrate availability, soil temperature, and soil ammonia. In RHESSys, soil organic nitrogen can be converted to inorganic N ($NH_4^+ - N$). Through nitrification, ammonium-N will be future converted into nitrate-N. Soil nitrate will be uptaken by plant, or washed away with subsurface flow, or be denitrified to N gases and lost to the atmosphere. Denitrification is controlled by

the maximum denitrification rate, soil respiration and soil moisture.

$$N(depth) = Coeff_1 \times N_{all} \times e^{-N\_decay \times depth} \times N\_decay \tag{3.1}$$

$$\int_{Max_d}^{depth} N(depth) = Coeff_1 \times N_{all} \times (e^{-N\_decay \times depth} - e^{-N\_decay \times Max_d}) \tag{3.2}$$

$depth$ is the soil depth, Max_d is the max soil depth, $N(depth)$ is the nitrate mass of the patch in the soil layer at depth = $depth$. $Coeff_1 = \frac{1}{1-e^{-N\_decay \times Max_d}}$ is the coefficients for $N(depth)$ calculation. N_{all} is the total amount of nitrate in that patch, and N_decay controls the vertical decay rate of the nitrate distribution. With the exponential distribution function, nitrate is assumed to concentrated near upper soil layers in semi-arid area, which is consistent with previous study [53]

3.2.4 Model Set Up

We consider a total of 36 different scenarios, including a combination of TIA and EIA settings and three vegetation types (Table 3.1). The vegetation types in this study are chaparral, lawn grass and coastal live oak, which are common for Southern California coastal area [93]. The ecophysiclogical parameters of these vegetation are estimated following previous studies [93]. For the grass vegetation type, we consider two different scenarios: one with and one without irrigation. In this study, we consider a single hillslope divided into 10 m^2 patches. While the observed max TIA on this hillslope is around 39%, we designed three levels of TIA coverage (12%, 25%, 39%) to examine the effects of total impervious area on the stream nitrate concentration (Figure 3.3). In RHESSys, once a patch is defined as impervious area, surface water won't infiltrate into the soil in this patch, but will either drain to the outlet of the hillslope or be routed to permeable patches

nearby, depending on whether it is the effective impervious area or not. For each TIA scenario, three levels of EIA fraction (10%, 50%, 100%) are assigned to the model setting to evaluate the impact of impervious surface connectivity on streamflow and stream nitrate concentration. The location of effective impervious patches are randomly chosen among the impervious patches assuming that all patches have an equal probability of being selected as an impervious patch.

RHESSys is used to estimate nutrient cycling and export for each combination of the TIA and EIA fraction. Key ecohydroological parameters are based on RHESSys parameter libraries and include parameters that define plant specific differences in N-cycling including fine root and leaf carbon-nitrogen ratios [93, 103], and using values come from averaged measurements across these vegetation types (Table 3.2). For each vegetation type, 240 years of pre-run were implemented to stabilize the soil carbon and the soil nitrate. Parameters for root depth and root distributions are calibrated so that the long-term stable root depth for these vegetation types is consistent with field observation [104, 105] (Table 3.3). The resulting states from pre-run are used as the initial condition for the 36 model scenarios. The spatial average soil nitrate, plant carbon, evapotranspiration over the whole hillslope are calculated and evaluated.

3.3 Results

3.3.1 Annual Transpiration

Grass scenarios have the lowest median-annual-transpiration (200 mm), widest variation of annual transpiration (70 380 mm), and greatest sensitivity to the annual precipitation (Figure 3.4). With irrigation the median-annual-transpiration in the grass scenario increases dramatically to 265 mm. Chaparral scenarios have a median-annual-

transpiration of 230 mm. The Oak scenario has the highest median-annual-transpiration (350 mm). The ranking order of the transpiration among different vegetation types is consistent with the previous study in this region [93].

The different impervious-surface-connectivity settings (low to high EIA scenarios) cause substantial variation in annual transpiration estimates (Figure 3.5). With the expansion of TIA from 12% to 39%, transpirations per hillslope area decrease in all scenarios. With less vegetation, the total transpiration decreases.

For each TIA level, the increase of EIA also leads to a decrease in the annual transpiration. The impact of EIA on the annual transpiration increases with TIA (Table 3.4) such that when TIA =12%, the median annual transpiration difference between low EIA and high EIA scenarios is smaller than that in TIA=39%. These results are consistent with Shields and Tague (2015). This increase in the sensitivity of transpiration estimates to EIA varies with vegetation type. Chaparral and oak have the similar results, with the annual transpiration difference between low and high EIA scenarios increasing from around 5 mm when TIA is 12% to around 20 mm when TIA is 39%. For grass-without-irrigation scenario, the annual transpiration difference between low and high EIA scenarios increases from 43 mm for TIA of 12% to 77 mm for TIA of 39% scenario. The larger variance in grass-without-irrigation scenarios than chaparral or oak scenarios can be explained by the shallower roots of grass than that of chaparral. As a result, the transpiration in grass-without-irrigation scenarios is more sensitive to the water availability and sensitive to the EIA changes. With irrigation, the additional water input reduces the water scarcity for all EIA levels, and the 'sensitivity increases with TIA' pattern is less significant in grass-with-irrigation scenario and the transpiration in grass-with-irrigation scenario shows less sensitivity to the EIA changes.

3.3.2 Annual Evaporation

Annual evaporation is sensitive to vegetation types but not to EIA. Oak and chaparral have higher annual evaporation ($\sim$ 75 mm and $\sim$ 80 mm) than the grass-without-irrigation scenarios ($\sim$ 50 mm). TOak and the chaparral have higher LAI (>2) than grass ($\sim$ 1) and consequently intercept more rain than grass. Oaks also intercept and retain more long and shortwave energy through the year than grassland [107], providing more energy for canopy interception evaporation in oak scenarios (Figure 3.6). Soil evaporation has less variation among the four vegetation scenarios. The grass-without-irrigation scenario has the least soil evaporation ($\sim$ 30 mm) than the rest of the scenarios ($\sim$ 40 mm)

3.3.3 Stream Discharge

Since oak and chaparral have higher transpiration and evaporation than grass, grass scenarios produce the highest stream discharge for the same climatic forcing. Grass-with-irrigation scenarios have additional water inputs and have the highest annual streamflow, followed by the grass-without-irrigation and chaparral scenarios (Figure 3.7). The oak scenarios have the lowest annual streamflow.

The TIA has a monotonic influence on the stream flow (Figure 3.8). The increase of TIA leads to increase in the mean stream flow for all scenarios.

The consequences of EIA changes on stream discharge are clear. The increase of EIA results in higher stream flow in all scenarios (Figure 3.8). The difference between high and low EIA is wider when TIA is 39% than that when TIA is 12% (Figure 3.10)

3.3.4 Plant Carbon

Oak scenarios have the highest mean plant carbon ($\sim 4\ kgC/m^2$) and second deepest root (chaparral has the deepest roots). Grass scenarios have the least mean plant carbon ($\sim 0.13\ kgC/m^2$) and shallowest roots ($\sim 0.2\ m$). Irrigation increases grass plant carbon, but the difference in grass plant carbon between irrigation and non-irrigation scenario is small. The mean plant carbon for the chaparral scenarios is around 3.7 kgC/m^2, and its root depth is around 4 m (Table 3.3 and 3.5).

The expansion of total impervious area (TIA) has a negative influence on the plant carbon in all scenarios (Figure 3.9). Given the same TIA, the increase of EIA leads to the decrease in the plant carbon. Figure 3.9 illustrates similar sensitivity of plant carbon to EIA increases with TIA when TIA shifts from 12% to 39%. When EIA increases from 10% to 50%, the decrease in plant carbon is larger than the decrease when EIA increases from 50% to 100%.

3.3.5 Soil Carbon and Soil Respiration

Oak scenarios have the highest soil carbon level ($\sim 1.2\ kgC/m^2$), followed by chaparral scenarios ($\sim 1.1\ kgC/m^2$). Grass scenarios have the lowest soil carbon ($\sim 0.9\ kgC/m^2$) (Table 3.4). With the irrigation, the soil respiration increases slightly and reduces soil carbon relative to grass without irrigation scenario. Vegetation types affect the soil carbon through litter and roots turn over, which controls both quantity and quality of carbon and nitrogen input for soil and through its impact on soil moisture. Table 3.4 shows the oak scenarios has the largest litter carbon pool ($\sim 0.06\ kgC/m^2$), followed by chaparral scenarios ($\sim 0.05\ kg/m^2$). Grass scenarios have the least litter carbon pool ($0.02\ kgC/m^2$). While with irrigation, the grass litter carbon pool increases to $0.027\ kgC/m^2$. However, different EIA/TIA settings have little influence on soil carbon

($< 1\%$).

Model output shows that oak and chaparral scenarios have the highest mean soil respiration rate ($> 120\ gC/m^2/year$). Grassland scenarios have a mean soil respiration rate of 70 $gC/m^2/year$. The soil in semi-arid area is drier and low in organic carbon. The soil respiration estimates in the results are low but still within the typical range of the soil respiration rate [108, 109, 110].

Both TIA and EIA level affects soil respiration rates (Figure 3.10). TIA has a more substantial impact on soil respiration rate ($10\% \sim 20\%$). With the increase of TIA, soil respiration rate decreases in all scenarios as expansion of TIA increases the impervious area and diverts water away from vegetated area and reduces water availability.

At the same TIA level, the increase of EIA reduces the soil respiration. The increase of EIA means less water availability for vegetated area, limiting the soil respiration. Again, the 'sensitivity of soil respiration to EIA' increases with TIA is observed. The soil respiration shows more sensitive to EIA in higher TIA scenarios than in lower TIA scenarios.

3.3.6 Soil Nitrate

All scenarios have similar soil nitrate values (Figure 3.11). The grass-without-irrigation scenarios have the highest mean soil nitrate level ($0.5 \sim 1.8\ gN/m^2$), followed by oak scenarios ($0.2 \sim 1.4\ gN/m^2$) and chaparral scenarios ($0.2 \sim 1.4\ gN/m^2$). While with irrigation, the mean soil nitrate level is reduced to $0.2 \sim 1.6\ gN/m^2$. The range of soil nitrate estimated here are comparable with previous studies in this region [32].

The expansion of TIA brings a monotonic increase in the soil nitrate level (Figure 3.12). The expansion of EIA has slightly different impacts on the three vegetation scenarios, given the same TIA. For chaparral and grass-w/o-irrigation scenarios, the increase of

EIA level builds up the soil nitrate. For oak, the EIA has little impact on the soil nitrate level.

3.3.7 Stream Nitrate Flux

Grass-with-irrigation scenarios have the lowest stream nitrate flux, followed by oak scenarios and chaparral scenarios (Figure 3.13). The modeled nitrate flux (0.005 0.06 gN/m2/year) is slightly lower than the estimations from observed data collected in station Rocky Nook ($\sim$ 0.1 $gN/m^2/year$) [100, **?**],and likely reflect that the simulation didnt consider additional nitrate source such as lawn fertilizer and leaking sewer pipes.

The EIA/TIA changes have a substantial influence on the stream nitrate flux (Figure 3.16). The increase of TIA leads to an increase of stream nitrate flux in all scenarios, except for the grass-with-irrigation one, which shows no increase, or even a slightly decrease in nitrate flux from low TIA (12%) scenario to high TIA (39%) scenario.

The responses of nitrate outflux to an increasing EIA is a similar to the responses to an increasing TIA. With the increase of EIA, the stream nitrate export flux increases, except for the transition from low EIA to medium EIA in 39% TIA for the chaparral and oak cases Figure 3.16.

3.3.8 Stream Nitrate Concentration

Nitrate concentration is calculated as the nitrate flux divided by stream flow. While grass-with-irrigation has the lowest nitrate fluxes, it has the highest stream flow, resulting in the lowest nitrate concentration in receiving water. Chaparral scenarios have the highest nitrate concentration. The max nitrate concentration in scenarios without irrigation is within the observed range from urban watershed in same area [51, 100].

The pattern of the influence of TIA and EIA on nitrate concentration follows the

pattern of the influence of EIA and TIA on nitrate exporting fluxes (Figure 3.17). The increase of TIA generally results in a rise in nitrate concentration, except for the grass-with-irrigation scenario. This is similar to results found in the nitrate flux analysis where the nitrate flux has a slight decline with expansion of TIA in the grass-with-irrigation scenario but otherwise increases with TIA. The increase of EIA does not always result in greater concentrations even though nitrate flux increases with EIA. For example, in scenarios with chaparral and oak tree with TIA=25% and 39%, the increase of EIA from low to medium leads to a decrease in nitrate concentration. In contrast in grass scenarios with TIA of 25% and 39%, the increase of EIA from low to medium results in an increase in nitrate concentration.

3.4 Discussion

Increasing TIA and EIA affect nitrate concentrations by altering nitrate availability, cycling, and transport and stream discharge (Figure 3.18 and 3.19).

An increase in TIA directly alters nitrate availability by reducing the vegetated areas, Reductions in vegetated areas can result in less plant uptake, less litter fall, and less nitrification. The reduced plant uptake may leave more soil nitrate for nitrate export. Decreasing nitrification and decomposition, on the other hand, may produce less nitrate in soil, and consequently less nitrate for outflux. However, this study found as previous studies suggest, that plant uptake is often the dominant process [53] compared with nitrification or mineralization.

However, nitrate concentration shows a more complex response to TIA because an increase of TIA also tends to increase stream discharge by decreasing the total evapotranspiration, thus increasing the peak flow and the total annual runoff [112, 85]. This additional water can lower the effective concentration associated with a given nitrate

flux.

Although TIA has impacts on both nitrate availability and stream discharge, the strength of these impacts is not the same. The net effect of an expansion in TIA for most scenarios is an increase in nitrate concentration, indicating that the influence of TIA on increasing nitrate flux is larger than the impact on increasing stream discharge. While previous studies emphases that the pollutant in impervious area carried by storm water may deteriorate the stream water quality [94, 113], our results indicate that the decrease in plant uptake may be the dominant factor affecting the water quality in urban streams in semi arid areas. Further we suggest that EIA as well as TIA will be a key control on the magnitude of the plant uptake effect.

For a given TIA, a change of EIA will moderate the nitrate availability through changing the amount of water diverted from HDIA to vegetated area (Figure 3.19). A conceptual model (Figure 3.20) explains how EIA controls the nitrate outflux. Many of these mechanisms have been demonstrated in field-based studies here we use the model to demonstrate the combined effect. An increase of EIA does not expand the total impervious area. However, it diverts more water to downstream directly and reduces the water availability on vegetated patches, leading to consequences for plant nutrient uptake and soil nitrate availability (Figure 3.20 A). The reduced water availability may decrease overall biomass and root nutrient uptake capacity [114], resulting in less vegetation uptake, and more nitrate left. Conversely, reduced soil moisture may reduce microbial activity [115, 116], and the mineralization and nitrification/denitrification processes [53], and result in less soil nitrate. The net effect of these contradictory factors is an increase in nitrate flux, indicating the reduced nitrate plant uptake is the dominant effect of the expansion of EIA (Figure 3.16).

Both TIA and EIA impact not only nitrate availability but also the amount of water available for export and resultant nitrate concentrations. The increase of EIA also diverts

more flow directly to the receiving water. For TIA of 25% and TIA of 39%, the increase of EIA from low to medium results in a lower nitrate concentration in chaparral and oak tree scenarios, indicating that in these cases, the rise of EIA has a more substantial impact on increasing the stream discharge than increasing the nitrate flux (Figure 3.17) and can offset the impact of an expanding TIA on increasing the nitrate flux. While EIA increases from medium to high, nitrate concentration increases in the chaparral and oak tree scenarios with TIA of 25% and TIA of 39%, indicating that in these scenarios, the rise of EIA has a more substantial impact on increasing the nitrate flux than increasing the stream discharge.

Vegetation types strongly influence both the impact of TIA and how this impact is moderated by EIA. If the landscape is dominated by more deeply rooted, larger biomass species such as oak and chaparral, the increase in nitrate flux with increasing TIA is greater that it is for grass, reflecting the greater nitrate uptake by shrubs and trees. The type of vegetation plays a role in terms of the sensitivity of nitrate concentration to EIA. EIA determines the amount of water being diverted to vegetated area, which controls the vegetation growth. Different plant types respond differently to water inputs and thus to the EIA, which in turn affects biochemical reaction rates, nitrate availability, nitrate export and stream discharge. Plants also differ in their nitrogen uptake rates. Chaparral uptakes more nitrate than grass, leaving less soil nitrate available for export (Figure 3.11), and potentially decreasing nitrate concentration. However, chaparral uses more water than grass for evapotranspiration, which decreases the volume of water in downstream and potentially increasing nitrate concentration. Figure 3.17 shows that in the end, the chaparral has lower nitrate concentration than grass, indicating that the plant nitrate uptake is the dominant controlling factor for nitrate concentration in downstream.

Vegetation types explain the different inter-annual-variance in nitrate ouflux and ni-

trate concentration. This is because with shorter roots, the nitrate uptake in grass scenarios in more sensitive to inter-annual variation in water availability associated with climate forcing, resulting in more inter-annual-variance. While under drought stress, the grass-without-irrigation uptakes less nitrate and leaves more soil nitrate than scenarios with adequate water supply. However, with irrigation, the water availability is more stable and the impact of climate variances on nitrate outflux is less substantial than it is in the grass-without-irrigation scenario.

The 'sensitivity increases with TIA' shows that EIA has a more substantial effect in higher TIA cases than lower TIA cases. This is particularly true for nitrate concentration (versus flux). The reason for this sensitivity increases with TIA pattern is that in higher TIA scenarios, both the EIA and HDIA have larger area than in lower TIA scenarios, and their impact on diverting water to either vegetated area or to receiving water is larger than that in the lower TIA case. Notice that in this study, the max TIA is 39%, which is much lower than the highly developed area (above 80%). However, the 'sensitivity increases with TIA' may still hold in higher TIA, unless there is a threshold where the vegetated area is small enough and the effects are negligible. Further more, 39% is high for this type of landuse and results of this paper are focused scenarios where landuse includes a mixture of impervious surface and vegetated patches found in low to medium density urban areas, places where connectivity to vegetated patches might be modified by suburban and urban design. Previous studies note that the EIA is a better indicator for impact of urbanization on stream ecosystem and emphasis its impact on geomorphic variables [117]. Our study focuses on the impact of EIA on plant nitrate uptake and subsurface nitrate export. While recent studies state the aim of storm water management should be restoring the flow regime [92], our results suggest that med EIA will not always result in lower nitrate concentration, especially for higher TIA case. To restore both the hydrologic and biogeochemical condition, one should design the EIA

based on TIA level and vegetation types.

The vertical distribution of nitrate in soil and its dynamic interaction with water table affects the nitrate export and downstream nitrate concentration. Soil nitrate is assumed to concentrated near upper soil layers in semi-arid area [53]. RHESSys uses exponential function to represent this distribution **??** and only moves nitrate out of patches from saturated zone. In the model, nitrate outflux from a given patch is proportional to the nitrate within the saturated zone (under the water table). When the saturation deficit is small (water table is high), the saturated zone accesses most of the patch nitrate pool, and is able to export larger portion of total soil nitrate. While the saturation deficit is high (water table is low), the total accessible nitrate is smaller, so the nitrate flux is a much smaller fraction of the total soil nitrate.

The type of modeling approach here may be used to estimate the role of vegetated patches and EIA in controlling n-export and concentration. However, there are several challenges to broad application of this approach. One of them is the modeling uncertainty from initial condition and the location of EIA or HDIA. Other modeling studies have shown that estimates of nitrate export are sensitive to the initial condition [118]. Although the total impervious area can be determined from landuse image, it is not easy to determine the location of the EIA patches or the HDIA patches. Previous research has attempted to estimate the fraction and the location of EIA [119, 93].Recently new methods have identified roads, side walks, parking lots, green sports fields, roofs and irrigated lawns in high-resolution [**?**], and may reduce the uncertainty in locations of EIA, and facilitate the application of this type of model based analysis to asses the impacts of current EIA-TIA-vegetation type setting.

3.5 Conclusion

In this study, we set up an eco-hydrogical model in an urban hillslope and explored the impact of impervious surface connectivity and vegetation types on stream discharge and stream nitrate concentration. These findings are specific to semi-arid regions where additional water inputs to vegetated patches from impervious surfaces can have substantial impacts on vegetation growth, water uptake and nitrogen cycling.

Modeling results show that a reduction of TIA leads to the decrease in nitrate concentration in all scenarios except for the grass-with-irrigation scenario, indicating that the enhanced plant uptake, rather than its impact on water balance, is the dominant mechanism through which TIA affects nitrate concentration in urban streams in semi-arid areas. Within a given TIA scenarios, a decreasing EIA provides more water for plants in vegetated area, stimulating growth and enhancing the plant nitrate uptake as well as soil nitrate generation. In most cases, the enhanced plant uptake dominates the impact of reduced EIA on nitrate concentration, and results in a decrease in nitrate flux and concentration. For some deeply rooted water consumptive species, however, reduced streamflow dominate the impact, and decreasing EIA actually leads to increasing nitrate concentration. While these results suggest that reducing both TIA and EIA can contribute to restoring a watersheds' hydrologic and biogeochemical conditions and improving water quality, consideration of vegetation type and non-linearities in TIA-EIA interactions is needed. Future studies will explore the impact of impervious area on mixed vegetation types in vegetation area, and their effects on nitrogen cycling and nitrate concentration in streams and receiving waters.

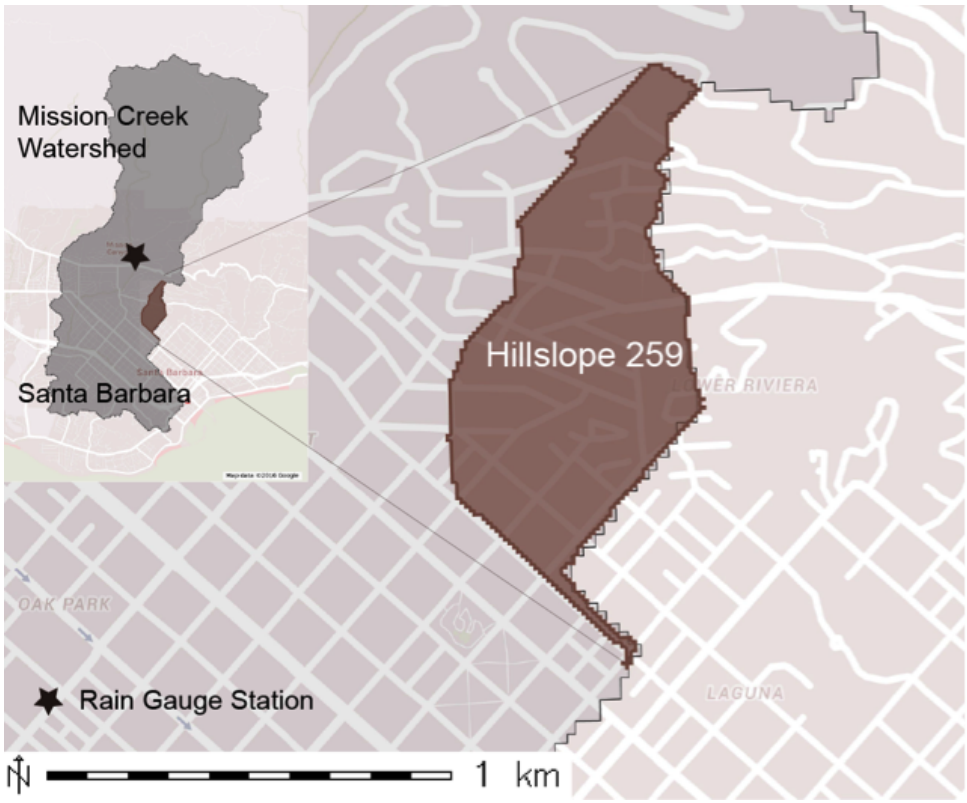

Figure 3.1: Study area is the hillslope #259 in the Mission Creek catchment in the northeast Santa Barbara (Google Maps, latitude: 34.4376, longitude: -119.7018, 2016).

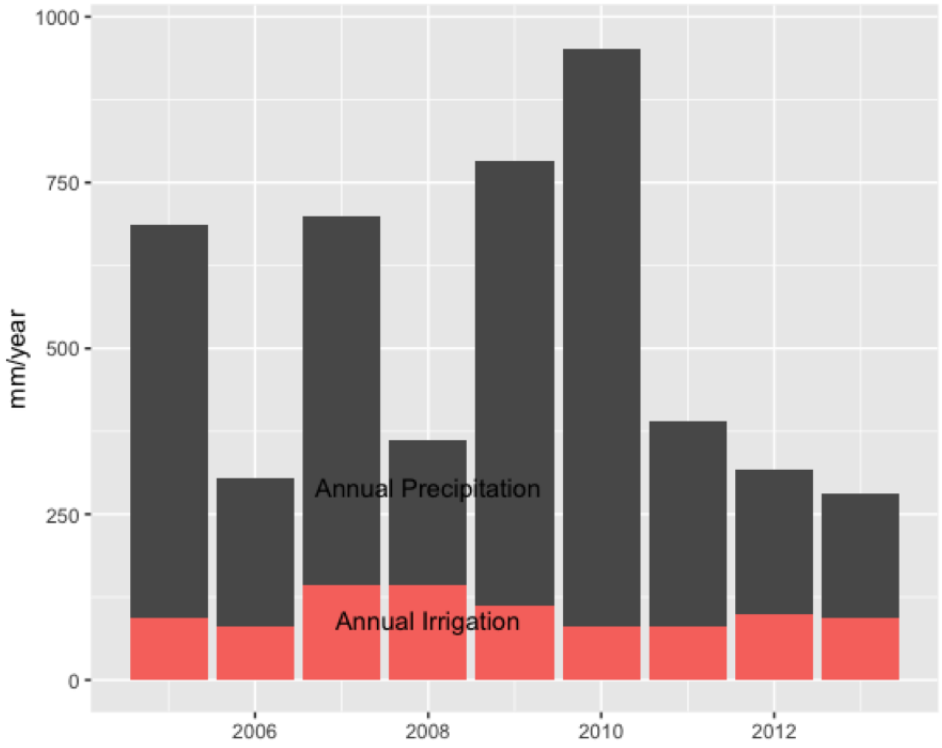

Figure 3.2: Precipitation records and estimated irrigation value for the study area from 2005 2013

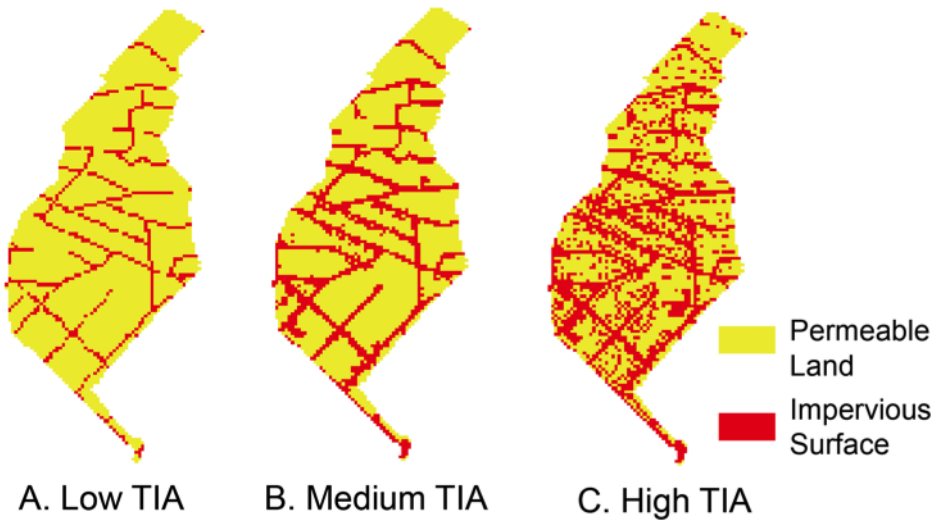

Figure 3.3: Three different TIA setting for the study area. Low, Medium, and High TIA are the scenarios with TIA = 12%, 25%, 39%. Yellow area represents the permeable surface, and the read area represents the impervious surface.

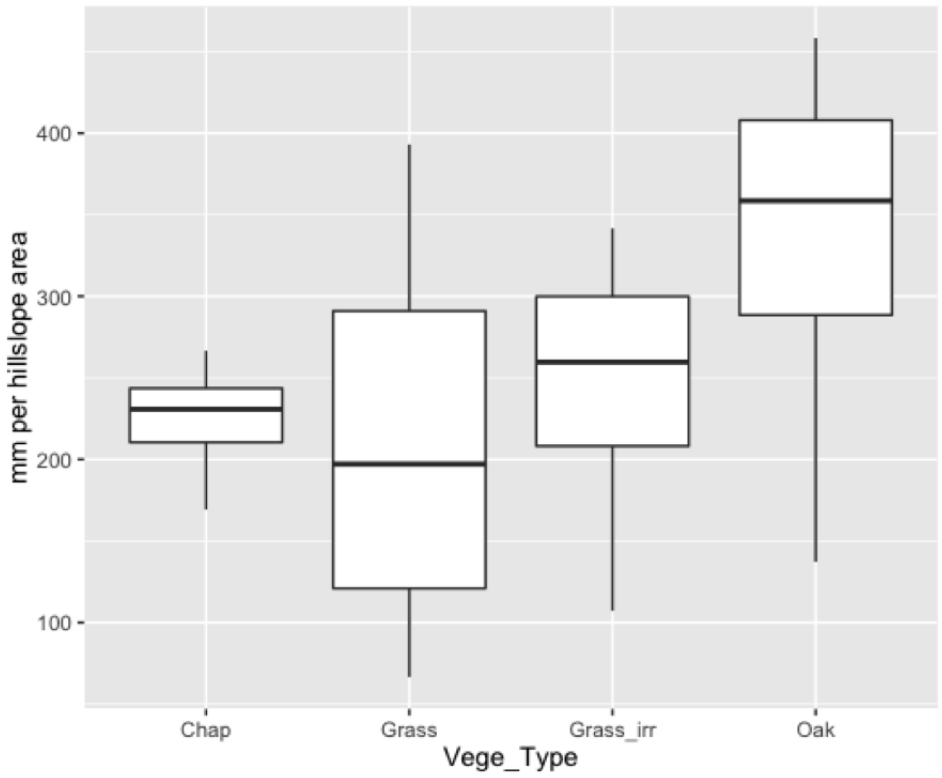

Figure 3.4: Annual transpiration (in mm) for the four scenarios: chap (chaparral), grass (grass lawn without irrigation), grass_irr (grass lawn with irrigation) and oak (coastal live oak). The box-plot is the annual transpiration across all EIA/TIA from water year 2005 to 2013.

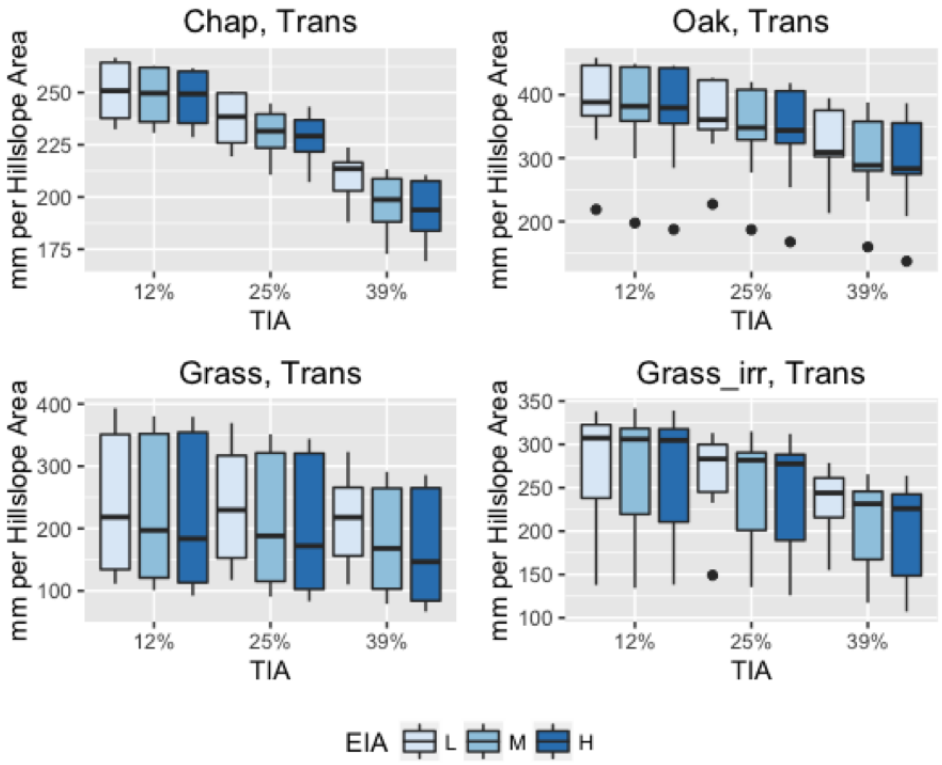

Figure 3.5: Annual transpiration with different EIA, TIA and vegetation settings. Three TIA scenarios are: 12%, 25%, and 39%. Three EIA scenarios are: L (10%), M (50%), H (100%). Four vegetation and irrigation scenarios are: chap (chaparral), oak (live oak), grass (grass lawn without irrigation), and grass_irr (grass lawn with irrigation). The box plot describes the variation of annual transpiration across water years 2005 to 2013.

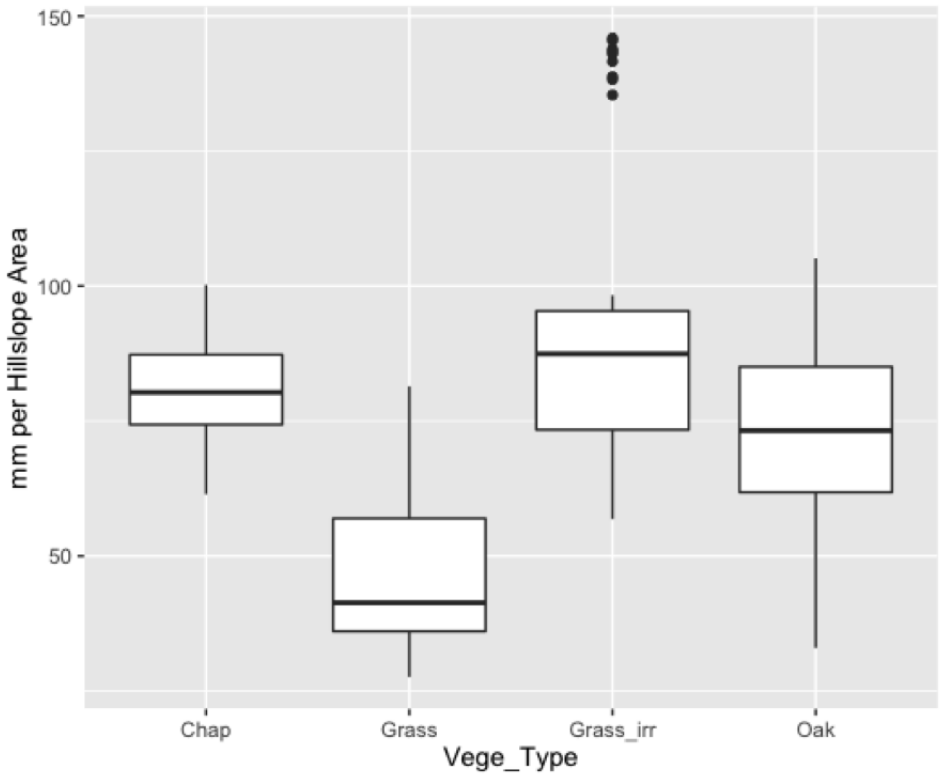

Figure 3.6: Annual evaporation (in mm) for the four scenarios: chap (chaparral), grass (grass lawn without irrigation), grass_irr (grass lawn with irrigation) and oak (coastal live oak). The box-plot is the annual evaporation across all EIA/TIA from water year 2005 to 2013.

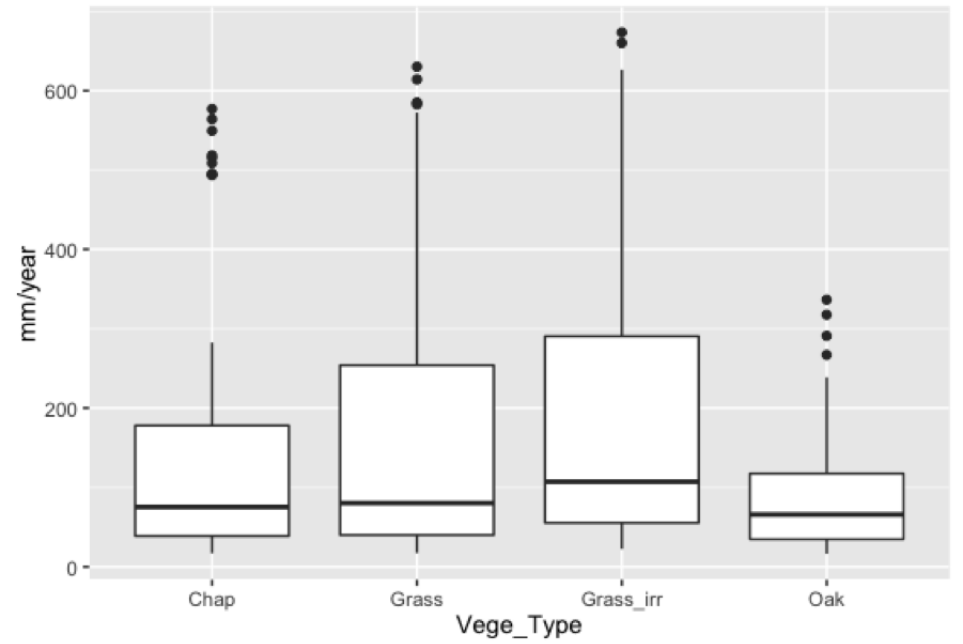

Figure 3.7: Annual runoff (in mm) for the four vegetation scenarios: chap (chaparral), grass (grass lawn without irrigation), grass_irr (grass lawn with irrigation) and oak (coastal live oak). The box-plot is the annual runoff across all EIA/TIA from water year 2005 to 2013.

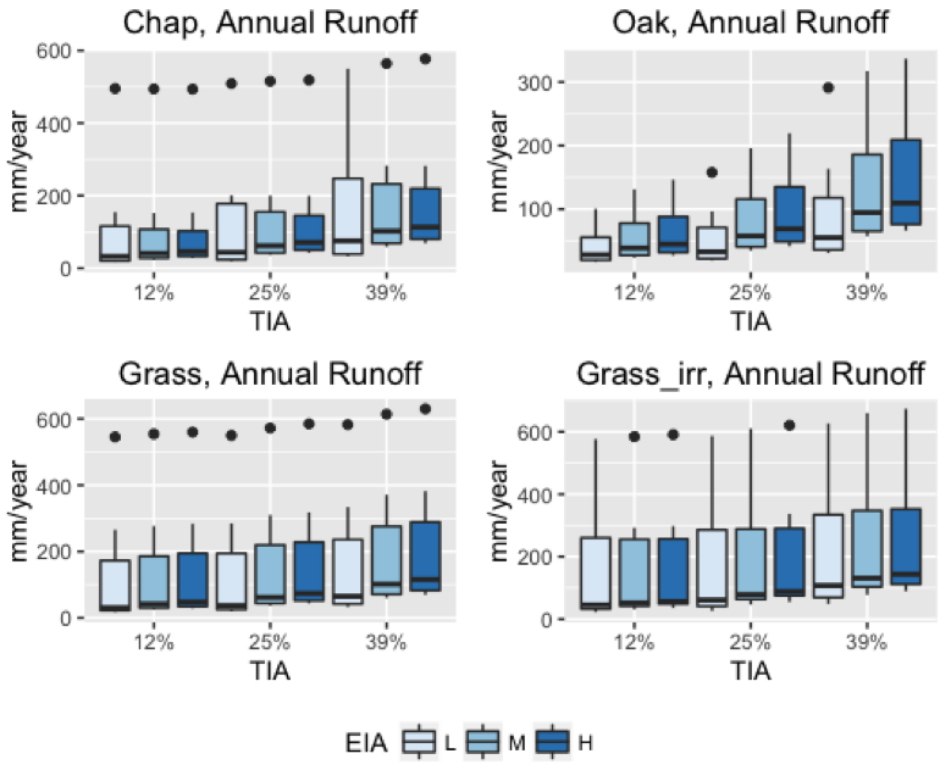

Figure 3.8: Annual runoff with different EIA, TIA and vegetation settings. Three TIA scenarios are: 12%, 25%, and 39%. Three EIA scenarios are: L (10%), M (50%), H (100%). Four vegetation and irrigation scenarios are: chap (chaparral), oak (live oak), grass (grass lawn without irrigation), and grass_irr (grass lawn with irrigation). The boxplot describes the variation of annual runoff across water years 2005 to 2013.

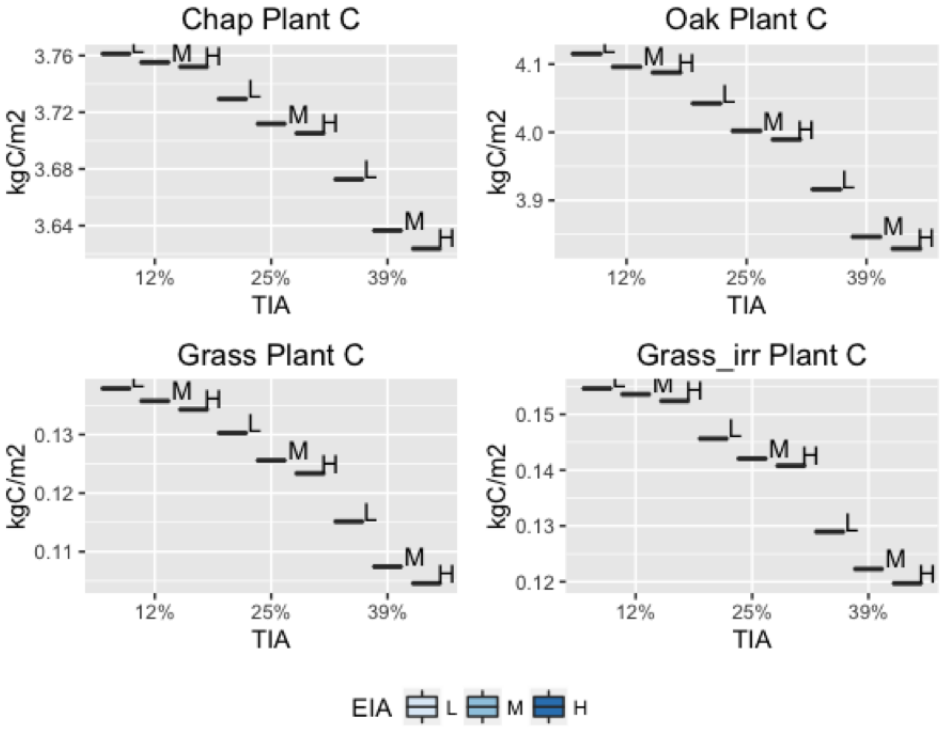

Figure 3.9: Plant carbon with different EIA, TIA and vegetation settings across water years 2005 to 2013. Three TIA scenarios are: 12%, 25%, and 39%. Three EIA scenarios are: L (10%), M (50%), H (100%). Four vegetation and irrigation scenarios are: chap (chaparral), oak (live oak), grass (grass lawn without irrigation), and grass_irr (grass lawn with irrigation).

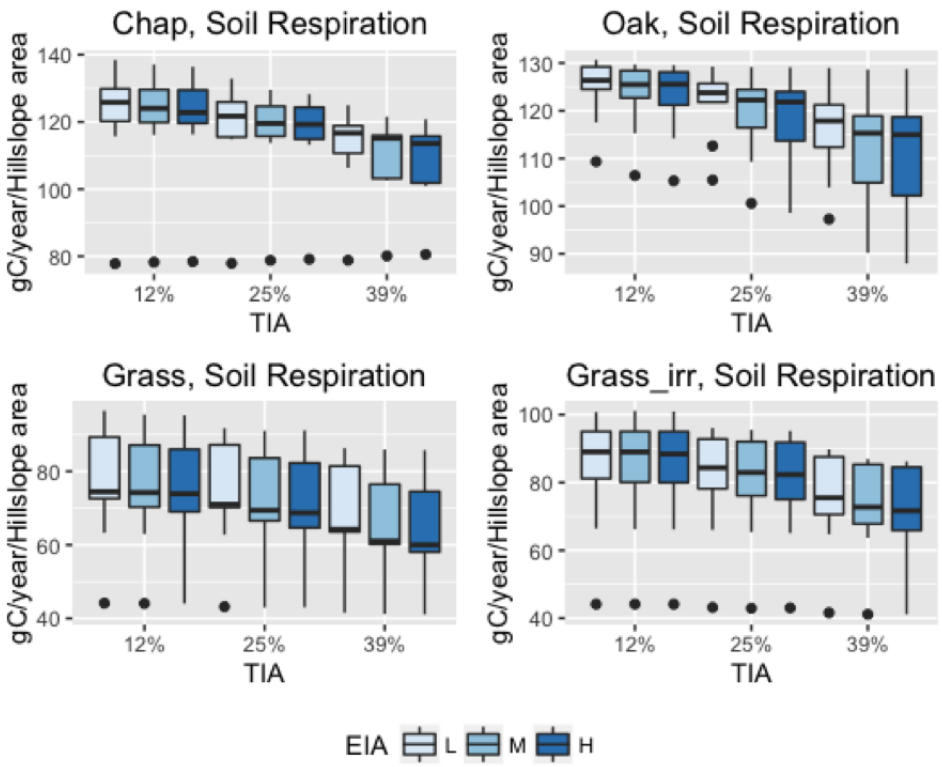

Figure 3.10: Soil respiration ($gC/year/m^2$) in different EIA, TIA and vegetation settings across water years 2005 to 2013. Three TIA scenarios are: 12%, 25%, and 39%. Three EIA scenarios are: L (10%), M (50%), H (100%). Four vegetation and irrigation scenarios are: chap (chaparral), oak (live oak), grass (grass lawn without irrigation), and grass_irr (grass lawn with irrigation).

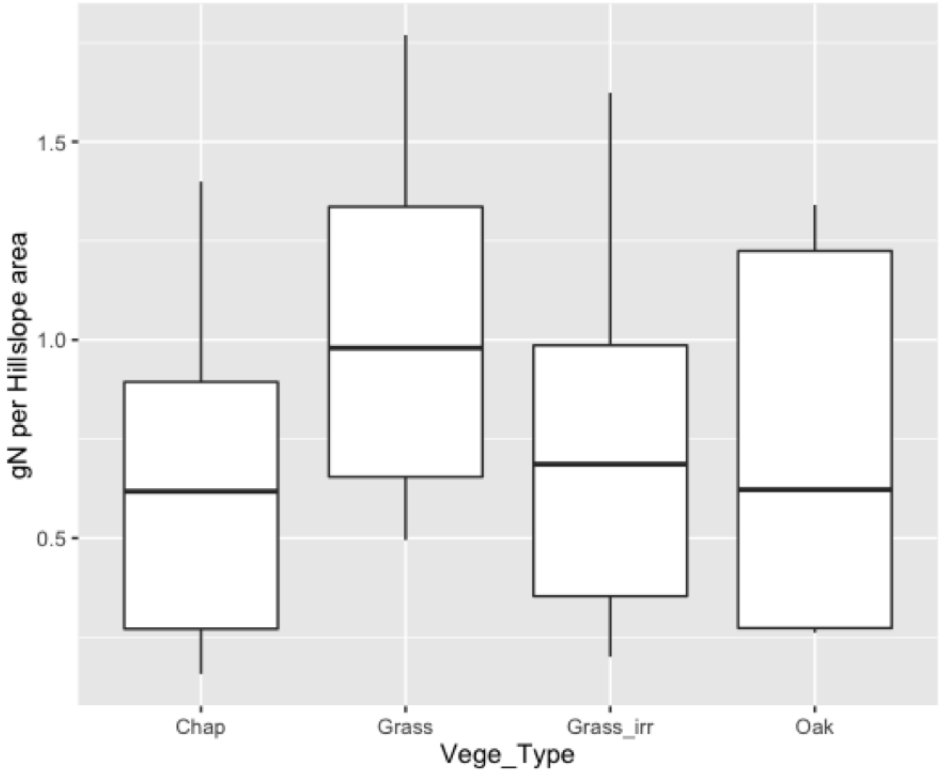

Figure 3.11: The box-plot is the soil nitrate (gN/m^2) across all EIA/TIA from water year 2005 to 2013. The four vegetation scenarios: chap (chaparral), grass (grass lawn without irrigation), grass_irr (grass lawn with irrigation) and oak (coastal live oak).

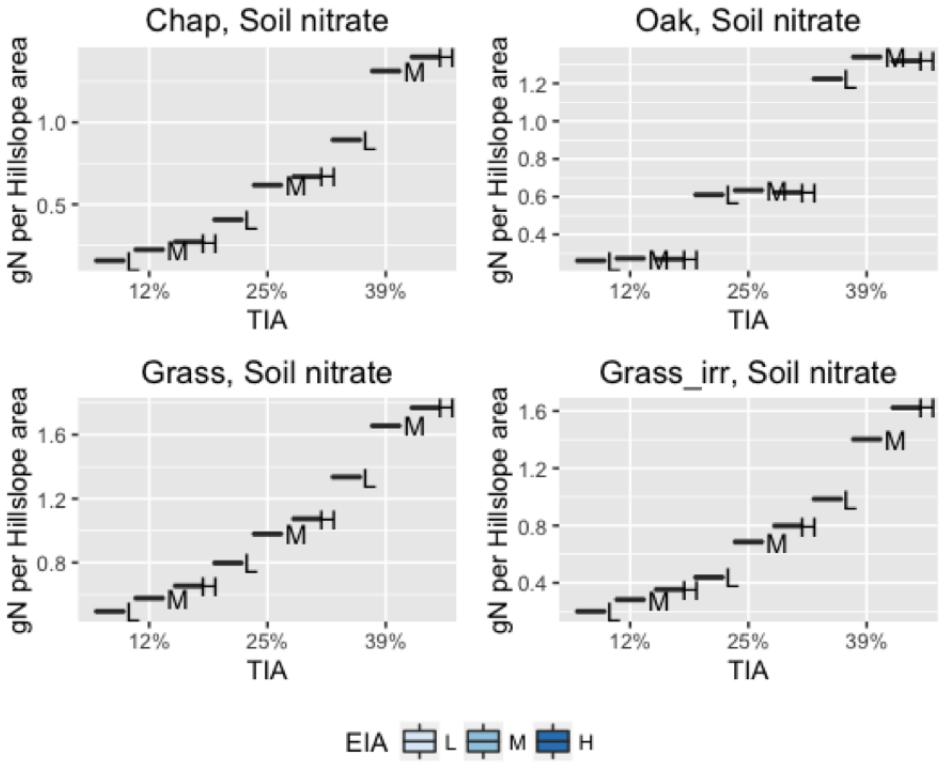

Figure 3.12: Soil nitrate (gN/m^2) across water year 2005 to 2013. Three TIA scenarios are: 12%, 25%, and 39%. Three EIA scenarios are: L (10%), M (50%), H (100%). Four vegetation and irrigation scenarios are: chap (chaparral), oak (live oak), grass (grass lawn without irrigation), and grass_irr (grass lawn with irrigation).

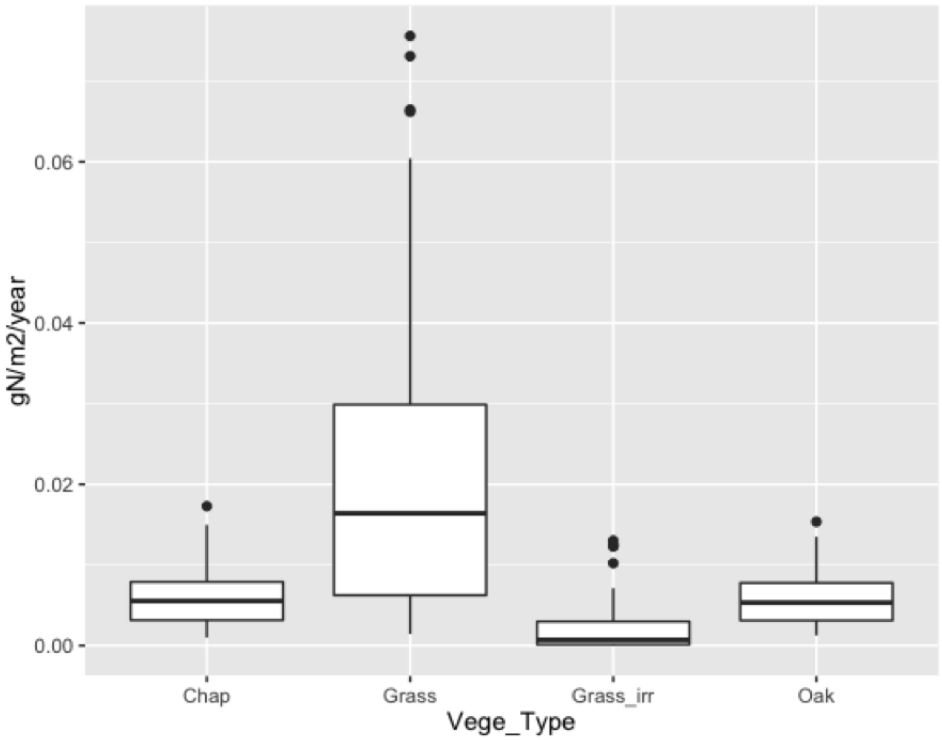

Figure 3.13: Nitrate flux, (gN/m^2) across all EIA/TIA from water year 2005 to 2013. The four vegetation scenarios: chap (chaparral), grass (grass lawn without irrigation), grass_irr (grass lawn with irrigation) and oak (coastal live oak).

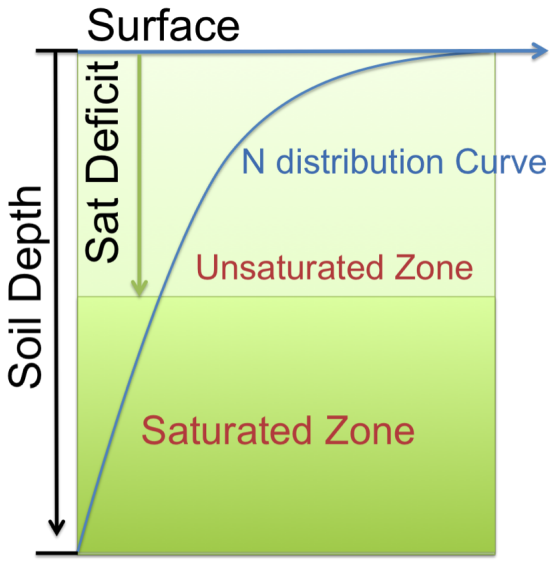

Figure 3.14: How nitrate is distributed in soil profile.

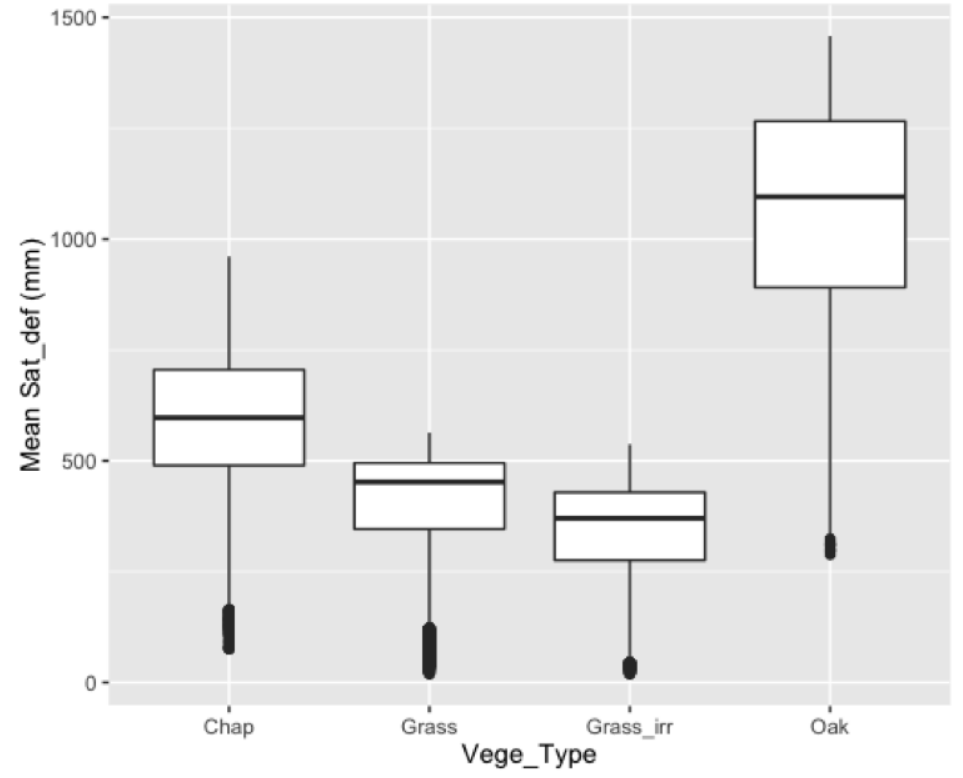

Figure 3.15: Mean saturation deficit (in mm) across all EIA/TIA from water year 2005 to 2013. The four vegetation scenarios: chap (chaparral), grass (grass lawn without irrigation), grass_irr (grass lawn with irrigation) and oak (coastal live oak).

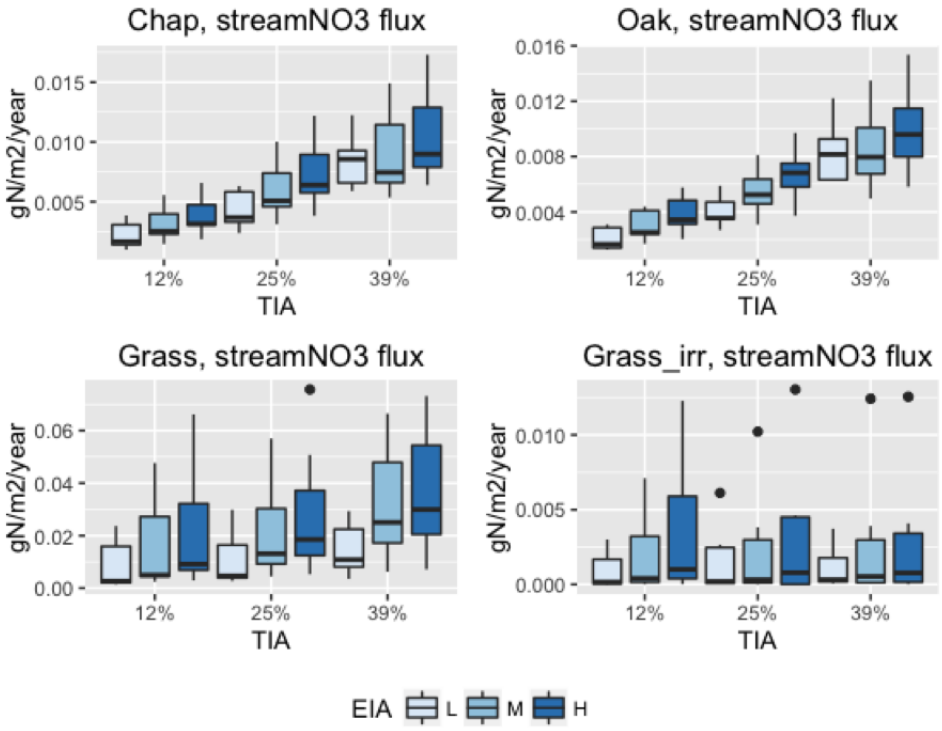

Figure 3.16: Annual nitrate exporting flux (gN/m2/year) across water year 2005 to 2013. Three TIA scenarios are: 12%, 25%, and 39%. Three EIA scenarios are: L (10%), M (50%), H (100%). Four vegetation and irrigation scenarios are: chap (chaparral), oak (live oak), grass (grass lawn without irrigation), and grass_irr (grass lawn with irrigation).

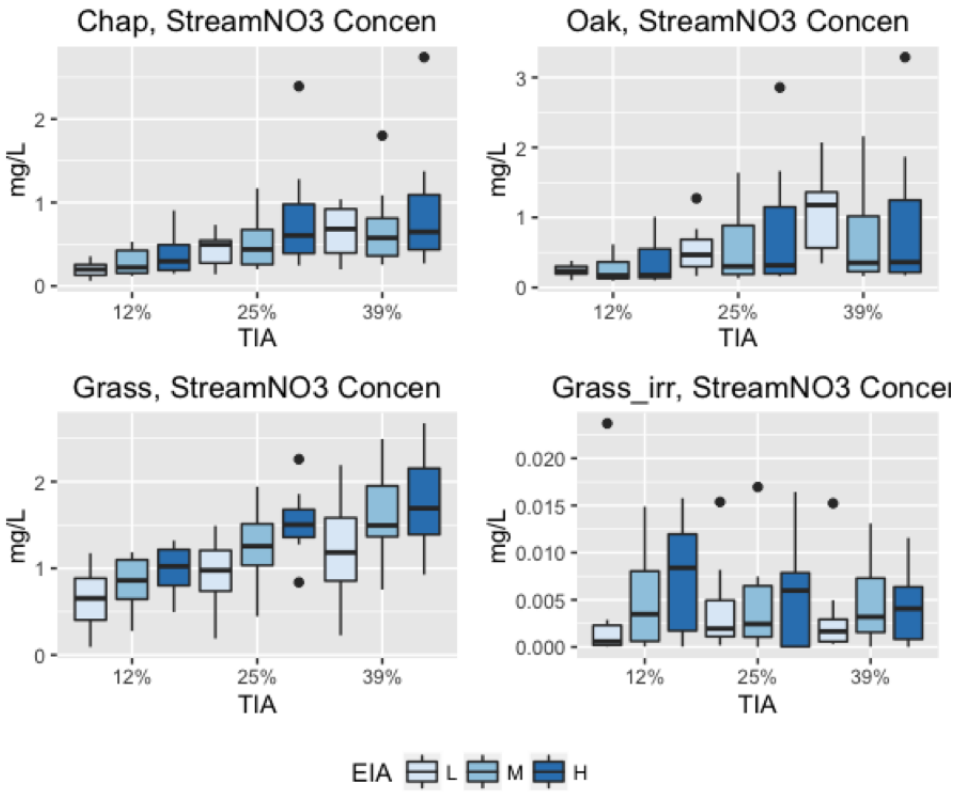

Figure 3.17: Mean annual stream nitrate concentration (mg/L) across water year 2005 to 2013. Three TIA scenarios are: 12%, 25%, and 39%. Three EIA scenarios are: L (10%), M (50%), H (100%). Four vegetation and irrigation scenarios are: chap (chaparral), oak (live oak), grass (grass lawn without irrigation), and grass_irr (grass lawn with irrigation).

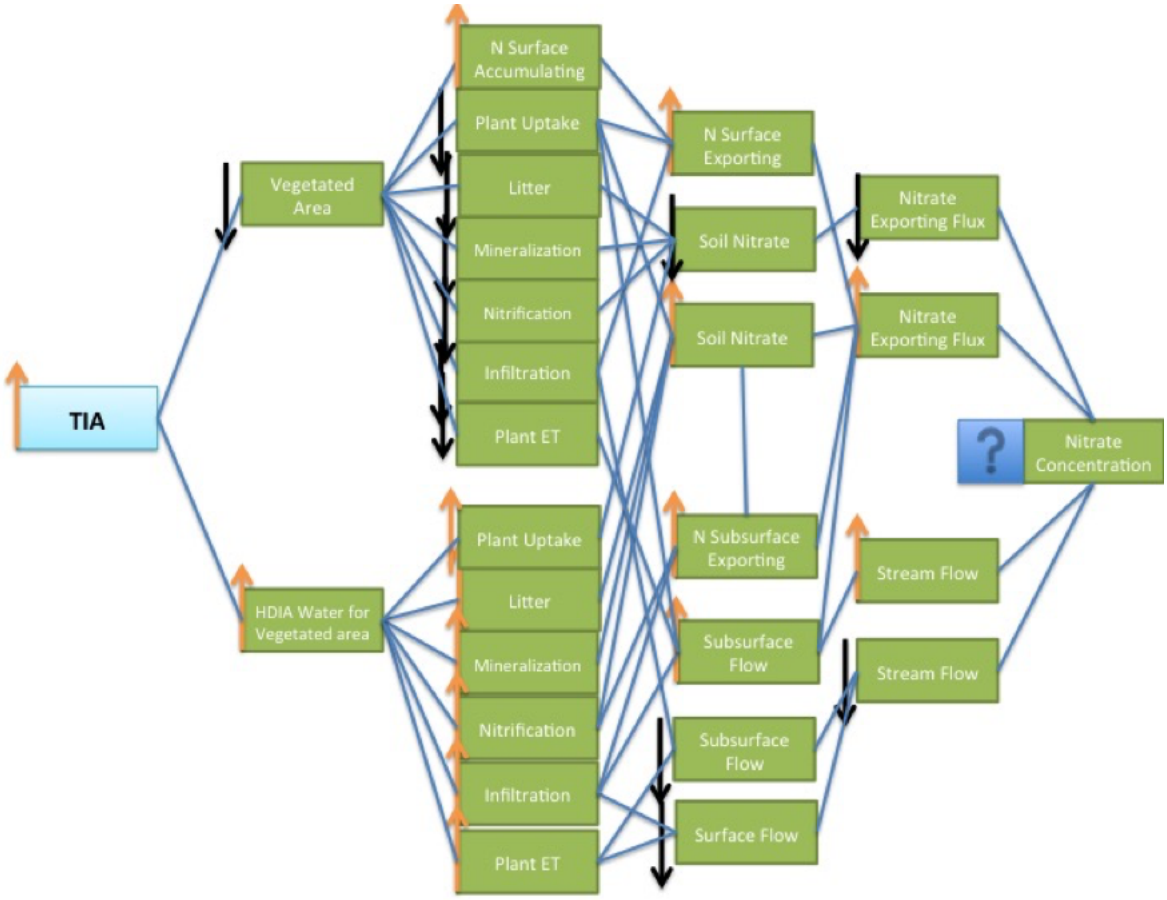

Figure 3.18: Summary of impact of an increase in TIA on nitrate concentration. Upper arrow means increase, and down arrow means decrease.

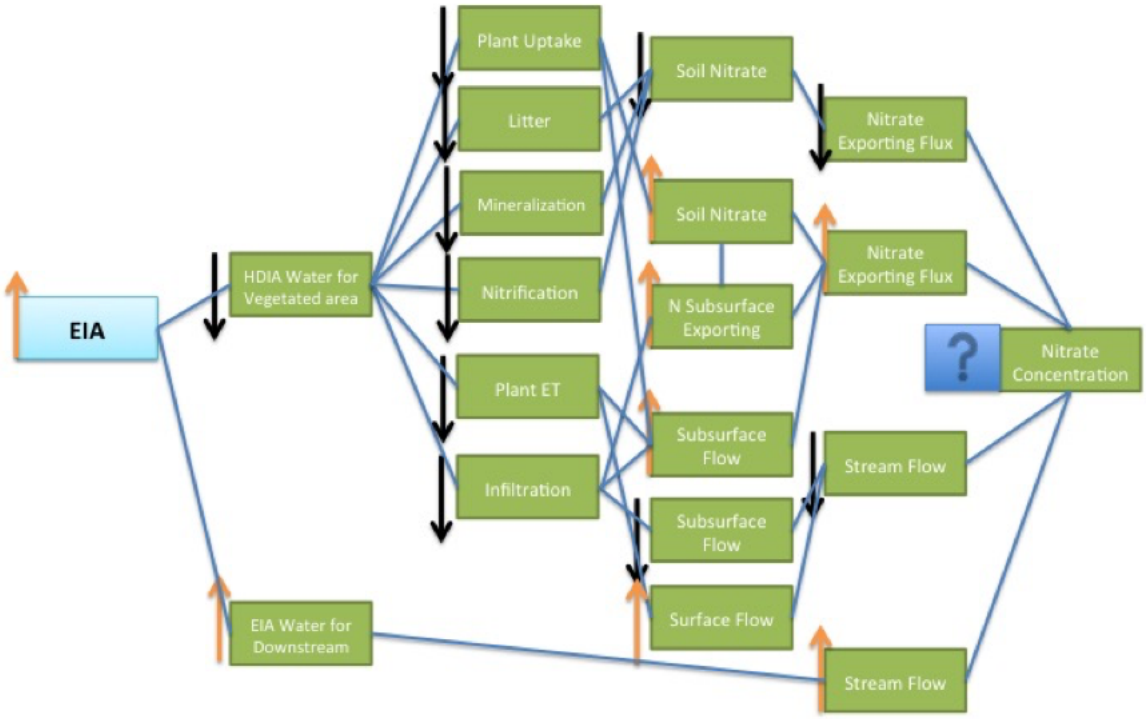

Figure 3.19: Summary of impact of an increase in EIA on nitrate concentration. Upper arrow means increase, and down arrow means decrease.

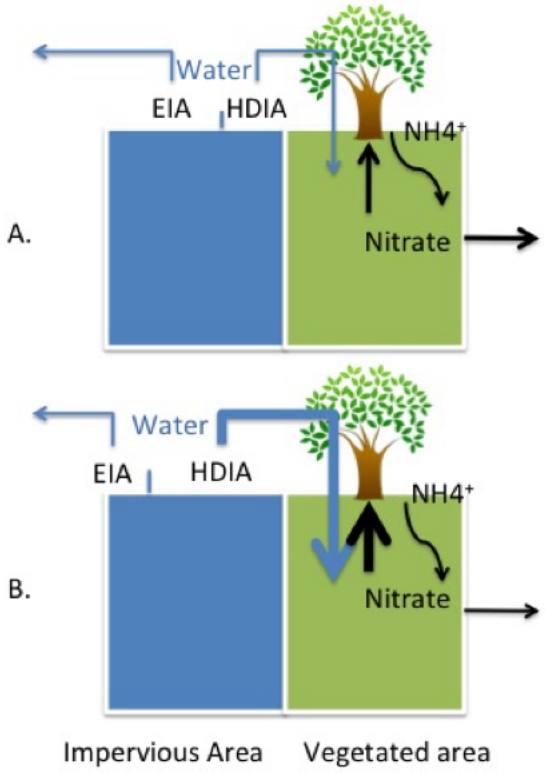

Figure 3.20: The decrease of EIA will divert more flow to the vegetated area, increase the infiltration in vegetated area, affect the nitrification and mineralization, increase the plant uptaking of nitrate and increase the subsurface flow. Model results show that the net effect of the decrease of EIA is the decrease of nitrate concentration. Blue arrow represents the water flow. Black arrow represents the nitrate flux.

Table 3.1: Scenario settings

TIA	EIA	Vegetation
12%	10%	Chaparral
25%	50%	Grass(w/o irrigation))
39%	100%	Oak

Table 3.2: Vegetation properties used in RHESSys model

Vegetation	Chaparral	Grass	Oak
Leaf Turnover Rate	0.28	0.00	0.27
Livewood Turnover Rate	0.25	0.00	0.5
Fine Root Turnover Rate	0.3	0.5	0.27
Daily Mortality Turnover	0.005	0.001	0.005
Leaf litter CN	90	40	90
Livewood CN	63.7	0.25	250
Fineroot CN	88	47.8	100

Table 3.3: Long-term stable root depth for three vegetation types in model output

Chaparral	Grass	Oak
∼4 m	∼ 0.2 m	∼ 4 m

Table 3.4: The difference of transpiration between low EIA and high EIA in series of TIA settings (in mm/unit area)

TIA	12%	15%	39%
Chap	2	8	19
Grass	43	62	77
Grass_irr	3	4	21
Oak	5	11	25

Table 3.5: Mean plant carbon (kgC/m^2), soil carbon(kgC/m^2), litter carbon(kgC/m^2) and soil respiration ($gC/m^2/year$) for different vegetation types

	Plant Carbon	Soil Carbon	Litter Carbon	Soil Respiration
Chap	~ 3.7	~ 1.1	$0.045 \sim 0.05$	122
Grass	0.13	~ 0.9	~ 0.02	70
$Grass\_irr$	0.14	~ 0.9	~ 0.03	72
Oak	~ 4.0	>1.2	$0.06\sim 0.07$	120

Bibliography

[1] M. Stieglitz, J. Shaman, J. McNamara, V. Engel, J. Shanley, and G. W. Kling, *An approach to understanding hydrologic connectivity on the hillslope and the implications for nutrient transport*, *Global Biogeochemical Cycles* **17** (2003), no. 4 n/a–n/a.

[2] L. E. Band, J. J. McDonnell, J. M. Duncan, A. Barros, A. Bejan, T. Burt, W. E. Dietrich, R. E. Emanuel, T. Hwang, G. Katul, Y. Kim, B. McGlynn, B. Miles, A. Porporato, C. Scaife, and P. A. Troch, *Ecohydrological flow networks in the subsurface*, *Ecohydrology* **7** (2014), no. 4 1073–1078.

[3] K. J. Beven and M. J. Kirkby, *A physically based, variable contributing area model of basin hydrology / un modle base physique de zone d'appel variable de l'hydrologie du bassin versant*, *Hydrological Sciences Bulletin* **24** (1979), no. 1 43–69.

[4] H. J. Tromp-van Meerveld and J. J. McDonnell, *Threshold relations in subsurface stormflow: 1. a 147-storm analysis of the panola hillslope*, *Water Resources Research* **42** (2006), no. 2. 021FX Times Cited:85 Cited References Count:41.

[5] M. Tani, *Runoff generation processes estimated from hydrological observations on a steep forested hillslope with a thin soil layer*, *Journal of Hydrology* **200** (1997), no. 14 84–109.

[6] H. J. Tromp-van Meerveld and J. J. McDonnell, *Threshold relations in subsurface stormflow: 2. the fill and spill hypothesis*, *Water Resources Research* **42** (2006), no. 2. 021FX Times Cited:122 Cited References Count:34.

[7] R. Z. Whipkey, *Subsurface stormflow from forested slopes*, *Internatioanl Association of Scientific Hydrology* **10** (1965), no. 2 74–85.

[8] L. Hopp and J. J. McDonnell, *Connectivity at the hillslope scale: Identifying interactions between storm size, bedrock permeability, slope angle and soil depth*, *Journal of Hydrology* **376** (2009), no. 34 378–391.

[9] A. L. James, J. J. McDonnell, I. Tromp-van Meerveld, and N. E. Peters, *Gypsies in the palace: experimentalist's view on the use of 3-d physics-based simulation of hillslope hydrological response*, *Hydrological Processes* **24** (2010), no. 26 3878–3893.

[10] D. Janzen and J. J. McDonnell, *A stochastic approach to modelling and understanding hillslope runoff connectivity dynamics*, *Ecological Modelling* **298** (2015), no. 0 64–74.

[11] P. Lehmann, C. Hinz, G. McGrath, H. J. Tromp-van Meerveld, and J. J. McDonnell, *Rainfall threshold for hillslope outflow: an emergent property of flow pathway connectivity*, *Hydrology and Earth System Sciences* **11** (2007), no. 2 1047–1063. 172NW Times Cited:64 Cited References Count:30.

[12] I. T.-v. Meerveld and M. Weiler, *Hillslope dynamics modeled with increasing complexity*, *Journal of Hydrology* **361** (2008), no. 12 24–40.

[13] N. van Schaik, A. Bronstert, S. M. de Jong, V. G. Jetten, J. C. van Dam, C. J. Ritsema, and S. Schnabel, *Process-based modelling of a headwater catchment in a semi-arid area: the influence of macropore flow*, *Hydrological Processes* **28** (2014), no. 24 5805–5816. ISI Document Delivery No.: AT6GB Times Cited: 0 Cited Reference Count: 34 van Schaik, N. L. M. B. Bronstert, A. de Jong, S. M. Jetten, V. G. van Dam, J. C. Ritsema, C. J. Schnabel, S. Deutsche Forschungsgemeinschaft (German Research Foundation) [SCHR1000/3-1] We gratefully acknowledge the colleagues from the University of Caceres as well as the students Koen Rutten and Joachim Hunnink for their support in gathering the field data and Iris Looijen for her cooperation. Furthermore, we acknowledge the funding of the Deutsche Forschungsgemeinschaft (German Research Foundation) in form of the research grant no. SCHR1000/3-1, which allowed us to write this article. Wiley-blackwell Hoboken.

[14] M. Weiler and J. J. McDonnell, *Conceptualizing lateral preferential flow and flow networks and simulating the effects on gauged and ungauged hillslopes*, *Water Resources Research* **43** (2007), no. 3 W03403.

[15] J. Latron, P. Llorens, and F. Gallart, *The hydrology of mediterranean mountain areas*, *Geography Compass* **3** (2009), no. 6 2045–2064.

[16] M. Niedda and M. Pirastru, *Field investigation and modelling of coupled stream discharge and shallow water-table dynamics in a small mediterranean catchment (sardinia)*, *Hydrological Processes* **28** (2014), no. 21 5423–5435.

[17] M. Weiler, J. J. McDonnell, I. Tromp-van Meerveld, and T. Uchida, *Subsurface Stormflow*. John Wiley and Sons, Ltd, 2006.

[18] S. Minor, K. Kellogg, R. Stanley, L. Gurrola, E. Keller, and T. Brandt, *Geologic map of the santa barbara coastal plain area, santa barbara county, california: U.s. geological survey scientific investigations map 3001,scale 1:25,000, 1 sheet, pamphlet, 38 p*, 2009.

[19] N. L. M. B. van Schaik, S. Schnabel, and V. G. Jetten, *The influence of preferential flow on hillslope hydrology in a semi-arid watershed (in the spanish dehesas)*, *Hydrological Processes* **22** (2008), no. 18 3844–3855.

[20] M. J. Kirkby, L. J. Bracken, and J. Shannon, *The influence of rainfall distribution and morphological factors on runoff delivery from dryland catchments in se spain*, *CATENA* **62** (2005), no. 23 136–156.

[21] S. M. Reaney, L. J. Bracken, and M. J. Kirkby, *Use of the connectivity of runoff model (crum) to investigate the influence of storm characteristics on runoff generation and connectivity in semi-arid areas*, *Hydrological Processes* **21** (2007), no. 7 894–906.

[22] J. P. Lesschen, J. M. Schoorl, and L. H. Cammeraat, *Modelling runoff and erosion for a semi-arid catchment using a multi-scale approach based on hydrological connectivity*, *Geomorphology* **109** (2009), no. 3-4 174–183. ISI Document Delivery No.: 468DO Times Cited: 52 Cited Reference Count: 72 Lesschen, J. P. Schoorl, J. M. Cammeraat, L. H. RECONDES; European Commission; Directorate-General of Research, Environment and Sustainable Development Programme; Natural Resources Management and Services [GOCE-CT-2003-505361] This research, within the RECONDES Project, was funded by the European Commission, Directorate-General of Research, Environment and Sustainable Development Programme, Natural Resources Management and Services, Project no. GOCE-CT-2003-505361 (1 February 2004-30 April 2007). Bas van Wesemael and Andre Meerkerk are thanked for the use of their observed connectivity map. Elsevier science bv Amsterdam.

[23] C. L. Tague and L. E. Band, *Rhessys: Regional hydro-ecologic simulation system-an object-oriented approach to spatially distributed modeling of carbon, water, and nutrient cycling*, *Earth Interactions* **8** (2004). V04oa Times Cited:1 Cited References Count:71.

[24] L. Christensen, C. L. Tague, and J. S. Baron, *Spatial patterns of simulated transpiration response to climate variability in a snow dominated mountain ecosystem*, *Hydrological Processes* **22** (2008), no. 18 3576–3588. ISI Document Delivery No.: 349LC Times Cited: 19 Cited Reference Count: 55 Christensen, Lindsey Tague, Christina L. Baron, Jill S. Usgs [04crag0004/4004cs0001]; epa star [r829640] This research is a product of the Western Mountain Initiative, funded by the USGS under contract 04CRAG0004/4004CS0001. and EPA STAR grant

Agreement Number: R829640. The authors thank two anonymous reviewers Don McKenzie, and David L. Peterson for comments, and Richard Menicke for graphic support. Wiley-blackwell Hoboken.

[25] E. S. Garcia, C. L. Tague, and J. S. Choate, *Influence of spatial temperature estimation method in ecohydrologic modeling in the western oregon cascades*, *Water Resources Research* **49** (2013), no. 3 1611–1624.

[26] S. E. Godsey, J. W. Kirchner, and C. L. Tague, *Effects of changes in winter snowpacks on summer low flows: case studies in the sierra nevada, california, usa*, *Hydrological Processes* **28** (2014), no. 19 5048–5064.

[27] J. I. Lpez-Moreno, J. Zabalza, S. M. Vicente-Serrano, J. Revuelto, M. Gilaberte, C. Azorin-Molina, E. Morn-Tejeda, J. M. Garca-Ruiz, and C. Tague, *Impact of climate and land use change on water availability and reservoir management: Scenarios in the upper aragn river, spanish pyrenees*, *Science of The Total Environment* **493** (2014), no. 0 1222–1231.

[28] C. Shields and C. Tague, *Assessing the role of parameter and input uncertainty in ecohydrologic modeling: Implications for a semi-arid and urbanizing coastal california catchment*, *Ecosystems* **15** (2012), no. 5 775–791.

[29] C. Tague, L. Seaby, and A. Hope, *Modeling the eco-hydrologic response of a mediterranean type ecosystem to the combined impacts of projected climate change and altered fire frequencies*, *Climatic Change* **93** (2009), no. 1-2 137–155.

[30] W. Heber Green and G. A. Ampt, *Studies on soil phyics*, *The Journal of Agricultural Science* **4** (1911), no. 01 1–24.

[31] J. Monteith, *Evaporation and the environment*, *The State and Movement of Water in Living Organisms* (1965) 205–234.

[32] E. J. Hanan, C. M. DAntonio, D. A. Roberts, and J. P. Schimel, *Factors regulating nitrogen retention during the early stages of recovery from fire in coastal chaparral ecosystems*, *Ecosystems* **19** (2016), no. 5 910–926.

[33] J. A. Warrick and L. A. K. Mertes, *Sediment yield from the tectonically active semiarid western transverse ranges of california*, *Geological Society of America Bulletin* **121** (2009), no. 7-8 1054–1070.

[34] R. E. Beighley, J. M. Melack, and T. Dunne, - *impacts of california's climatic regimes and coastal land use change on streamflow characteristics1*, . - 1419.

[35] G. W. Brunner, *Hec-ras (river analysis system).*, 1997.

[36] J. M. Melack, *Sbc lter: Land: Hydrology: Santa barbara county flood control district - precipitation at el deseo (eldeseo255). santa barbara coastal lter. knb-lter-sbc.5008.5. (http://metacat.lternet.edu/knb/metacat/knb-lter-sbc.5008.5/lter)*, .

[37] J. M. Melack, *Sbc lter: Land: Hydrology: Stream discharge and associated parameters at rattlesnake creek, las canoas rd (rs02). santa barbara coastal lter. knb-lter-sbc.3013.6 (http://metacat.lternet.edu/knb/metacat/knb-lter-sbc.3013.6/lter).*, .

[38] J. E. Nash and J. V. Sutcliffe, *River flow forecasting through conceptual models part i a discussion of principles*, *Journal of Hydrology* **10** (1970), no. 3 282–290.

[39] R. E. Beighley, T. Dunne, and J. M. Melack, - *impacts of climate variability and land use alterations on frequency distributions of terrestrial runoff loading to coastal waters in southern california1*, . - 62.

[40] P. A. Troch, G. A. Carrillo, I. Heidbchel, S. Rajagopal, M. Switanek, T. H. M. Volkmann, and M. Yaeger, *Dealing with landscape heterogeneity in watershed hydrology: A review of recent progress toward new hydrological theory*, *Geography Compass* **3** (2009), no. 1 375–392.

[41] J. O. Adegoke and A. M. Carleton, *Relations between soil moisture and satellite vegetation indices in the u.s. corn belt*, *Journal of Hydrometeorology* **3** (2002), no. 4 395–405.

[42] T. Chen, R. A. M. de Jeu, Y. Y. Liu, G. R. van der Werf, and A. J. Dolman, *Using satellite based soil moisture to quantify the water driven variability in ndvi: A case study over mainland australia*, *Remote Sensing of Environment* **140** (2014) 330–338.

[43] K. Beven and A. Binley, *The future of distributed models: Model calibration and uncertainty prediction*, *Hydrological Processes* **6** (1992), no. 3 279–298.

[44] J. W. Kirchner, *Getting the right answers for the right reasons: Linking measurements, analyses, and models to advance the science of hydrology*, *Water Resources Research* **42** (2006), no. 3 n/a–n/a.

[45] R. B. Grayson, A. W. Western, F. H. S. Chiew, and G. Blschl, *Preferred states in spatial soil moisture patterns: Local and nonlocal controls*, *Water Resources Research* **33** (1997), no. 12 2897–2908.

[46] D. Patten, *Riparian ecosytems of semi-arid north america: Diversity and human impacts*, *Wetlands* **18** (1998), no. 4 498–512.

[47] A. Porporato, F. Laio, L. Ridolfi, and I. Rodriguez-Iturbe, *Plants in water-controlled ecosystems: active role in hydrologic processes and response to water stress: Iii. vegetation water stress*, *Advances in Water Resources* **24** (2001), no. 7 725–744.

[48] J. N. Galloway, J. D. Aber, J. W. Erisman, S. P. Seitzinger, R. W. Howarth, E. B. Cowling, and B. J. Cosby, *The nitrogen cascade*, *BioScience* **53** (2003), no. 4 341–356.

[49] L. O. Hedin, J. J. Armesto, and A. H. Johnson, *Patterns of nutrient loss from unpolluted, old-growth temperate forests: Evaluation of biogeochemical theory*, *Ecology* **76** (1995), no. 2 493–509.

[50] H. M. Page, D. C. Reed, M. A. Brzezinski, J. M. Melack, and J. E. Dugan, *Assessing the importance of land and marine sources of organic matter to kelp forest food webs*, *Marine Ecology Progress Series* **360** (2008).

[51] B. M. Goodridge and J. M. Melack, *Land use control of stream nitrate concentrations in mountainous coastal california watersheds*, *Journal of Geophysical Research: Biogeosciences* **117** (2012), no. G2 n/a–n/a.

[52] P. Homyak, J. Sickman, A. Miller, J. Melack, T. Meixner, and J. Schimel, *Assessing nitrogen-saturation in a seasonally dry chaparral watershed: Limitations of traditional indicators of n-saturation*, *Ecosystems* (2014) 1–20.

[53] S. S. Parker and J. P. Schimel, *Soil nitrogen availability and transformations differ between the summer and the growing season in a california grassland*, *Applied Soil Ecology* **48** (2011), no. 2 185–192.

[54] C. A. Shields, L. E. Band, N. Law, P. M. Groffman, S. S. Kaushal, K. Savvas, G. T. Fisher, and K. T. Belt, *Streamflow distribution of nonpoint source nitrogen export from urban-rural catchments in the chesapeake bay watershed*, *Water Resources Research* **44** (2008), no. 9 n/a–n/a.

[55] S. E. Godsey, J. W. Kirchner, and D. W. Clow, *Concentration-discharge relationships reflect chemostatic characteristics of us catchments*, *Hydrological Processes* **23** (2009), no. 13 1844–1864. Times Cited: 100 Godsey, Sarah E. Kirchner, James W. Clow, David W.

[56] W. A. House and M. S. Warwick, *Hysteresis of the solute concentration/discharge relationship in rivers during storms*, *Water Research* **32** (1998), no. 8 2279–2290.

[57] G. M. Hornberger, K. E. Bencala, and D. M. McKnight, *Hydrological controls on dissolved organic-carbon during snowmelt in the snake river near montezuma, colorado*, *Biogeochemistry* **25** (1994), no. 3 147–165. ISI Document Delivery No.:

NY664 Times Cited: 291 Cited Reference Count: 26 Hornberger, gm bencala, ke mcknight, dm Kluwer academic publ Dordrecht.

[58] C. J. Ocampo, C. E. Oldham, M. Sivapalan, and J. V. Turner, *Hydrological versus biogeochemical controls on catchment nitrate export: a test of the flushing mechanism*, *Hydrological Processes* **20** (2006), no. 20 4269–4286.

[59] I. F. Creed, L. E. Band, N. W. Foster, I. K. Morrison, J. A. Nicolson, R. S. Semkin, and D. S. Jeffries, *Regulation of nitrate-n release from temperate forests: A test of the n flushing hypothesis*, *Water Resources Research* **32** (1996), no. 11 3337–3354. ISI Document Delivery No.: VQ428 Times Cited: 205 Cited Reference Count: 90 Creed, IF Band, LE Foster, NW Morrison, IK Nicolson, JA Semkin, RS Jeffries, DS Amer geophysical union Washington.

[60] I. F. Creed and L. E. Band, *Export of nitrogen from catchments within a temperate forest: Evidence for a unifying mechanism regulated by variable source area dynamics*, *Water Resources Research* **34** (1998), no. 11 3105–3120. ISI Document Delivery No.: 132WA Times Cited: 177 Cited Reference Count: 109 Creed, IF Band, LE Amer geophysical union Washington.

[61] I. F. Creed and L. E. Band, *Exploring functional similarity in the export of nitrate-n from forested catchments: A mechanistic modeling approach*, *Water Resources Research* **34** (1998), no. 11 3079–3093. ISI Document Delivery No.: 132WA Times Cited: 74 Cited Reference Count: 46 Creed, IF Band, LE Amer geophysical union Washington.

[62] T. K. Harms and N. B. Grimm, *Influence of the hydrologic regime on resource availability in a semi-arid stream-riparian corridor*, *Ecohydrology* **3** (2010), no. 3 349–359. ISI Document Delivery No.: 648KC Times Cited: 12 Cited Reference Count: 57 Harms, Tamara K. Grimm, Nancy B. Sustainability of Semi-Arid Hydrology and Riparian Areas Science and Technology Center [NSF OIA-9876800] D. Lewis and J. Schade initiated data collection at this site, while C. Kochert and T. Colella provided expertise with laboratory analyses. We thank T. Johns, J. Koehler, R. Martin, M. McCrackin, S. Norlin, J. Schampel, and H. Van Vleck for field assistance. S. Anderson provided access to a protected field site. T. Burt, J. Elser, S. Fisher, S. Hall, and J. Sabo provided comments that significantly improved the manuscript. The Sustainability of Semi-Arid Hydrology and Riparian Areas Science and Technology Center (NSF OIA-9876800) provided funding for this research. John wiley and sons inc Hoboken.

[63] K. A. Lohse, J. Sanderman, and R. Amundson, *Identifying sources and processes influencing nitrogen export to a small stream using dual isotopes of nitrate*, *Water Resources Research* **49** (2013), no. 9 5715–5731. ISI Document Delivery No.: 238ZO Times Cited: 6 Cited Reference Count: 89 Lohse, Kathleen A.

Sanderman, Jonathan Amundson, Ronald Kearney Foundation of Soil Science; University of Arizona Lohse Start up funds; National Science Foundation [EPS-0814387] This work was funded with a grant to R. Amundson by the Kearney Foundation of Soil Science and funding from University of Arizona Lohse Start up funds. Kathleen Lohse, now at Idaho State University, was supported by the National Science Foundation under award EPS-0814387 to complete analysis and writing. We also thank three reviewers and the comments of the editor that vastly improved the manuscript. Amer geophysical union Washington.

[64] R. Jiang, R. Hatano, R. Hill, K. Kuramochi, T. Jiang, and Y. Zhao, *Water connectivity in hillslope of upland-riparian zone and the implication for stream nitrate-n export during rain events in an agricultural and forested watershed*, *Environmental Earth Sciences* **74** (2015), no. 5 4535–4547. Times Cited: 0 Jiang, Rui Hatano, Ryusuke Hill, Robert Kuramochi, Kanta Jiang, Tao Zhao, Ying.

[65] K. G. Jencso, B. L. McGlynn, M. N. Gooseff, K. E. Bencala, and S. M. Wondzell, *Hillslope hydrologic connectivity controls riparian groundwater turnover: Implications of catchment structure for riparian buffering and stream water sources*, *Water Resources Research* **46** (2010), no. 10 n/a–n/a.

[66] M. L. Macrae, M. C. English, S. L. Schiff, and M. Stone, *Influence of antecedent hydrologic conditions on patterns of hydrochemical export from a first-order agricultural watershed in southern ontario, canada*, *Journal of Hydrology* **389** (2010), no. 12 101–110.

[67] A. Swarowsky, R. A. Dahlgren, and A. T. O'Geen, *Linking subsurface lateral flowpath activity with streamflow characteristics in a semiarid headwater catchment*, *Soil Science Society of America Journal* **76** (2012), no. 2.

[68] M. J. Bowes, H. P. Jarvie, S. J. Halliday, R. A. Skeffington, A. J. Wade, M. Loewenthal, E. Gozzard, J. R. Newman, and E. J. Palmer-Felgate, *Characterising phosphorus and nitrate inputs to a rural river using high-frequency concentration-flow relationships*, *Science of the Total Environment* **511** (2015) 608–620. Times Cited: 7 Bowes, M. J. Jarvie, H. P. Halliday, S. J. Skeffington, R. A. Wade, A. J. Loewenthal, M. Gozzard, E. Newman, J. R. Palmer-Felgate, E. J.

[69] A. A. Ameli, J. J. McDonnell, and K. Bishop, *The exponential decline in saturated hydraulic conductivity with depth: a novel method for exploring its effect on water flow paths and transit time distribution*, *Hydrological Processes* (2016) n/a–n/a.

[70] K. Beven and P. Germann, *Macropores and water flow in soils*, *Water Resources Research* **18** (1982), no. 5 1311–1325.

[71] H. Schlesinger and T. J. Gray, *Atmospheric precipitation as a source of nutrients in chaparral ecosystems*, *Symposium on Dynamics and Management of Mediterranean-type Ecosystems* (1982).

[72] J. M. Melack, *Sbc lter: Land: Stream chemistry in the santa barbara coastal drainage area. santa barbara coastal lter. knb-lter-sbc.6.13 (http://metacat.lternet.edu/knb/metacat/knb-lter-sbc.6.13/lter).*, .

[73] S. Neitsch, J. Arnold, J. Kiniry, and J. Williams, *Soil and water assessment tool theoretical documentation verstion 2009*, tech. rep., 2009.

[74] A. J. Wade, P. Durand, V. Beaujouan, W. W. Wessel, K. J. Raat, P. G. Whitehead, D. Butterfield, K. Rankinen, and A. Lepisto, *A nitrogen model for european catchments: Inca, new model structure and equations*, *Hydrol. Earth Syst. Sci.* **6** (2002), no. 3 559–582. HESS.

[75] J. J. McDonnell, *A rationale for old water discharge through macropores in a steep, humid catchment*, *Water Resources Research* **26** (1990), no. 11 2821–2832. Times Cited: 335.

[76] D. L. Peters, J. M. Buttle, C. H. Taylor, and B. D. Lazerte, *Runoff production in a forested, shallow soil, canadian shield basin*, *Water Resources Research* **31** (1995), no. 5 1291–1304. Times Cited: 151.

[77] P. E. Thornton, *Regional ecosystem simulation: combining surface- and satellite-based observations to study linkages between terrestrial energy and mass budgets*. Ph.d. dissertation, 1998.

[78] W. J. Parton, A. R. Mosier, D. S. Ojima, D. W. Valentine, D. S. Schimel, K. Weier, and A. E. Kulmala, *Generalized model for n2 and n2o production from nitrification and denitrification*, *Global Biogeochemical Cycles* **10** (1996), no. 3 401–412.

[79] D. K. Benbi, C. R. Biswas, and J. S. Kalkat, *Nitrate distribution and accumulation in an ustochrept soil profile in a long term fertilizer experiment*, *Fertilizer research* **28** (1991), no. 2 173–177.

[80] J. Zhou, B. Gu, W. H. Schlesinger, and X. Ju, *Significant accumulation of nitrate in chinese semi-humid croplands*, *Scientific Reports* **6** (2016) 25088.

[81] L. R. Sherson, D. J. Van Horn, J. D. Gomez-Velez, L. J. Crossey, and C. N. Dahm, *Nutrient dynamics in an alpine headwater stream: use of continuous water quality sensors to examine responses to wildfire and precipitation events*, *Hydrological Processes* **29** (2015), no. 14 3193–3207. Times Cited: 2 Sherson, Lauren R. Van Horn, David J. Gomez-Velez, Jesus D. Crossey, Laura J. Dahm, Clifford N.

[82] D. o. E. United Nations and P. D. Social Arrairs, *World urbanization prospects: The 2014 revision, (st/esa/ser.a/366).*, tech. rep., 2015.

[83] T. D. Fletcher, H. Andrieu, and P. Hamel, *Understanding, management and modelling of urban hydrology and its consequences for receiving waters: A state of the art*, *Advances in Water Resources* **51** (2013) 261–279. ISI Document Delivery No.: 078NN Times Cited: 52 Cited Reference Count: 252 Fletcher, T. D. Andrieu, H. Hamel, P. Elsevier sci ltd Oxford.

[84] W. D. Shuster, J. Bonta, H. Thurston, E. Warnemuende, and D. R. Smith, *Impacts of impervious surface on watershed hydrology: A review*, *Urban Water Journal* **2** (2005), no. 4 263–275.

[85] L. B. Leopold, *Hydrology for urban land planning–a guidebook on the hydrologic effects of urban land use*, Report 554, 1968.

[86] K. Price, *Effects of watershed topography, soils, land use, and climate on baseflow hydrology in humid regions: A review*, *Progress in Physical Geography* **35** (2011), no. 4 465–492. ISI Document Delivery No.: 794IN Times Cited: 58 Cited Reference Count: 223 Price, Katie US Environmental Protection Agency Science to Achieve Results (STAR) [F6C20808]; National Science Foundation (NSF) [BCS-0702857]; University of Georgia (UGA); University of Georgia Women's Club; Coweeta LTER (NSF) [DEB-0218001] Funding was provided by the US Environmental Protection Agency Science to Achieve Results (STAR) fellowship F6C20808, National Science Foundation (NSF) Doctoral Dissertation Improvement award BCS-0702857, the University of Georgia (UGA) Research Foundation, and the University of Georgia Women's Club. Additional support was generously provided by the Coweeta LTER (NSF cooperative agreement DEB-0218001). Sage publications ltd London.

[87] C. J. Walsh, T. D. Fletcher, and M. J. Burns, *Urban stormwater runoff: A new class of environmental flow problem*, *Plos One* **7** (2012), no. 9. ISI Document Delivery No.: 014PP Times Cited: 51 Cited Reference Count: 54 Walsh, Christopher J. Fletcher, Tim D. Burns, Matthew J. Melbourne Water; Australian Research Council's; Linkage Projects scheme [LP0883610]; Council's Future Fellowship scheme This work was supported by Melbourne Water (www.melbournewater.com.au) and the Australian Research Council's (www.arc.gov.au) Linkage Projects scheme (project number LP0883610) and TDF is supported by the Council's Future Fellowship scheme. The views expressed herein are those of the authors and not necessarily those of the funding bodies. The funders had no role in study design, data analysis, decision to publish, or preparation of the manuscript. Other than the acknowledged hydrographic data used in the paper that were collected by Melbourne Water, the funders had no role in data collection. Public library science San francisco.

[88] C. J. Walsh, A. H. Roy, J. W. Feminella, P. D. Cottingham, P. M. Groffman, and R. P. Morgan, *The urban stream syndrome: current knowledge and the search for*

a cure, *Journal of the North American Benthological Society* **24** (2005), no. 3 706–723. ISI Document Delivery No.: 965NI Times Cited: 694 Cited Reference Count: 76 Walsh, CJ Roy, AH Feminella, JW Cottingham, PD Groffman, PM Morgan, RP Symposium on Urbanization and Stream Ecology Dec, 2003 Univ Melboune, Melbourne, AUSTRALIA North amer benthological soc Lawrence.

[89] A. M. Coutts, N. J. Tapper, J. Beringer, M. Loughnan, and M. Demuzere, *Watering our cities: The capacity for water sensitive urban design to support urban cooling and improve human thermal comfort in the australian context*, *Progress in Physical Geography* **37** (2013), no. 1 2–28. ISI Document Delivery No.: 080KK Times Cited: 18 Cited Reference Count: 128 Coutts, Andrew M. Tapper, Nigel J. Beringer, Jason Loughnan, Margaret Demuzere, Matthias collaborative Cities as Water Supply Catchments research program This research was funded by a large number of government and industry partners as part of the collaborative Cities as Water Supply Catchments research program. A list of funding partners can be found at http://www.waterforliveability.org.au/ page id89 Sage publications ltd London.

[90] C. J. Walsh and J. Kunapo, *The importance of upland flow paths in determining urban effects on stream ecosystems*, *Journal of the North American Benthological Society* **28** (2009), no. 4 977–990. ISI Document Delivery No.: 547KM Times Cited: 40 Cited Reference Count: 37 Walsh, Christopher J. Kunapo, Joshphar 2nd Symposium on Urbanization and Stream Ecology May, 2008 Salt Lake City, UT North amer benthological soc Lawrence.

[91] D. E. Pataki, M. M. Carreiro, J. Cherrier, N. E. Grulke, V. Jennings, S. Pincetl, R. V. Pouyat, T. H. Whitlow, and W. C. Zipperer, *Coupling biogeochemical cycles in urban environments: ecosystem services, green solutions, and misconceptions*, *Frontiers in Ecology and the Environment* **9** (2011), no. 1 27–36. ISI Document Delivery No.: 714XQ Times Cited: 148 Cited Reference Count: 84 Pataki, Diane E. Carreiro, Margaret M. Cherrier, Jennifer Grulke, Nancy E. Jennings, Viniece Pincetl, Stephanie Pouyat, Richard V. Whitlow, Thomas H. Zipperer, Wayne C. US Forest Service, Northern Global Change Program and Research Work Unit [NE-4952]; US National Science Foundation [DEB 97-14835, DEB 99-75463, DEB 0423476, BCS 0948914, HSD 0624177]; Center for Urban Environmental Research and Education, University of Maryland Baltimore County (NOAA) [NA06O AR4310243, NA07OAR4170518]; NOAA EPP Environmental Cooperative Science Center [NA06O AR4810164]; Florida Department of Environmental Protection Nonpoint Source Management Section [G0188, G0262] Funding support came from the US Forest Service, Northern Global Change Program and Research Work Unit (NE-4952); the US National Science Foundation (grants DEB 97-14835, DEB 99-75463, DEB 0423476, BCS 0948914, and HSD 0624177); the Center for Urban Environmental Research and Education, University of Maryland

Baltimore County (NOAA grants NA06O AR4310243 and NA07OAR4170518); NOAA EPP Environmental Cooperative Science Center (grant NA06O AR4810164); and the Florida Department of Environmental Protection Nonpoint Source Management Section (grants G0188 and G0262). We thank the organizers of the Coupled Biogeochemical Cycles sessions at the 2009 ESA Annual Meeting in Albuquerque, New Mexico, for initiating the discussions that led to this paper. Ecological soc amer Washington Si.

[92] C. J. Walsh, D. B. Booth, M. J. Burns, T. D. Fletcher, R. L. Hale, L. N. Hoang, G. Livingston, M. A. Rippy, A. H. Roy, M. Scoggins, and A. Wallace, *Principles for urban stormwater management to protect stream ecosystems*, *Freshwater Science* **35** (2016), no. 1 398–411. ISI Document Delivery No.: DE9XS Times Cited: 12 Cited Reference Count: 111 Walsh, Christopher J. Booth, Derek B. Burns, Matthew J. Fletcher, Tim D. Hale, Rebecca L. Hoang, Lan N. Livingston, Grant Rippy, Megan A. Roy, Allison H. Scoggins, Mateo Wallace, Angela US National Science Foundation (NSF) [DEB 1427007]; NSF Partnerships for International Research and Education [OISE-1243543]; NSF [EPSCoR IIA 1208732]; UK Engineering and Physical Sciences Research Council [EP/K013661/1]; Melbourne Water, through the Melbourne Waterway Research Practice Partnership; Australian Research Council Future Fellowship [FT10010044] This paper arose from a discussion session at the 3rd Symposium on Urbanization and Stream Ecology in Portland, Oregon, in May 2014, which was funded in part by the US National Science Foundation (NSF) award DEB 1427007. The authors acknowledge financial support from the NSF Partnerships for International Research and Education (OISE-1243543, MAR); NSF grant EPSCoR IIA 1208732 (RLH); the UK Engineering and Physical Sciences Research Council Grant EP/K013661/1 (LNH); Melbourne Water, through the Melbourne Waterway Research Practice Partnership (CJW, MJB, TDF); and Australian Research Council Future Fellowship (FT10010044, TDF). Any use of trade, firm, or product names is for descriptive purposes only and does not imply endorsement by the US Government. Univ chicago press Chicago.

[93] C. Shields and C. Tague, *Ecohydrology in semiarid urban ecosystems: Modeling the relationship between connected impervious area and ecosystem productivity*, *Water Resources Research* **51** (2015), no. 1 302–319. ISI Document Delivery No.: CB8OO Times Cited: 2 Cited Reference Count: 29 Shields, Catherine Tague, Christina Santa Barbara Coastal Long-Term Ecological Research project - National Science Foundation [OCE-9982105, OCE-0620276]; National Science Foundation Graduate Research Fellowship This work was supported by the Santa Barbara Coastal Long-Term Ecological Research project, funded by the National Science Foundation (OCE-9982105 and OCE-0620276), and a National Science Foundation Graduate Research Fellowship. The data for this research are

available at http://sbc.lternet.edu. The model code is available at https://github.com/RHESSys/RHESSys. Amer geophysical union Washington.

[94] E. Brabec, S. Schulte, and P. L. Richards, *Impervious surfaces and water quality: A review of current literature and its implications for watershed planning*, *Journal of Planning Literature* **16** (2002), no. 4 499–514. ISI Document Delivery No.: 545QF Times Cited: 179 Cited Reference Count: 92 Brabec, E Schulte, S Richards, PL Sage publications inc Thousand oaks.

[95] P. Gbel, C. Dierkes, and W. G. Coldewey, *Storm water runoff concentration matrix for urban areas*, *Journal of Contaminant Hydrology* **91** (2007), no. 12 26–42.

[96] S. B. Grant, T. D. Fletcher, D. Feldman, J. D. Saphores, P. L. M. Cook, M. Stewardson, K. Low, K. Burry, and A. J. Hamilton, *Adapting urban water systems to a changing climate: Lessons from the millennium drought in southeast australia*, *Environmental Science and Technology* **47** (2013), no. 19 10727–10734. ISI Document Delivery No.: 295CT Times Cited: 14 Cited Reference Count: 53 Grant, Stanley B. Fletcher, Tim D. Feldman, David Saphores, Jean-Daniel Cook, Perran L. M. Stewardson, Mike Low, Kathleen Burry, Kristal Hamilton, Andrew J. U.S. National Science Foundation Partnerships for International Research and Education [OISE-1243543]; ARC [FT100100144] The authors gratefully acknowledge data provided by Melbourne Water, comments on the manuscript from A. Deletic and R. Brown, and financial support from the U.S. National Science Foundation Partnerships for International Research and Education (OISE-1243543). Fletcher is supported by an ARC Future Fellowship (FT100100144). Amer chemical soc Washington.

[97] M. C. Gromaire-Mertz, S. Garnaud, A. Gonzalez, and G. Chebbo, *Characterisation of urban runoff pollution in paris*, *Water Science and Technology* **39** (1999), no. 2 1–8. ISI Document Delivery No.: 174AC Times Cited: 125 Cited Reference Count: 11 Gromaire-Mertz, MC Garnaud, S Gonzalez, A Chebbo, G Conference on Innovative Technologies in Urban Storm Drainage 1998 (NOVATECH 98) May 04-07, 1998 Lyon, france Pergamon-elsevier science ltd Oxford.

[98] B. D. McVeety and R. A. Hites, *Atmospheric deposition of polycyclic aromatic-hydrocarbons to water surfaces - a mass balance approach*, *Atmospheric Environment* **22** (1988), no. 3 511–536. ISI Document Delivery No.: N0511 Times Cited: 267 Cited Reference Count: 76 Mcveety, bd hites, ra Pergamon-elsevier science ltd Oxford.

[99] R. Tobar, R. Azcon, and J. M. Barea, *Improved nitrogen uptake and transport from n-15-labeled nitrate by external hyphae of arbuscular mycorrhiza under*

water-stressed conditions, *New Phytologist* **126** (1994), no. 1 119–122. ISI Document Delivery No.: MW080 Times Cited: 165 Cited Reference Count: 21 Tobar, r azcon, r barea, jm Cambridge univ press New york.

[100] J. Melack, *Sbc lter: Land: Hydrology: Santa barbara county flood control district - precipitation at botanic garden, 321 (botanicgarden321), ongoing since 2005-10-01.*, 2015.

[101] G. D. Farquhar and S. von Caemmerer, *Modelling of Photosynthetic Response to Environmental Conditions*, pp. 549–587. Springer Berlin Heidelberg, Berlin, Heidelberg, 1982.

[102] M. G. Ryan, *Effects of climate change on plant respiration*, *Ecological Applications* **1** (1991), no. 2 157–167.

[103] M. A. White, P. E. Thornton, S. W. Running, and R. R. Nemani, *Parameterization and sensitivity analysis of the biomebgc terrestrial ecosystem model: Net primary production controls*, *Earth Interactions* **4** (2000), no. 3 1–85.

[104] S. De Baets, J. Poesen, A. Knapen, G. G. Barber, and J. A. Navarro, *Root characteristics of representative mediterranean plant species and their erosion-reducing potential during concentrated runoff*, *Plant and Soil* **294** (2007), no. 1 169–183.

[105] G. Moreno, J. J. Obrador, E. Cubera, and C. Dupraz, *Fine root distribution in dehesas of central-western spain*, *Plant and Soil* **277** (2005), no. 1 153–162.

[106] C. Kurz-Besson, D. Otieno, R. Lobo do Vale, R. Siegwolf, M. Schmidt, A. Herd, C. Nogueira, T. S. David, J. S. David, J. Tenhunen, J. S. Pereira, and M. Chaves, *Hydraulic lift in cork oak trees in a savannah-type mediterranean ecosystem and its contribution to the local water balance*, *Plant and Soil* **282** (2006), no. 1 361–378.

[107] M. T. Divers, E. M. Elliott, and D. J. Bain, *Quantification of nitrate sources to an urban stream using dual nitrate isotopes*, *Environmental Science and Technology* **48** (2014), no. 18 10580–10587.

[108] F. Bastida, J. L. Moreno, T. Hernndez, and C. Garca, *The long-term effects of the management of a forest soil on its carbon content, microbial biomass and activity under a semi-arid climate*, *Applied Soil Ecology* **37** (2007), no. 12 53–62.

[109] J. W. Raich and W. H. Schlesinger, *The global carbon dioxide flux in soil respiration and its relationship to vegetation and climate*, *Tellus B* **44** (1992), no. 2 81–99.

[110] A. Rey, E. Pegoraro, C. Oyonarte, A. Were, P. Escribano, and J. Raimundo, *Impact of land degradation on soil respiration in a steppe (stipa tenacissima l.) semi-arid ecosystem in the se of spain*, *Soil Biology and Biochemistry* **43** (2011), no. 2 393–403.

[111] A. Deschaseaux and J.-F. Ponge, *Changes in the composition of humus profiles near the trunk base of an oak tree (quercus petraea (mattus.) liebl.)*, *European Journal of Soil Biology* **37** (2001), no. 1 9–16.

[112] L. Cuo, D. P. Lettenmaier, M. Alberti, and J. E. Richey, *Effects of a century of land cover and climate change on the hydrology of the puget sound basin*, *Hydrological Processes* **23** (2009), no. 6 907–933. ISI Document Delivery No.: 419OM Times Cited: 58 Cited Reference Count: 44 Cuo, Lan Lettenmaier, Dennis P. Alberti, Marina Richey, Jeffrey E. University of Washington; University of Washington [NA17RJ1232] The work reported herein was supported by the University of Washington under its PRISM (Puget Sound Regional Synthesis Model) initiative, and by the Joint Institute for the Study of the Atmosphere and Ocean (JISAO) at the University of Washington under NOAA Cooperative Agreement NA17RJ1232, Contribution 1451. John wiley and sons ltd Chichester.

[113] R. L. Hale, L. Turnbull, S. R. Earl, D. L. Childers, and N. B. Grimm, *Stormwater infrastructure controls runoff and dissolved material export from arid urban watersheds*, *Ecosystems* **18** (2015), no. 1 62–75. ISI Document Delivery No.: CB2CN Times Cited: 11 Cited Reference Count: 57 Hale, Rebecca L. Turnbull, Laura Earl, Stevan R. Childers, Daniel L. Grimm, Nancy B. National Science Foundation [BCS-1026865, DEB-0918457, 0504248] We thank the cities of Tempe, Phoenix, and Scottsdale for permission and assistance in stormwater sampling and for providing datasets describing stormwater infrastructure. The Environmental Remote Sensing and Geoinformatics Lab at Arizona State University provided land-cover classification data. This material is based upon the work supported by the National Science Foundation under Grant numbers BCS-1026865 (CAP LTER) and DEB-0918457 (Impacts of urbanization on nitrogen biogeochemistry in xeric ecosystems). Hale received additional funding from National Science Foundation Grant number No. 0504248, IGERT in Urban Ecology at Arizona State University. Kate Lindekugel, Cathy Kochert, Quincy Stewart, Nicholas Weller, Sarah Moratto, and Danielle Shorts provided valuable field and lab assistance. Springer New york.

[114] A. Gessler, K. Jung, R. Gasche, H. Papen, A. Heidenfelder, E. Brner, B. Metzler, S. Augustin, E. Hildebrand, and H. Rennenberg, *Climate and forest management influence nitrogen balance of european beech forests: microbial n transformations and inorganic n net uptake capacity of mycorrhizal roots*, *European Journal of Forest Research* **124** (2005) 95–111.

[115] R. Gasche and H. Papen, *A 3-year continuous record of nitrogen trace gas fluxes from untreated and limed soil of a n-saturated spruce and beech forest ecosystem in germany. 2. no and no2 fluxes*, *Journal of Geophysical Research* **104** (1999) 18505–18520.

[116] M. Reichstein, A. Rey, A. Freibauer, J. Tenhunen, R. Valentini, J. Banza, P. Casals, Y. F. Cheng, J. M. Grunzweig, J. Irvine, R. Joffre, B. E. Law, D. Loustau, F. Miglietta, W. Oechel, J. M. Ourcival, J. S. Pereira, A. Peressotti, F. Ponti, Y. Qi, S. Rambal, M. Rayment, J. Romanya, F. Rossi, V. Tedeschi, G. Tirone, M. Xu, and D. Yakir, *Modeling temporal and large-scale spatial variability of soil respiration from soil water availability, temperature and vegetation productivity indices*, *Global Biogeochemical Cycles* **17** (2003), no. 4. ISI Document Delivery No.: 749BH Times Cited: 102 Cited Reference Count: 74 Reichstein, M Rey, A Freibauer, A Tenhunen, J Valentini, R Banza, J Casals, P Cheng, YF Grunzweig, JM Irvine, J Joffre, R Law, BE Loustau, D Miglietta, F Oechel, W Ourcival, JM Pereira, JS Peressotti, A Ponti, F Qi, Y Rambal, S Rayment, M Romanya, J Rossi, F Tedeschi, V Tirone, G Xu, M Yakir, D Amer geophysical union Washington.

[117] G. J. Vietz, M. J. Sammonds, C. J. Walsh, T. D. Fletcher, I. D. Rutherfurd, and M. J. Stewardson, *Ecologically relevant geomorphic attributes of streams are impaired by even low levels of watershed effective imperviousness*, *Geomorphology* **206** (2014) 67–78.

[118] N. McIntyre, B. Jackson, A. J. Wade, D. Butterfield, and H. S. Wheater, *Sensitivity analysis of a catchment-scale nitrogen model*, *Journal of Hydrology* **315** (2005), no. 14 71–92.

[119] W. Han and S. Burian, *Determining effective impervious area for urban hydrologic modeling*, *Journal of Hydrologic Engineering* **14** (2009), no. 2 111–120.